FACULTY OF BIOSCIENCE ENGINEERING

# COMPUTATIONAL STUDY OF 2,2-DICHLORO-*N*-(CHLOROMETHYL)ACETAMIDE FORMATION DURING ATTEMPTED STAUDINGER 2,2-DICHLORO-$\beta$-LACTAM SYNTHESIS

Number of words: 21810


Hannes Naeyaert

Student number: 01206374

Promoters: Prof. dr. ir. Matthias D'hooghe
Prof. dr. ir. Veronique Van Speybroeck

Tutors: ir. Elias Van Den Broeck
ir. Sari Deketelaere



Master's Dissertation submitted to Ghent University in partial fulfilment of the requirements for the degree of Master of Science in Bioscience Engineering: Chemistry and Bioprocess Technology

Academic year: 2019 – 2020


UNIVERSITEIT GENT

# Preambule

# Impact van de Coronamaatregelen op de Thesis

Het onderzoek, uitgevoerd in deze thesis, was louter computationeel. De optie was er om dit te combineren met experimenteel onderzoek, maar de beslissing om het enkel bij berekeningen te houden werd al redelijk vroeg tijdens het proces genomen. Er werd van mij verwacht om regelmatig aanwezig te zijn op het CMM. Dit kwam neer op een tweetal dagen per week dat ik direct contact had met mijn begeleider, Elias Van Den Broeck. Op het moment dat de coronamaatregelen van kracht gingen was ik al vertrouwd genoeg met de praktische kant van het modelleren en kon ik zelfstandig gebruik maken van de toepassingen die ik nodig had om mijn onderzoek verder te zetten. Voor vragen en feedback kon ik steeds gebruik maken van online platforms waarmee ik mijn begeleiders op ieder moment kon bereiken. Deze communicatie verliep zeer vlot en zonder problemen. De coronamaatregelen hadden dus zo goed als geen impact op het verloop van mijn thesis. Ik kon mijn onderzoek van thuis uit verderzetten terwijl ik de nodige communicatie met mijn begeleiders en promotoren kon onderhouden. Bijgevolg was er geen heroriëntering van de thesis nodig.

Deze preambule werd in overleg tussen de student en de promotoren opgesteld en door beiden goedgekeurd.

# Acknowledgements

Now my last months as a student draw to a close, I reflect on the past years that made me the person I am today. This education was much more than courses, classes and books. It taught me to be assertive, critical, to think outside the box and solve problems in efficient and creative ways. The skills and knowledge I obtained in the past years were put to the test in this final task. The way I experienced this thesis is similar to my entire carreer as a student. It was hard work with ups and downs and I could not have done it without the help of others.

First, I want to thank my promoters, Prof. dr. ir. Matthias D'hooghe and Prof. dr. ir. Veronique Van Speybroeck for the guidance and feedback. The concept of this thesis and the field of computational chemistry in general is something I am sincerely passionate about and it's an honor to provide this very modest contribution to the scientific realm.

To the people of the CMM, thank you for the assistance and for the quick replies whenever I was facing technical issues.

The people that definitely deserve the most credit are my tutors. To Sari, since this was a computational study, I did not see you that much during the first half of the thesis. But once I got to a point where my simulations started to deliver results, you were there to help us interpret these results. Your experimental input was very fruitful and it gave us a better sense of direction for further calculations. To Elias, a thesis student could not wish for a better tutor. You were very committed to my work and had faith in my capabilities which was a huge motivation for me. Even in times when you were very busy with your own work, you managed to find spare time to help out your thesis students. Sari and Elias, I wish you both all the luck with the further course of your academic careers!

Furthermore, I want to say a few words to the people in my personal life. To Wenke, thank you for supporting me and to her family, thank you for letting me stay at your home during these unusual times in quarantine. To my brother to whom I've always looked up and my closest friends for giving me the much needed confidence. And last but not least, thank you "Moeke en Vake" for the financial support and for being patient with me. I know I have never been the best student and still you gave me the opportunity to continue my studies. I am not taking this for granted!

# Contents

# Chapter 1

# Background and Goals

## 1.1 Background

Since the discovery of penicillin by Alexander Fleming in 1928, azetidin-2-ones or β-lactams have been one of the most intensively studied classes of heterocyclic compounds due to their medical [1]–[4] and synthetic [5] value. Fleming was growing *Staphylococcus* cultures in his lab when one day he noticed that bacteria were dying in the vicinity of a fungus which had contaminated one of his plates and named the active compound after the producing genus *Penicillium*. [6] The accidental discovery of this antibacterial compound revealed its pharmaceutical usefulness as it was only active towards some types of bacteria and not towards animals and humans. The biological activity of penicillin and derivatives is dictated by their characteristic β-lactam structure. They are structurally similar to the peptidoglycan subunits which are the building blocks of the bacteria's cell wall. Penicillins bind irreversibly to the active catalytic site of the proteins responsible for the crosslinking of these peptidoglycan subunits. This way cell wall formation is inhibited and growing cells undergo lysis. Excessive use of penicillin antibiotics gave bacteria the opportunity to develop mechanisms to counteract penicillin's biological activity, resulting in an increasing number of resistant strains. Researchers were well aware of this danger and they understood the importance of modifying the side chains to fight off resistance. The first generations of penicillin antibiotics were produced exclusively via fermentation. [7] Addition of various additives, for example acetic acids, to the *Penicillium* fermentation medium gave newly derived penicillins with different activity spectra. However, a purely synthetic route would enable the production of a much wider range of β-lactam antibiotics, an absolute necessity to arm humanity against the threat of resistant bacteria. This was not possible yet because there was still dissension about the actual structure of the compounds. It was not until 1945, when Dorothy Crowfoot, Hodgkin and Barbara Low completed a successful X-ray crystallographic analysis, that the β-lactam structure was shown beyond question to be correct.

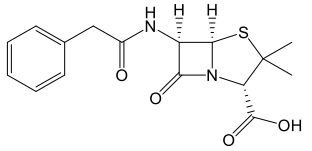


**Figure 1**: Structure of penicillin

Nowadays, the Staudinger β-lactam synthesis is the most widely used method for the production of substituted β-lactams. Apart from their biological activity, β-lactams are very useful starting compounds for the stereoselective synthesis of a variety of organic compounds. [5] This is why the Staudinger β-lactam synthesis is so relevant today and why so many experimental and theoretical studies are published in the last 50 years tackling this specific reaction.

## 1.2 Goals

Although the reaction between ketenes and imines has been known since 1907, the exact nature of the underlying mechanisms was not well understood until a few decades ago. β-lactams **4** (**Figure 2**) are formed via a [2+2]-cyclocondensation of imines **3** with ketenes **2**. [7] The latter are relatively unstable compounds and are not suitable for storage, so they need to be generated *in situ*. This can be done by adding the corresponding acid chlorides **1** to the mixture which contains an excess amount of a suitable base. Other methods for ketene generation include a Wolff rearrangement of α-diazoketones induced by light, heat or a transition metal catalyst, or via photolysis of metal-carbene complexes. [8], [9] The advantages of the acid chloride method are the mild conditions which can be applied to a one-pot reaction. Room temperature is sufficient to obtain high product yields. A disadvantage is the potential formation of unwanted side products such as *N*-(chloromethyl)amides **5** [10]–[13] and enamides **6**. (**Figure 2**) [14], [15]

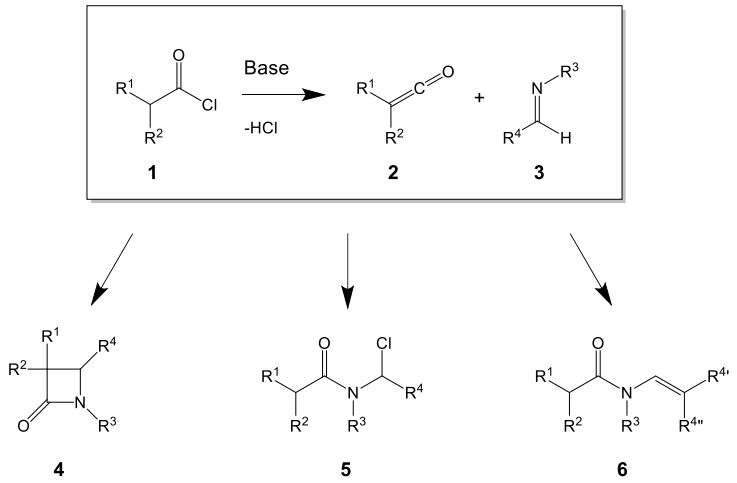


**Figure 2**: Observed products **4**, **5** and **6** after reaction of acid chlorides **1** with imines **3** in the presence of a base.

This thesis is a computational continuation on the experimental findings of D. Deturck and L. Cools. [16], [17] With the original aim of producing spiro-fused β-lactams **10**, the Staudinger synthesis protocol was applied in an attempt to make precursor **9a** using (*S*)-1-(2,2-dimethyl-1,3-dioxolan-4-yl)-*N*-(4-methoxyphenyl)methanimine **7a** and 2,2-dichloroacetyl chloride **8**. (**Scheme 1**) The purpose of the 2,2-dimethyl-1,3-dioxolan side chain is to initiate a series of modification resulting in a spiro-fused side chain at the C4 terminus. The two chlorine groups are required to protect the C3 carbon from deprotonation, since proton abstraction at the C3 position could lead to the formation of bicyclic β-lactams.

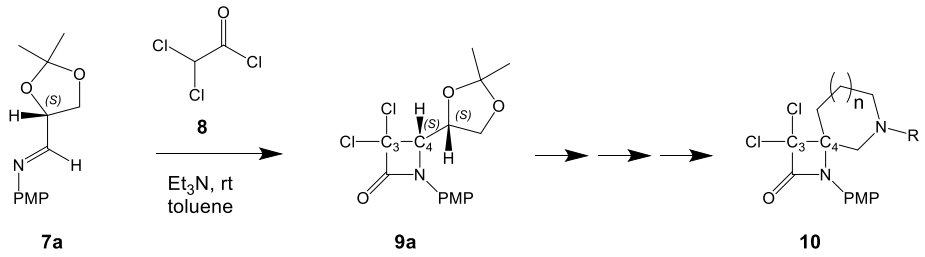


**Scheme 1**: Synthesis of spiro-fused β-lactams **10** from precursor **9a**. [16]

However, the attempts to make precursor **9a** did not result in the formation of the envisioned β-lactam structure, but 2,2-dichloro-*N*-(chloromethyl)acetamide **11a** was formed instead. (**Scheme 2**)

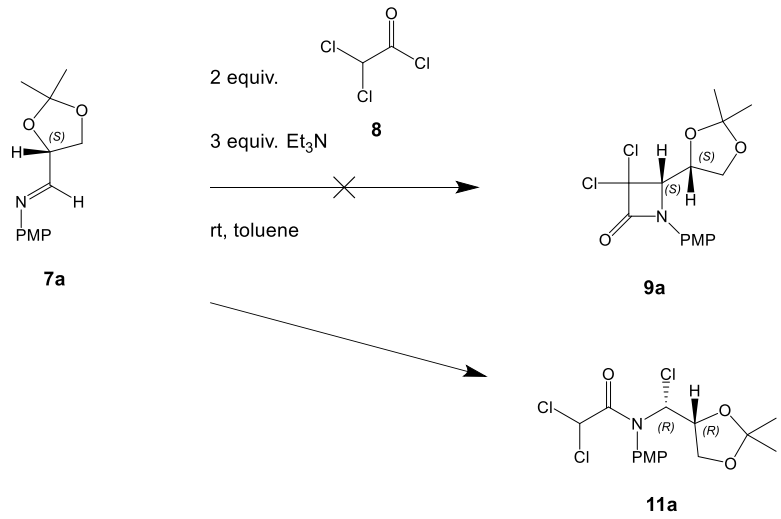


**Scheme 2**: Unexpected reactivity of imine **7a** with 2,2-dichloroacetyl chloride **8**, observed in the experimental thesis of D. Deturck. [16], confirmed and further investigated in experimental thesis of L. Cools. [17]

This behaviour was rather unexpected, since (*S*)-1-(2,2-dimethyl-1,3-dioxolan-4-yl)-*N*-(4-methoxyphenyl)methanimine **7a** has been used before in combination with other acid chlorides **12** to succesfully produce β-lactams **13**. (**Scheme 3**) [18] Also, reactions of 2,2-dichloroacetyl chloride **8** with a variety of imines under Staudinger conditions have already been reported to yield β-lactams. [19], [20] The problem thus lies in the specific combination of (*S*)-1-(2,2-dimethyl-1,3-dioxolan-4-yl)-*N*-(4-methoxyphenyl)methanimine **7a** with 2,2-dichloroacetyl chloride **8**.

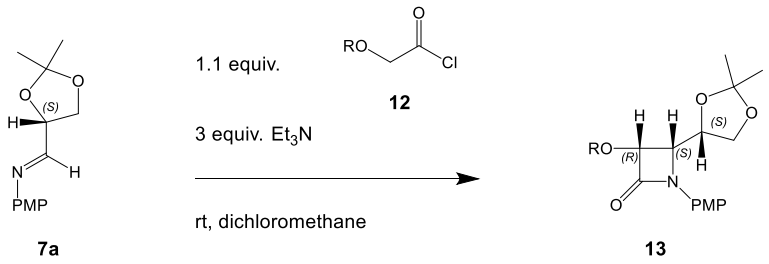


**Scheme 3**: Successful application of imine **7a** in combination with acid chlorides **12** to yield β-lactams **13**, observed in thesis of D. Deturck. (R=Bn: 60%, R=Me: 22%) [16]

The reactivity of imine **7a** with 2,2-dichloroacetyl chloride **8** will be investigated by means of a DFT study. Gibbs free energy profiles will be constructed for the mechanisms dictating this unexpected reactivity and for the mechanisms which are common in the Staudinger β-lactam synthesis. These profiles will be made for different acid chloride and imine combinations in order to investigate the effect of the side chains on the preferential formation of different products. In addition, the hydrolytic stability of 2,2-dichloro-*N*-(chloromethyl)acetamide **11a** will be examined since the observation of this compound was always accompanied by the observation of it's hydrolysis product. The latter is most probably formed during aqueous workup in the attempts to isolate 2,2-dichloro-*N*-(chloromethyl)acetamide **11a**.

# Chapter 2

# Literature Study

This chapter presents an overview of experimental and computational studies concerning the reaction of imines with acid chlorides applying Staudinger conditions. It was suggested that multiple mechanisms could operate simultaneously. (**Scheme 4**) [21] These different pathways can interfere with the stereoselectivity of the reaction and can result in lower yields of the desired products. The mechanisms proposed in the literature are discussed with the main focus on stereochemistry. In the end, a more recent computational technique that was used to investigate mechanochemical activation of the Staudinger β-lactam synthesis is reviewed.

## 2.1 Reactions of Imines with Acid Chlorides

In the literature, three intertwined paths are formulated that lead to β-lactams **4** from acid chlorides **1** and imines **3** in the presence of a base. **Scheme 4** outlines the main mechanisms that were proposed to rationalize experimental findings. [22] The addition order of the reagents has a distinct influence on the preference for the different paths that are given. When acid chlorides are added over a solution which contains imine and excess base, ketene generation occurs almost instantly and path I is operative. Path II and path III can occur in situations where a base is added dropwise over a solution containing imines and acid chlorides. This procedure is widely applied when *trans*-selectivity is desired. [23]

Path I follows the mechanisms which are specific to the Staudinger β-lactam synthesis and in the section where the results are discussed, this path shall be referred to as the 'Staudinger Path'. Acid chlorides **1** are activated carbonyl compounds that generate ketenes **2** and hydrogen chloride by the action of a base. Suitable bases are tertiary amines and in most reported procedures triethylamine is used. [4], [18]-[20] The essential step in path I is the nucleophilic addition of imines **3** onto ketenes **2**. This way zwitterionic intermediates **15** are formed that subsequently undergo a conrotatory ring-closure producing β-lactams **4**.

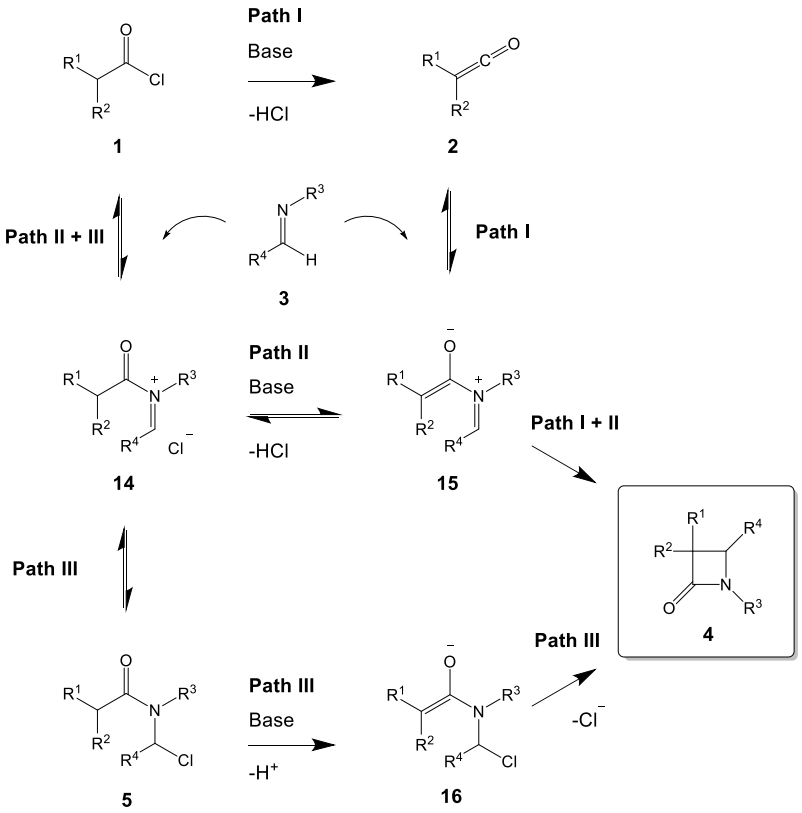


**Scheme 4**: Reaction paths leading to β-lactams **4** starting from acid chlorides **1** and imines **2**.

Parallel to this, *N*-(chloromethyl)amides **5** have been reported in the literature as intermediates during the Staudinger β-lactam synthesis using the acid chloride method for ketene generation. [10]–[13] In some cases these intermediates were isolated, which indicates that other reaction paths are active during the reaction of imines with acid chlorides, apart from Path I. In the presence of a suitable base, Lynch et al. showed in a low temperature FT-IR spectroscopic study that β-lactam formation goes exclusively via a zwitterionic intermediate because ketene generation occurs very quickly when excess amounts of base are present in the mixture. [24] However, in the absence of a base or when the base is added slowly over the mixture, direct acylation of the imines occurs, resulting in *N*-acyliminium salts **14**. [22] This intermediate opens up two other possible routes for β-lactam formation. Path II can be seen as a bridge between path I and path III. When addition occurs prior to ketene generation, delayed proton abstraction from cations **14** by a base will still result in the formation of zwitterionic intermediates **15**. Alternatively, recombination of the chloride anion with the ammonium cations gives rise to *N*-(chloromethyl)amides **5**. Some authors suggest that deprotonation of the ketene moiety in these compounds could lead to stable anions **16**. [22] Subsequent ring-closure of the latter compounds via an intramolecular $S_N2$-displacement could be an alternative route for β-lactam formation.

The reversibility of the initial addition steps of acid chlorides **1** to imines **3** was proven experimentally by Bose et al. [11] They studied the $^1$H-NMR spectra of a carbon tetrachloride solution containing equimolar amounts of acetyl chloride **17a** and benzalaniline **18** (**Scheme 5**). At 40 °C, 95% of acetyl chloride **17a** had been converted to covalent adduct **20a**, at 65 °C the proportion was reduced to 90% and after cooling to 40 °C, the spectrum returned to its original form. This feature highlights the reversibility of the reaction, in which an equilibrium exist between the starting materials and *N*-(chloromethyl)amide **20a**. Addition of triethylamine to this mixture did not lead to 1,4-diphenylazetidin-2-one **21a**, while other acid chlorides **17b-d** did react with benzalaniline **18** in these conditions to form *trans*-β-lactams **21b-d**. This indicates the side chain dependence on this particular reaction.

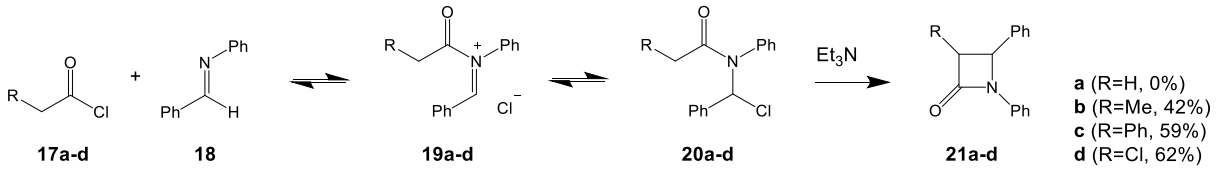


17a-d 18 19a-d 20a-d 21a-d

**Scheme 5**: Reversible relationship between starting components **17a-d** and **18**, and covalent adducts **20a-d**, observed experimentally by Bose et al. [11]

Duran et al. [10] investigated the dependence of the addition order of the base and the reaction conditions on the different pathway's given in **Scheme 4**. They observed *N*-(chloromethyl)amide **22** as the sole product when no triethylamine was added to a mixture of 2,2-dichloroacetyl chloride **8** and benzalaniline **18** in benzene at room temperature. (**Scheme 6**) However when compound **22** was heated under reflux in a benzene solution, β-lactam **23** formation was observed. Addition of triethylamine to a solution containing **22** at room temperature also yielded **23**. On the other hand, yields of almost 100% were obtained when 2,2-dichloroacetyl chloride **8** was added to a solution where an excess amount of triethylamine was already present. This lead to the conclusion that, considering the applied reaction conditions, **22** should be excluded as the main precursor for **23** and path I is favored over path III. Although, small contributions of path III cannot be ruled out completely.

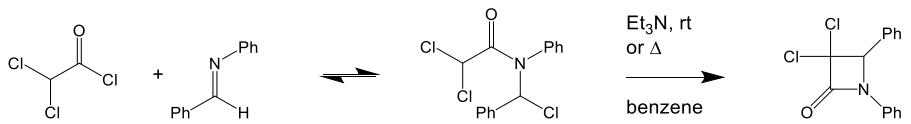


8 18 22 23

**Scheme 6**: Formation of β-lactam **23** through covalent adduct **22**, observed experimentally by Duran et al. [10]

Similar trends were observed by David A. Nelson. [13] Chloroacetyl chloride **24** was added over a solution of benzalaniline **18** in DMF at 80 °C and yielded a mixture of *cis*- and *trans*-cycloadducts **26** (**Scheme 7**). When the proposed intermediate *N*-(chloromethyl)amide **25** was stirred in DMF at 25 °C, no β-lactam was formed, but when added to refluxing DMF, a diastereomeric mixture of β-lactam **26** was obtained (*trans/cis = 47/53*). Treatment of *N*-(chloromethyl)amide **25** with triethylamine in either DMF or benzene at 25 °C yielded only *trans*-**26**. No β-lactam formation was observed when *N*-(chloromethyl)amide **25** was heated under reflux in benzene, so they stated that solvent participation cannot be neglected.

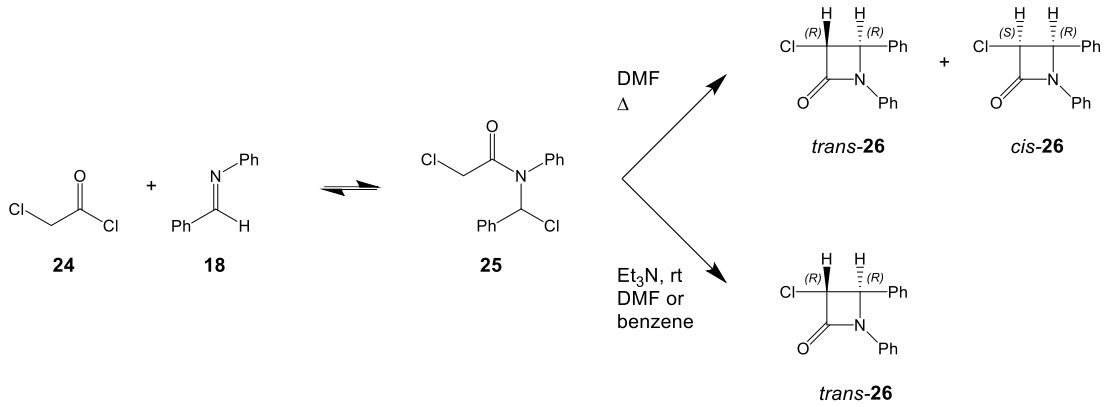


**Scheme 7**: Formation of β-lactam **26** via heating *N*-(chloromethyl)amide **25** under reflux in DMF or by treatment with triethylamine, observed experimentally by Nelson et al. [13]

The articles discussed in this section provided experimental evidence that β-lactam synthesis does not always go exclusively through a zwitterionic intermediate (path I and II, **Scheme 4**). Depending on the conditions applied, path III can occur to some degree and alter the stereochemistry of the final product. In the next section a more detailed overview of the mechanisms governing the stereoselectivity in the Staudinger β-lactam synthesis is given.

## 2.2 Stereoselectivity

### 2.2.1 Origins of Stereoselectivity

When acid chlorides and imines combine to form substituted β-lactams, two chiral centers are created at the C3 and C4 terminals. This leads to four different enantiomers, namely (*3S,4S*)-, (*3S,4R*)-, (*3R,4S*)- and (*3R,4R*)-β-lactam.

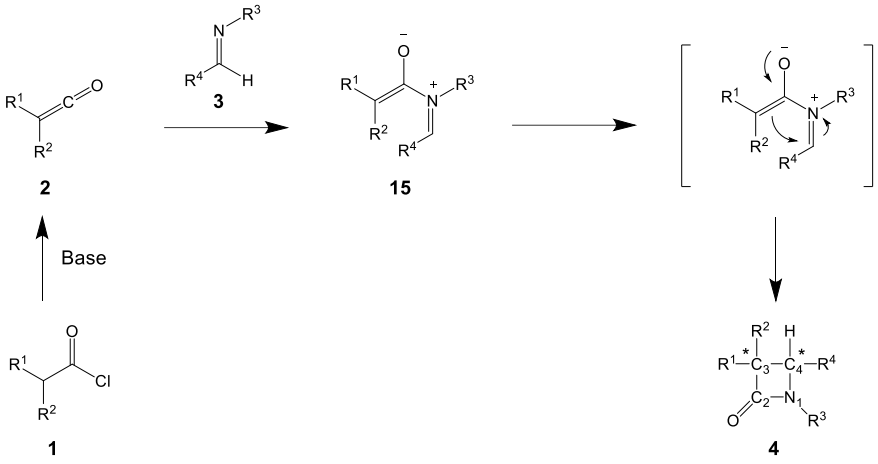


**Scheme 8**: Chiral centers (indicated with '*') created in Staudinger β-lactam synthesis.

The first nucleophilic addition of ketene to imine is mostly a low energy, reversible process. [25] A first distinction is made between the *endo*- and *exo*-attack, where the larger ketene substituent is directed towards the imine (left side in **Scheme 9**) or away from the imine (right side in **Scheme 9**), respectively. Besides the different attack options, the ketene can be approached by the imine from the bottom face (upper half in **Scheme 9**) or top face (lower half in **Scheme 9**), to produce two intermediates which are basically the same zwitterion but their newly formed N1-C2 bonds have a different dihedral angle. For example, when the ketene is approached from the bottom face by the imine in an *endo* fashion, zwitterion **15a** will be formed. Rotation around the N1-C2 bond leads to **15b**. In order to subsequently form the planar four-membered ring structure, a 90° rotation of the N1-C2 bond is needed alongside torsions of the enolate and imine π-systems of the zwitterions **15**. According to the torque-electronic model this has to happen in a conrotatory fashion. [26] For intermediate **15a**, the π-systems can only rotate counterclockwise because a clockwise torsion of the enolate and imine systems in **15a** would cause the $R^1$ and $R^4$ groups to collide. In this model the *endo*-attack produces intermediate **15a** or **15b**, and both form to the final product in *trans* configuration, but with an opposite absolute configuration. The same applies for the *exo*-

attack where two transition states both form *cis*-cycloadducts with opposite absolute configuration.

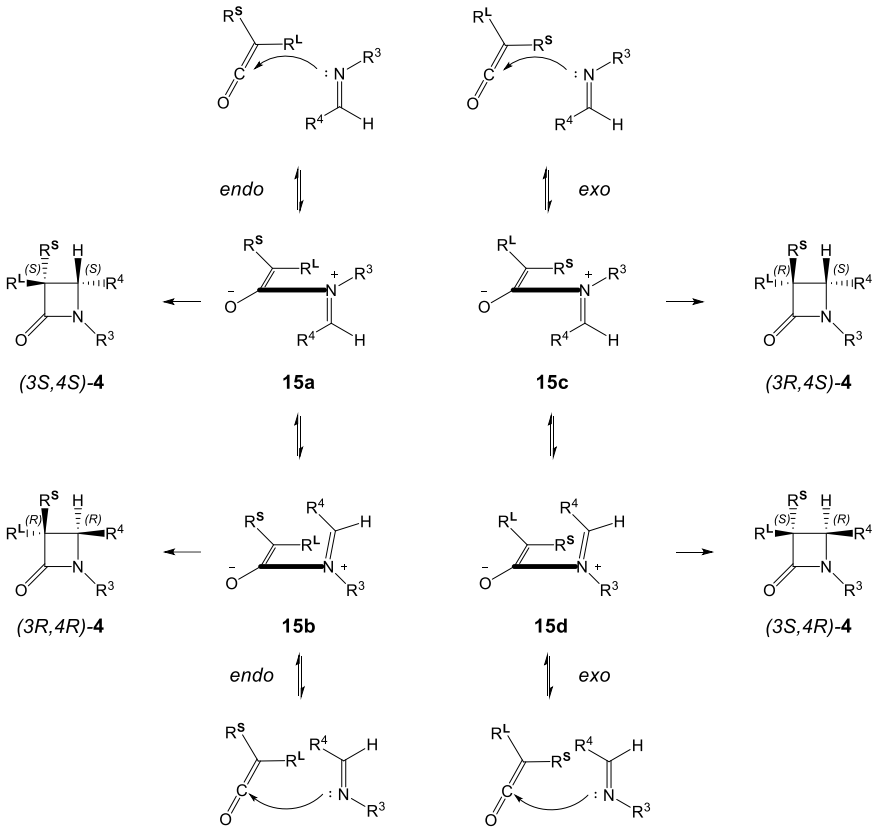


**Scheme 9***:* Illustration of the different addition conformations of imines and ketenes, leading to the four enantiomers of the corresponding β-lactam

According to this model, the stereochemistry will be a result of the differences in energy between the transition states originating from **15a-d**. Apart from this, other models have been developed to explain and predict the stereoselectivity in the Staudinger β-lactam synthesis. Xu et al. proposed that the latter is due to the competition between direct ring-closure of the zwitterionic intermediate **15** and isomerization of the imine moiety in **15** to form intermediate **15'** in **Scheme 10**. [27] For the substrates that were used in their experiments, they found that addition of ketene **2** to imine **3** went exclusively via an *exo*-attack. Subsequent cyclization of **15** leads to the formation of the *cis*-cycloadduct **4** while cyclization of **15'** results in *trans*-cycloadduct **4**. Intermediate **15'** is sterically more favorable than intermediate **15** due to the outward position of the $R^4$ group in **15'**. Therefore, $k_2$ is much larger than $k_2$' and the ratio [*cis*-**4**]/[*trans*-**4**] can be predicted via the ratio $k_1/k_2$.

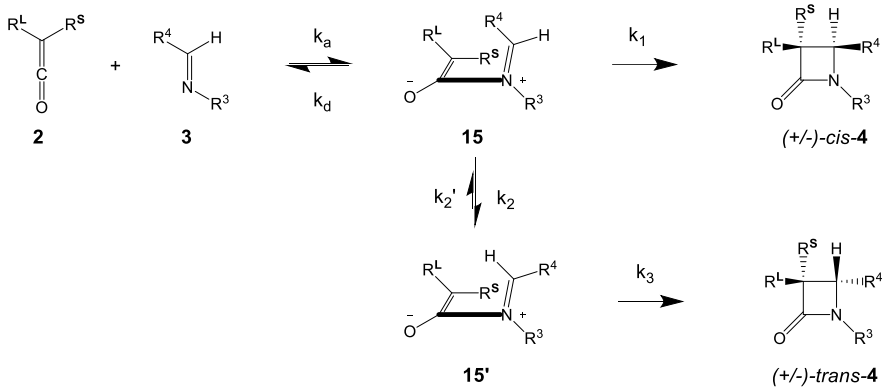


**Scheme 10**: Reaction rates associated with isomerization of the imine moiety in the Staudinger β-lactam synthesis.

It should be stressed that this model is only valid when β-lactam formation goes exclusively via a zwitterionic intermediate. As was mentioned before, delayed addition of the base to a mixture of acid chlorides and imines can cause reaction path III to become operative. Here the final $S_N2$ displacement dictates the stereospecific outcome of the reaction. [28]

## 2.2.2 Influences of the Starting Reactants on the Stereoselectivity

The electronic structures of the starting ketenes and imines play a crucial role in the kinetic model described by Xu et al. The final cyclization step of the zwitterionic intermediate, described by $k_1$ and $k_3$, can be seen as an intramolecular nucleophilic attack of the electron-rich enolate system to the C4 atom of the imine moiety. Electron-donating groups on the ketene thereby accelerate direct ring-closure (increase $k_1$), favoring *cis*-products, while electron-withdrawing groups decrease *cis*-selectivity. [29] In the literature three types of ketenes are mentioned: 1) "Bose-Evans ketenes", possessing strong electron-donating substituents (*O*-alkyl, *O*-aryl or *N*-alkylaryl) favor the formation of *cis*-β-lactams, 2) "Sheehan ketenes", (PhthN) produce complex stereochemical mixtures due to the moderate rate constant for direct cyclization, and 3) "Moore ketenes", carrying very weak electron-donating groups (*S*-alkyl, *S*-aryl, alkyl or aryl) have a preference for the formation of *trans*-β-lactams due to the very small rate constant for direct cyclization. [27]

The effect of the imine substituents $R^3$ and $R^4$ is not as biased as the effect of the ketene substituents. According to the experimental findings of Xu et al. the effect of $R^3$ and $R^4$ is two-sided. Electron-withdrawing groups lower the electron density on C4 making it more susceptible for nucleophilic attack of C3. On the other hand, decreased electron density on the imine double bond increases the possibility of isomerization of the zwitterionic intermediate.

Thus, electron-withdrawing groups $R^3$ and $R^4$ can accelerate both direct ring-closure and isomerization (increase both $k_1$ and $k_2$) complicating stereo-control of the synthesis. This effect can be counteracted by introducing bulky groups on N1. If the N1-substituent $R^3$ is a bulky group, such as isopropyl, isomerization can be slowed down due to steric effects favoring the *E*-configuration of the imine moiety. This means lower values for $k_2$ and *cis*-products are favored. [27]

Until now, only the preference for *cis*- or *trans*-β-lactam formation was discussed. But most production processes rely on the synthesis of enantiomerically pure products. This is where chiral auxiliaries come into play in order to control the absolute stereochemistry. Cossío et al. showed in a computational study the effectiveness of using chiral starting imines or ketenes. The HF/6-31+G* transition structure **29** in **Scheme 11** [30] was calculated to be 6.3 kJ/mol more stable than transition structure **30**, which is in good agreement with experimental results. The difference in energies of these two transition structures, both originating from the initial *exo*-attack of chiral imine **28** onto ketene **27**, is due to a steric hindrance between the 2,2-dimethyl-1,3-dioxolane group and the β-lactam ring being formed in **30**. The same reasoning can be applied to the use of chiral ketene substituents for enantioselective Staudinger β-lactam syntheses. [30]

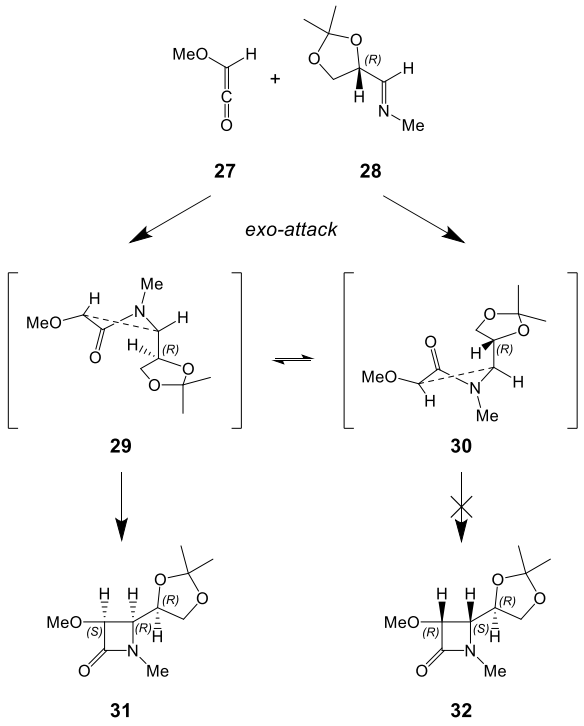


**Scheme 11**: Illustration of how chiral auxiliaries can control the absolute stereochemistry in the Staudinger β-lactam synthesis. Transition structures **29** and **30** were calculated at the HF/6-31+G* level of theory by Cossío et al. [30]

### 2.2.3 Influences of the Reaction Conditions on the Stereoselectivity

In this section, the conclusions from a series of papers on the influences of reaction conditions on the Staudinger reaction of imines with ketenes, published by Xu and coworkers, will be discussed. [27]–[29], [31] First, it was investigated if the ketene generation method had an effect on the stereoselectivity. The two major methods that were compared are the dehydrohalogenation of acid chlorides and the thermal Wolff-rearrangement of α-diazo carbonyl compounds. Their results indicated that the ketene formation pathways did not have an obvious effect on the stereoselectivity.

The reaction temperature, however, did have a distinct effect on the stereoselectivity. Their experiments were designed to distinguish between three possibilities for this temperature dependency: 1) products can epimerize at higher temperatures, 2) there is a competition between *endo*- and *exo*-attack at higher temperatures, dictating the final stereochemistry, and 3) the ratio between $k_1$ and $k_2$ is the major temperature dependent effect. From the obtained results, they concluded that the third possibility is the major contributing factor. They observed that *cis*-selectivity decreased with increasing temperature because the rate constant for isomerization $k_2$ increases faster than the rate constant for direct ring-closure $k_1$ when temperature is raised.

According to calculations performed by Arrieta et al., transition structures leading to *cis*-products are generally more polar than their *trans*-counterparts, so they argued that increasing the polarity of the solvent should affect the stereoselectivity. However, Xu et al. doubted the computational accuracy of the method used by Arrieta et al. and stated that this was not the major factor in the solvent's effect on the stereoselectivity. [28] Again, they proposed that the real influence of the solvent on the stereoselectivity lies in the competition between direct ring-closure and isomerization of the zwitterionic intermediate. The latter is highly ionic in nature and increasing the polarity of the solvent should increase their half-life and moreover, increase the possibility of isomerization thus favoring the formation of *trans*-cycloadducts. On the other hand, nonpolar solvents should favor direct ring-closure and hence increase *cis*-selectivity. In terms of rate constants, this means that $k_2$ increases when more polar solvents are used. This was investigated by performing a series of Staudinger β-lactam syntheses in different solvents. The results indicated that, as anticipated, nonpolar solvents are favorable for the synthesis of *cis*-β-lactams while polar solvents increase the formation of *trans*-β-lactams. The same conclusion was confirmed by Nagy et al. in a recent computational study where solvent effects in the Staudinger β-lactam synthesis were evaluated with the IEFPCM method. [32]

## 2.2.4 Relation between Stereochemistry and the Reaction Paths participating in the Staudinger β-lactam Synthesis

When reaction path III is responsible for the formation of β-lactams, there is a distinct preference for the formation of *trans*-cycloadducts. This was shown in a computational analysis performed by Arrieta and coworkers using the B3LYP/6-31+G* level of theory. [22] The free energy barriers for the final cyclization steps in path I and path III were calculated and compared. It was found that transition structure **34** in **Scheme 12**, which leads to the *cis*-cycloadduct *(3R,4S)*-**38** via conrotatory cyclization, was 34.4 kJ/mol lower in energy than the corresponding transition structure **35** that would lead to the *trans*-cycloadduct *(3S,4S)*-**38**. On the other hand, transition structure **36**, which leads to *(3R,4R)*-**38** via an $S_N2$-displacement of chloride, was 26.4 kcal/mol lower in energy than the transition state **37** that would form *cis*-cycloadduct *(3S,4R)*-**38**.

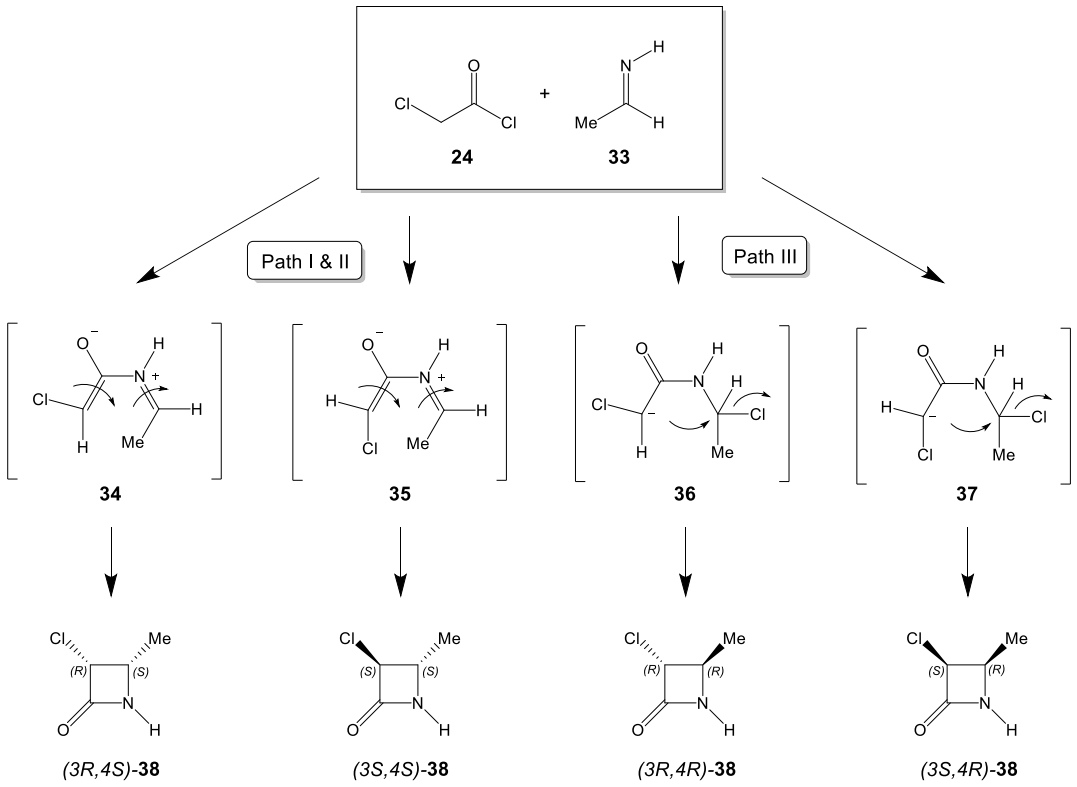


**Scheme 12**: Formation of β-lactam **38** via conrotatory cyclization of zwitterionic intermediates **34-35** or via an $S_N2$-displacement of a chloride anion in **36-37**. (The arrows in **34-35** are used to indicate the clockwise rotation in the conrotatory cyclization step) [22]

The zwitterionic intermediates in transition structures **34** and **35** have a more rigid structure due to the enolate and imine π-systems and are stuck in the conformation determined by the direction of ketene-imine addition. The *N*-(chloromethyl)amide obtained via path III on the other hand has a higher degree of rotational freedom, hence giving it the possibility to adopt a more stable conformation prior to enolate formation in **36** and **37**. Steric effects between the chlorine atom at C3 and the methyl group at C4 favor the *trans*-configuration for the final $S_N2$-displacement. This explains the decreased *cis*-selectivity when β-lactam formation does not go exclusively through the formation of a zwitterion. **Scheme 13** gives an detailed overview of the processes leading to these different cyclization transition state structures.

In order to distinguish between the pathways responsible for the formation of β-lactams **4** (**Scheme 13**), Xu et al. conducted a series of experiments. [28] In Path I and II, the conrotatory cyclization of zwitterionic intermediates **15** favors the formation of *cis*-β-lactams in most cases. When Path III is operative, *cis*-selectivity of the reaction is reduced considerably. The *cis/trans* ratios of β-lactam products formed from a series of ketenes and imines were compared for different addition methods and different ketene generation methods. Addition method A) a solution of acid chloride in toluene was added into a solution of imine and triethylamine in toluene, addition method B) a solution of triethylamine in toluene was added over a solution of imine and acid chloride in toluene immediately, and addition method C) a solution of triethylamine in toluene was added after the solution of imine and acyl chloride in toluene was stirred for 4 hours at 80 °C.

For addition method A, *cis/trans*-β-lactam ratios were the same as those formed from ketenes which were generated via a Wolff-rearrangement. Path II and III can be excluded when ketenes are generated via this method due to the absence of the reactive acid chlorides **1**. This means that for addition mode A, β-lactam formation goes exclusively via path I (**Scheme 13**).

For addition method B there was a higher amount of *trans*-product **4** observed, meaning that path I was not fully responsible for β-lactam formation and path III had a share in the final stereochemical outcome. However, for imines carrying strong electron-donating groups and for imines carrying strong electron-withdrawing groups, the results were the same as for addition mode A. This can be ascribed to the electron-rich group increasing the nucleophilicity of the imine and decreases the possibility of the nucleophilic addition of a chlorine ion to the imine moiety in the formed iminium ion **16**. The slowly added triethylamine immediately abstracts a proton from iminium ion **16** to give rise to zwitterionic intermediate **17**, which is further responsible for β-lactam **4** formation (Path II). Thus, delayed addition of base gives acid chloride **1** the opportunity to react directly with imine **3**, but from the moment base is added, equilibrium shifts towards the formation of zwitterionic intermediate **17**. Imines with strong electron-withdrawing groups have a decreased nucleophilicity, disfavoring direct addition of imines to acid chlorides. Consequently, all acid chloride can be converted to the corresponding ketene when base is added and path I is the major process.

Finally, addition method C yielded predominately *trans*-β-lactams, meaning that path III was the stereochemistry determining factor here.

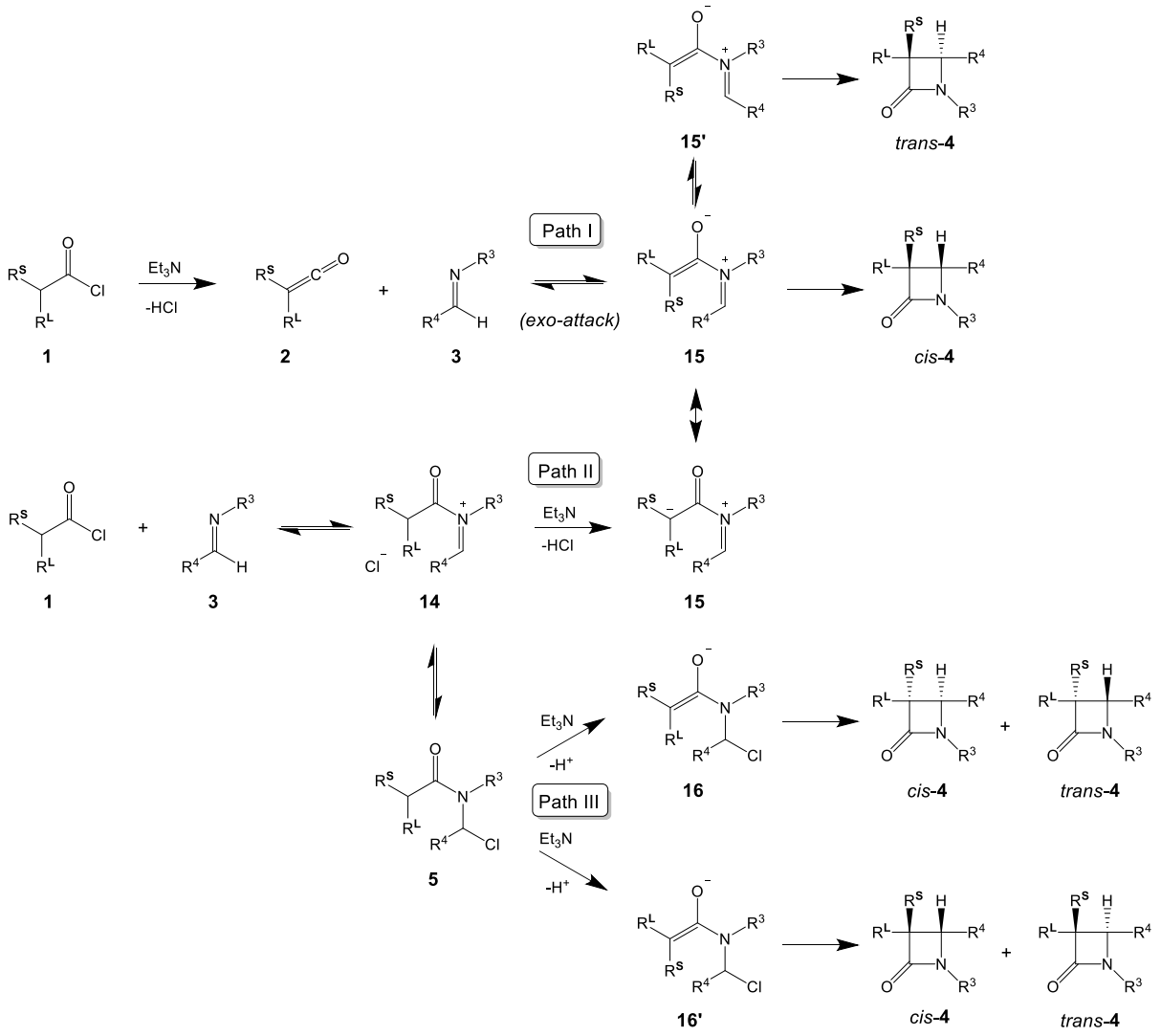


**Scheme 13**: Overview of the three reaction paths, responsible for the formation of β-lactams **4** starting from acid chlorides **1** and imines **3**. Note that for Path I only the case for *exo*-attack is drawn. The structures formed after *endo*-attack are included in **Scheme 9**.

## 2.3 Recent Advances: increasing Reactivity via mechanochemical Activation, a computational Analysis

Chemical reactions are associated with an activation barrier that needs to be overcome. Addition of energy to a reaction can assist the system to get over this barrier more easily, hence decreasing the duration of syntheses. This energy can come in different forms, such as heat, irradiation or mechanical energy. The first step in the Staudinger β-lactam synthesis, that is the nucleophilic addition of the imine to the ketene, is mostly a low-energy reversible process. [25] The conrotatory ring-closure of the zwitterionic intermediate however is the rate-limiting irreversible step that needs to be activated if shorter reaction times are desired. Many concepts have been developed to enhance the reactivity of imines with ketenes, including microwave- and photochemical-induced methods. [9], [33]–[36] Until now, less attention has been given to mechanochemical activation in the Staudinger β-lactam synthesis. [37], [38] Yet, some experimental work reported that ultrasonication methods provided shorter reaction times and higher β-lactam yields. [39] Where chromophores are capable of transforming light energy into electronic excitations, mechanophores can convert mechanical energy into force. [40] The mechanochemical ring opening of β-lactams has been investigated and it was demonstrated that a β-lactam ring is indeed a mechanophore capable of undergoing a mechanically activated cycloelimination reaction (**Figure 3**). [41] The force-assisted synthesis of β-lactams on the other hand has not been investigated computationally up until recently by Menéndez et al. [42]

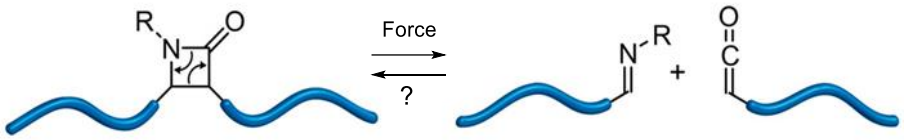


**Figure 3**: Force-assisted cycloelimination of β-lactams.

This force-assisted synthesis can be explained as follows. During the Staudinger β-lactam synthesis, the double bond in the imine reactant is converted into a single bond in the β-lactam product (red bonds in **Figure 4**), so Menéndez and coworkers suggested that specific mechanical activation leading to the weakening of that particular strong bond in the reactant species could accelerate β-lactam formation.

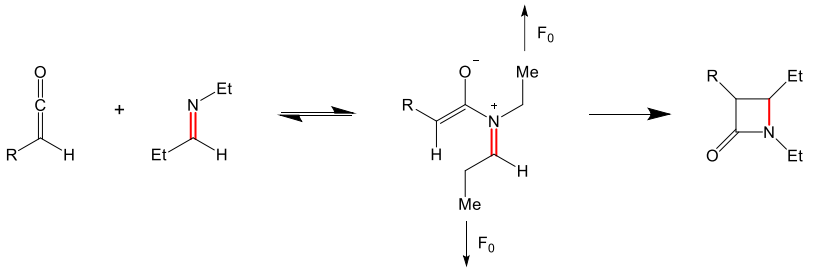


**Figure 4**: Force-assisted synthesis of β-lactams from ketenes and imines.

A computational technique was used that resembles atomic force microscopy (AFM) [37], where force versus extension curves are measured by pulling apart chain molecules which are anchored both at the tip and to a support surface. Theoretically, this is mimicked by imposing a distance constraint $q(\mathbf{x}) = |\mathbf{x_i} - \mathbf{x_j}|$ connecting two atoms at positions $\mathbf{x_i}$ and $\mathbf{x_j}$ and minimizing equation 1.

$$V_{COGEF}(\mathbf{x}, q) = V_{BO}(\mathbf{x}) - \lambda(q(\mathbf{x}) - q_0) \qquad \textit{Eq. 1}$$

Here, $V_{BO}(\mathbf{x})$ is the ground-state Born-Oppenheimer potential energy surface (PES), $q_0$ is the control parameter and $\lambda$ is a Lagrange multiplier. This constrained minimization yields the "COnstrained Geometries simulate External Force" potential $V_{COGEF}(q_0)$ as a function of $q_0$, the distorted molecular structures $\mathbf{x}_0(q_0)$ and the force/extension curves $F(q_0)$. Analogically, the changes in the PES can be simulated as a function of the external force $F_0$ directly when $F_0$ is taken as the control parameter rather than a structural constraint $q_0$. An exact, fully nonlinear and self-consistent approach can be formulated by applying the external force directly on the respective atoms and minimizing equation 2 with respect to $\mathbf{x}$ by structure optimization.

$$V_{EFEI}(\mathbf{x}, F_0) = V_{BO}(\mathbf{x}) - F_0 q(\mathbf{x}) \qquad \textit{Eq. 2}$$

At stationarity, $\nabla_x V_{EFEI}(\mathbf{x}_0, F_0)|_{F_0} = 0$ and the external force $F_0$ cancels out the internal force $F = -\nabla_q V_{BO}(\mathbf{x}_0)$ at the determined minimum $\mathbf{x}_0$ and $q(\mathbf{x}_0) = q_0$ is obtained. This technique, in which the "External Force is Explicitly Included" (EFEI), yields the exact distortion of the molecular structure $\mathbf{x}_0(F_0)$ as a function of the external force $F_0$. It can be shown that $V_{EFEI}(F_0)$ is the Legendre transform of $V_{COGEF}(q_0)$ at stationarity.

$$V_{EFEI}(F_0) = V_{COGEF}(q_0) - F_0 q_0 \qquad \textit{Eq. 3}$$

Furthermore, $V_{EFEI}(\mathbf{x},F_0)$ is the correct force-transformed Born-Oppenheimer PES and $\mathbf{x}_0(F_0)$ describes exactly the deformation of the molecular structure $\mathbf{x}_0$ as a function of a specified external force $F_0$. This way, properties such as reactant and transition state structures or activation energies can be evaluated as a function of $F_0$, without invoking any approximation. [40]

The stereochemistry of β-lactam products is an important issue for the Staudinger β-lactam synthesis. Therefore, when activation methods such as sonication techniques are used to increase reactivity of the system, stereoselectivity should be preserved as much as possible. To tackle this topic, Menéndez et al. [42] calculated the free activation energies for the *endo*- and *exo*-pathways of diethylimine **39** with two different monosubstituted ketenes **40** and **43**. (**Scheme 14**) Varying tensile forces ($F_0$), ranging from 0 nN up to 4.0 nN, were applied on the methyl-terminals of the imine moieties in **41** and **44**, using the isotensional EFEI computational approach. [40] Structure optimizations were performed at the B3LYP/TZVP level of theory and the PCM solvent model was used to represent a dichloromethane solution.

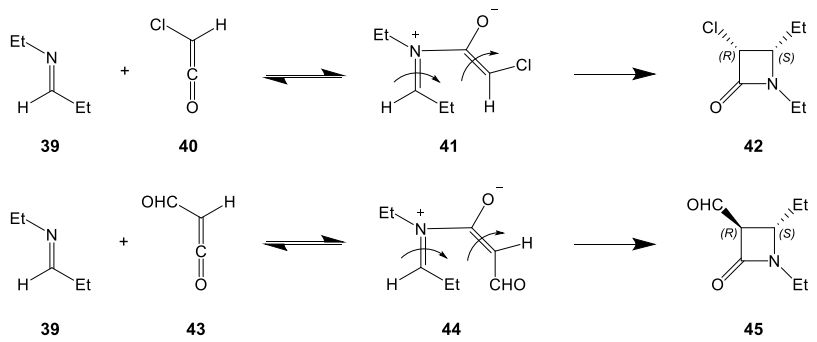


**Scheme 14**: Reaction of diethylimine **39** with ketenes **40** and **43**, modelled in the computational study of Menéndez et al. [42]

The second step in **Scheme 14** is the rate-limiting irreversible step where the torque-electronic rules dictate the stereoselectivity. [43] The electronic character of the ketene substituent and the substituent on the C-terminus of the imine determine if clockwise or counterclockwise rotation is preferred for cyclization of **41** and **44**. [44] A π-electron-donating group like chlorine tends to place itself on the outside during the final ring-closing step of **41** to minimize repulsive filled-filled orbital interactions between the donor orbital of the enolate system and the σ-orbital of the partially formed C3-C4 σ-bond. In contrast, π-electron-accepting groups such as formyl rather prefer the inside position in **44** to maximize favorable overlap of the empty π* orbital of the formyl substituent and the HOMO of the partially formed C3-C4 bond.

Indeed, in the absence of tensile forces, Menéndez and coworkers found that chloroketene **40** preferred the *exo*-attack over the *endo*-attack by 50.2 kJ/mol and for formylketene, *endo*-attack was favored by 2.1 kJ/mol. When tensile forces were applied with increasing steps of 0.1 nN, they observed that the preference for the *exo*- and *endo*-pathways for chloro- and formylketene respectively, remained the same for every amount of external force, meaning that torque-selectivity is not affected by the applied tensile forces. Furthermore, for tensile forces larger than 1.4 nN, a continuous decrease of the free energy barriers was obtained up until the breaking point of the imine chain at 3.9 nN. The key conclusion of this computational study is that mechanochemical activation can be applied to obtain the desired reactivity, while keeping the stereoselectivity of the Staudinger β-lactam synthesis unchanged.

## 2.4 Conclusion

This chapter gave an overview of the possible mechanisms occurring in the Staudinger β-lactam synthesis when dehydrohalogenation of acid chlorides by a base is used as a method for *in situ* generation of ketenes. There was an emphasis on studies tackling the stereoselectivity in the Staudinger β-lactam synthesis since the final stereochemistry can explain a lot about the paths that were favored during reaction. Many models developed to predict stereochemistry are based on the conrotatory cyclization of the zwitterionic intermediates formed by addition of imines onto ketenes. However, in many cases this conventional depiction of the Staudinger β-lactam synthesis does not satisfy experimental observations. A considerable portion of the reactivity can be induced by the direct acylation of imines and the subsequent formation of intermediate *N*-(chloromethyl)amides.

# Chapter 3

# Computational Part

## 3.1 Theoretical Introduction to DFT

### 3.1.1 A brief History in molecular Physics

The scientific progress during the first half of the 20th century was characterized by our fundamental understanding of nature and the development of quantum mechanics. At that time it was believed that the atom was comprised of electrons embedded in a homogeneous distribution of positive charge. However, this model was not able to describe scattering experiments with alpha-particles by golden foil. [45] In 1911 Rutherford came up with a new model. Most of the atomic mass was concentrated at the core of the atom which carried the positive charge and was very small compared to the dimensions of the atom. Electrons moved around this 'nucleus' in planetary orbitals, much like a miniature solar system. Rutherford was able to describe the scattering experiments but his model failed drastically on other fronts. There was a lack of atom stability due to the attractive Coulomb force and it was impossible to verify the spectral lines emitted by atoms. Two years later, in 1913, Niels Bohr managed to describe the latter. [46] He postulated that the orbital momenta of the electrons are 'quantized' and electrons can make transitions between these quantized orbitals, leading to the observed spectral lines of the H atom. However, his model had some major shortcomings, as it was only able to reproduce the spectrum of atomic species with one electron (H, $He^{+}$, $Li^{2+}$) and failed otherwise.

In 1926, Erwin Schrödinger paved the road for future physicists and theoretical chemists with his famous equation and thereby created a mathematical framework to describe the wavelike character of matter. [47] This lead to a deeper understanding in the fundamental nature of the chemical bond and chemistry in general.

$$i\hbar\frac{\delta}{\delta t}\psi(r,t) = \left[\frac{-\hbar^2}{2m}\nabla^2 + V(r,t)\right]\psi(r,t) \qquad \textit{Eq. 4}$$

Equation 4 shows the time-dependent Schrödinger equation for a non-relativistic particle subjected to an external potential V(r,t). From this the time independent Schrödinger equation can be derived for a bound particle where $\psi_n(r)$ are the eigenfunctions, also called stationary states, corresponding to discrete eigenvalues $E_n$ (equation 5). This discretization is a consequence of the boundary conditions implied upon the particle and the solution to this eigenvalue equation is a set of standing waves.

$$\left[\frac{-\hbar^2}{2m}\nabla^2 + V(r)\right]\psi_n(r) = E_n\psi_n(r) \qquad \textit{Eq. 5}$$

The left term in equation 5 represents a hermitic operator which acts upon the wavefunction and thereby computes the quantized energy levels $E_n$ associated with every stationary state $\psi_n(r)$. In terms of atoms and molecules the Schrödinger equation can be rewritten as shown in equation 6 and 7.

$$\left[\hat{T}_N + \hat{T}_e + \hat{V}_{NN} + \hat{V}_{Ne} + \hat{V}_{ee}\right]\psi_n(r) = E_n\,\psi_n(r) \qquad \textit{Eq. 6}$$

$$\hat{H}\,\psi_n(r) = E_n\,\psi_n(r) \qquad \textit{Eq. 7}$$

$\hat{H}$ in equation 7 is called the molecular Hamiltonian operator and consists of 5 terms: $T_N$ and $T_e$ represent the kinetic energy of the nuclei and the electrons respectively. The Coulomb potential energies are represented by $V_{NN}$ : between the nuclei reciprocally, $V_{Ne}$ : between nuclei and electrons and $V_{ee}$ : between electrons reciprocally.

### 3.1.2 Born-Oppenheimer Approximation

For computational purposes, Max Born and J. Robert Oppenheimer developed a flow scheme to solve molecular problems based on some assumptions since it is impossible to find an exact analytical solution for the molecular Schrödinger equation. [48] Their methodology, called the Born-Oppenheimer approximation (BOA), is one of the founding principles for computational chemistry.

The mass of the nuclei is several orders of magnitude larger than the mass of the electrons while their momenta are similar. This means that on the timescale of the nuclear motion, electrons almost instantaneously relax to their ground state. Hence, the BOA assumes that the nuclei are stationary point-particles and therefore $T_N$ can be neglected for computations involving electronic motion. Basically, the BOA implies that the motion of electrons does not depend on the motion of the nuclei and vice versa. Obviously, this is not the case in reality. In mathematical terms, the BOA translates to expressing the total wavefunction $\psi(r_i,R_\alpha)$ of a

molecule as the product of the electronic wavefunction $\varphi(r_i,R_\alpha)$ and the nuclear wavefunction $\chi(R_\alpha)$. In equation 8, $r_i$ and $R_\alpha$ refer to the spatial coordinates of electron i and nucleus α respectively.

$$\psi(r_i, R_\alpha) \overset{BOA}{\Longleftrightarrow} \varphi(r_i, R_\alpha)\, \chi(R_\alpha) \qquad \textit{Eq. 8}$$

Consequently, the molecular Hamiltonian operator $\hat{H}$ can be separated into the electronic and the nuclear Hamiltonian where the former still depends parametrically on the nuclear positions $R_\alpha$.

$$\widehat{H}_{elec}(r_i, R_\alpha)\, \varphi_n(r_i, R_\alpha) = U_n(R_\alpha)\, \varphi_n(r_i, R_\alpha) \qquad \textit{Eq. 9}$$

$$\left(\hat{T}_N + U_n(R_\alpha)\right) \chi_{nm}(R_\alpha) = E_{nm}\chi_{nm}(R_\alpha) \qquad \textit{Eq. 10}$$

Starting from an initial set of nuclear coordinates $R_\alpha$ the electronic Schrödinger equation is solved. An electronic surface is constructed by varying the nuclear positions $R_\alpha$ and each electronic eigenvalue $U_n$ will give rise to what is called a Born-Oppenheimer surface. On these surfaces the nuclear Schrödinger equation can be solved, yielding a set of vibrational and rotational energy levels $E_{nm}$ (indicated with index n and m in equation 10). In order to minimize the energy, the nuclei are moved until convergence is reached, resulting in a self-consistent solution of the coupled equations.

### 3.1.3 Hartree-Fock

The electronic Hamiltonian (equation 11) is comprised of three terms. The first one is the sum of the kinetic energies of the electrons, the second one represents the electron-nuclei Coulomb interaction and the last term represents the potential energy between electrons reciprocally. The former two terms do not depend on the positions of other electrons while the last term does and is thus called 'non-seperable'. The location and hence the charge of an electron is not fixed at a specific position, but rather smeared out over space. Therefore, there is no convenient way to compute the repulsive interaction between electrons and approximating techniques are required to solve the electronic Schrödinger equation.

$$\widehat{H}_{elec} = \sum_i -\frac{\nabla_i^2}{2} - \sum_i \sum_\alpha \frac{Z_\alpha}{r_{i\alpha}} + \sum_i \sum_j \frac{1}{r_{ij}} \qquad \textit{Eq. 11}$$

In 1928, Douglas Hartree published a set of equations aiming to compute many-electron systems in a self-consistent field, which were later generalized by Vladimir Fock to include exchange phenomena between two electrons. [49], [50] This method is known as the Hartree-Fock (HF) approximation and plays a pivotal role in many quantum computational methods up to this day, including DFT. Firstly, the BOA is inherently assumed and relativistic effects are completely neglected. In order to treat the non-separable term of the electronic Hamiltonian (Equation 11) as a one-particle operator, the interaction of electron i with all electrons in the system is averaged over a 'mean field'. To meet the requirements for a many-body electronic wavefunction which correctly treats the statistics of fermions, the Slater determinant was introduced as an approximation for the electronic wavefunction. [51] This is a normalized product of one-electron wavefunctions which satisfies the anti-symmetry requirement for electrons. The variational principle is applied to obtain a solution for the eigenvalue equation. This solution is a linear combination of a finite and complete set of orthogonal functions, called basis functions. Equation 12 shows the Slater determinant $\phi$ for a N-electron system where $\psi_i$ represent one-electron spin-orbitals and $x_i$ the spatial and spin coordinates.

$$\phi(x_1, x_2, \dots, x_N) = \frac{1}{\sqrt{N!}} \begin{vmatrix} \psi_1(x_1) & \cdots & \psi_N(x_1) \\ \vdots & \ddots & \vdots \\ \psi_1(x_N) & \cdots & \psi_N(x_N) \end{vmatrix} \qquad \textit{Eq. 12}$$

The energy of the Slater determinant (Equation 13) is given by the usual quantum mechanical expression applying the 'bra-ket' notation.

$$E_{Sl}(\phi) = \langle \phi | \hat{H}_{elec} | \phi \rangle \qquad \textit{Eq. 13}$$

After a lengthy evaluation of equation 13, this expression can be rewritten in terms of integrals of one- and two-electron operators.

$$E_{Sl}(\phi) = \sum_{j=i+1}^{N} \langle \psi_i \left| \hat{h} \right| \psi_i \rangle + \sum_{i=1}^{N-1} \sum_{j=i+1}^{N} (J_{ij} - K_{ij}) \qquad \textit{Eq. 14}$$

$$J_{ij} = \langle \psi_i \psi_j | \hat{v}_{ee} | \psi_i \psi_j \rangle \qquad \textit{Eq. 15}$$

$$K_{ij} = \langle \psi_i \psi_j | \hat{v}_{ee} | \psi_j \psi_i \rangle \qquad \textit{Eq. 16}$$

The one-electron operator $\hat{h}$ or 'core Hamiltonian' is comprised of the kinetic energy and the electron-nuclei attraction energy. Evaluation of the Slater determinant with the two-electron operator yields two terms: $J_{ij}$, the Coulomb intergral and $K_{ij}$, the exchange intergral (Equation 15 and 16, respectively). The former represents the electrostatic repulsion potential and does not depend on the spin coordinate while $K_{ij}$ quantifies the exchange energy. The latter effect arises due to the wave function of indistinguishable particles being subject to exchange

symmetry and is related to the Pauli exclusion principle. [52] It is interpreted as the interaction between a given state and a second state in which the coordinates of two identical electrons are switched. Physically, $K_{ij}$ contributes to the energy when an electron (ex)changes position or spin in a molecule, while in the Coulomb integral $J_{ij}$ the electron always stays in the same orbital. Computing the actual Hartree-Fock energy $E_{HF}$ of a system is done using the variational theorem. This theorem states that $E_{Sl}(\phi)$ will always be higher than the true energy $E_0$ of a system. Hence, the best approximation for the wavefunction is found by varying the parameters of the basis functions until a Slater determinant is obtained whose energy is minimized.

$$E_0 \leq E_{HF} = \min_{\{\psi_i\}} E_{Sl}(\phi) \qquad \textit{Eq. 17}$$

The one-particle Hartree-Fock energy $\varepsilon^{HF}{}_{\alpha}$ (Equation 18) of orbital α is calculated using the Fock operator $\hat{f}$ (Equation 19). These expressions are required for implementation of the numerical solution method.

$$\varepsilon_{\alpha}^{HF} = \langle \psi_{\alpha} | \hat{f}(\{\psi_i\}_{i=1}^{N}; x) | \psi_{\alpha} \rangle \qquad \textit{Eq. 18}$$

$$\hat{f}(\{\psi_i\}_{i=1}^{N}; x) \equiv \hat{h}(r) + \hat{j}(\{\psi_i\}_{i=1}^{N}; r) - \hat{k}(\{\psi_i\}_{i=1}^{N}; x) \qquad \textit{Eq. 19}$$

In practice an iterative process is used to implement the Hartree-Fock method numerically, which is illustrated in **Figure 6**.

### 3.1.4 Post Hartree-Fock

Due to all the approximations introduced in the HF method, there will always be a significant gap between the HF energy and the true energy of a system, which is always lower than $E^{HF}$. The collection of all the effects causing this deviation is termed electron correlation and is mainly attributed to the mean field approximation to describe repulsive electron interaction. In order to improve the HF method and obtain energies closer to the true energy, the electron correlation has to be included in some way. Therefore, a lot of post-HF methods have been developed with the aim to obtain more accurate approximations for the exact energy. A good example is the Møller-Plesset method which uses the Rayleigh-Schrödinger perturbation theory to add electron correlation. [53] Because of its relatively low computational

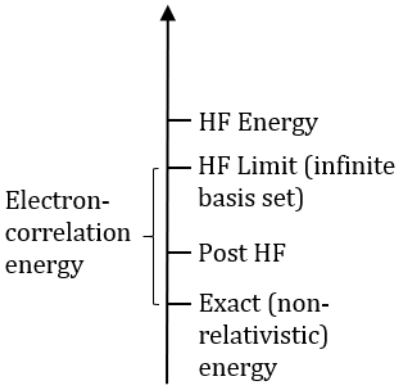


**Figure 5**: Electron correlation energy.

cost the MP theory is still widely used today as a reference method to benchmark new functionals for larger molecules. [54]

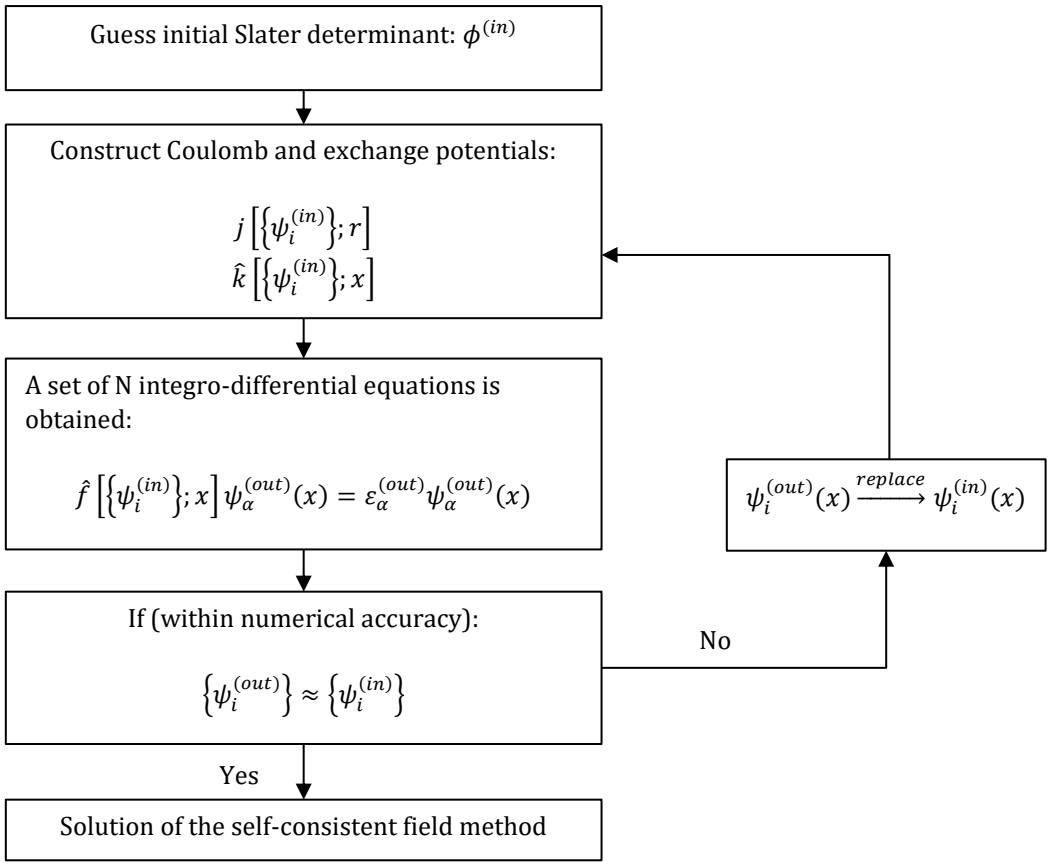


**Figure 6**: Iterative proces to solve Hartree-Fock equations.

### 3.1.5 Density Functional Theory (DFT)

Considerable progress was made in the field of computational chemistry during the second half of the 20th century. An increasing amount of papers dealt with the expansion of the HF-equations and the application of molecular orbital theory. In 1964 P. Hohenberg and W. Kohn published a paper which dealt with the ground state of an interacting electron gas in an external potential v(r). [55] They introduced two theorems later known as the foundation of DFT. Their first theorem (HK I) reads that the external potential v(r), and hence the total energy E(ρ), is a unique functional of the electron density ρ(r). Furthermore, it was proven that there exists a universal functional of the density F(ρ), independent of v(r), such that minimization of equation 20 yields the exact ground state energy of a system associated with

v(r). The latter statement is defined in the second Hohenberg-Kohn theorem (HK II) and provides a variational principle for the ground state electron density.

$$E(\rho) \equiv F(\rho) + \int v(r)\rho(r)dr \qquad \textit{Eq. 20}$$

The HK theorems show that the electron density can be used, instead of the wavefunction itself, as a variable to find any measurable of a N-electron system. However, they do not provide a computational scheme to solve such a problem and the difficulties in developing such a scheme are again related to the electron-electron interaction term in the Hamiltonian. One year after the publication of the HK theorems, W. Kohn and L. J. Sham released a paper tackling this difficulty. [56] They projected the interacting N-electron system onto a non-interacting reference system (Kohn-Sham system) whose ground-state wave-function can be described by a single Slater determinant. The resulting Kohn-Sham (K-S) equations are a set of N one-electron Schrödinger equations which are defined by a local fictious external potential $v_{eff}(r)$, also called the Kohn-Sham potential (Equation 21). The K-S potential $v_{eff}(r)$ is the potential associated with the non-interacting system which gives rise to the same electron density associated with the interacting system.

$$\left(-\frac{\hbar^2}{2m}\nabla^2 + v_{eff}(r)\right)\varphi_i(r) = \varepsilon_i\varphi_i(r) \qquad \textit{Eq. 21}$$

The K-S theory suggests that the exact electronic energy of a molecule can be expressed as the sum of 4 terms given in equation 22.

$$E(\rho) = T_S(\rho) + \int v(r)\rho(r)dr + J(\rho) + E_{xc}(\rho) \qquad \textit{Eq. 22}$$

$T_S(\rho)$ is the kinetic energy of the non-interacting electrons, the second term is the attractive electron-nuclei potential energy, $J(\rho)$ is the classical electron-electron Coulomb energy and $E_{xc}(\rho)$ represents the exchange-correlation energy, which is a correction term for the errors introduced by $T_s(\rho)$ and $J(\rho)$.

$$E_{xc}(\rho) = T(\rho) - T_S(\rho) + V_{ee}(\rho) - J(\rho) \qquad \textit{Eq. 23}$$

$T(\rho)$ and $V_{ee}(\rho)$ in equation 23 represent the exact kinetic and potential energy of the interacting system and therefore, equation 22 ensures that $E(\rho)$ is the true energy of the interacting system but expressed as if it were a non-interacting system. The aim for a good DFT method is thus to find a good approximation for $E_{xc}$. Again, numerical implementation in practice is done using an iterative process, shown in **Figure 7**.

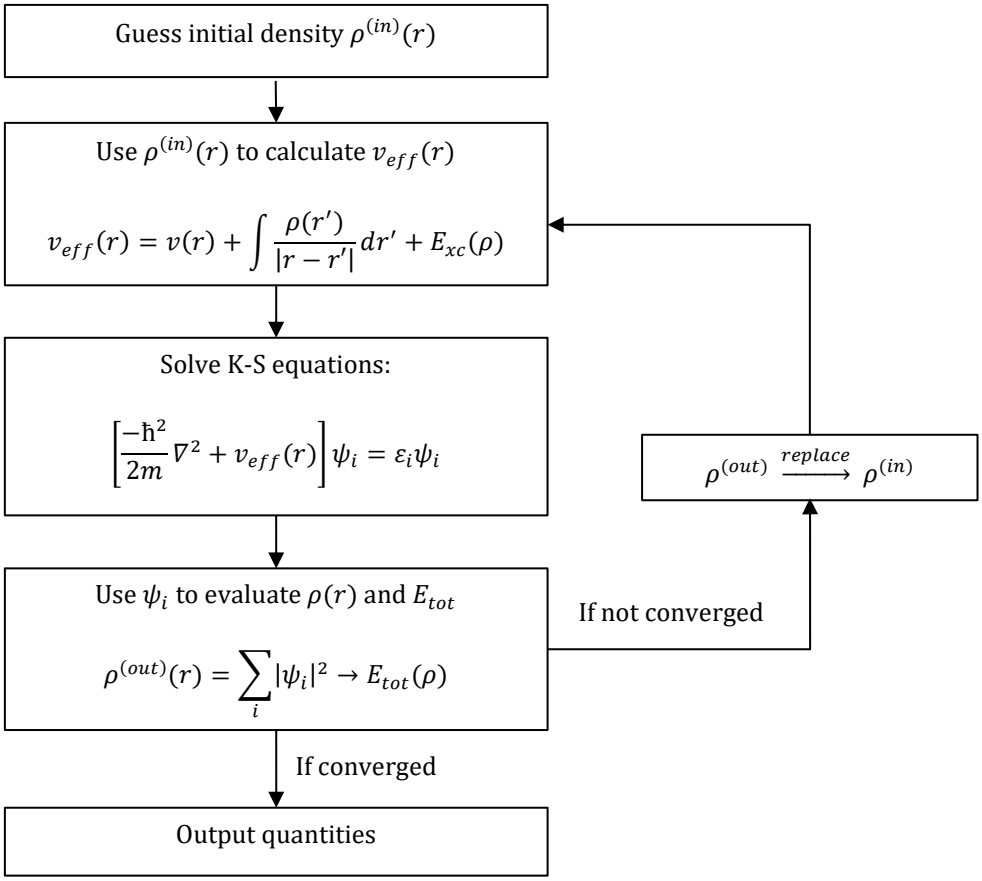


**Figure 7**: Iterative process to solve Kohn-Sham equations.

## 3.2 Computational Methodology

### 3.2.1 Calculation and Construction of Gibbs free Energy Profiles

All calculations will be performed using the Gaussian 16 package. Transition-, reactant - and product states will be identified via frequency analysis. Transition states are first order saddle points on the potential energy surface (PES) characterized by exactly one imaginary frequency. Product and reactant states are minima on the PES and are identified by frequencies which are all positive. Thorough conformational analyses will be performed to ensure that intermediate -, reactant -, product- and transition states are in the lowest energy conformation. Pre- and post-reactive complexes will be identified via IRC calculations. [57] This type of calculation follows a reaction path in the forward and reverse direction starting from an initial transition state structure by integrating the intrinsic reaction coordinate.

Gibbs free energies are always reported with respect to a certain reference. Since this thesis deals with multiple reaction paths which will be visualized in the same Gibbs free energy profile, an appropriate reference is required to construct these profiles. The best option is to use the combined Gibbs free energies of the separate reactants as the reference value. In order to maintain the same atom balance within one specific profile, intermediates that are not participating in certain reaction steps have to be included in the Gibbs free energy value associated with that particular step. An example is presented in **Figure 8**. Consider a hypothetical reaction mixture, containing three solutes A, B and C. The following two consecutive reactions are known to occur:

$$A + B \xrightarrow[-X]{} Y \xrightarrow[+C]{} Z$$

In a first step, reactants A and B combine with the formation of intermediate products X and Y. In a following step, intermediate product Y reacts with component C yielding final product Z. In this case the seperate reactants are A, B and C and thus the reference value is given by equation 24.

$$G_{REF} = G_A + G_B + G_C \qquad Eq.\ 24$$

Take now for example the final product Z, equation 25 is used to calculate the Gibbs free energy difference of Z with respect to the separate reactants, while taking into account the prior formation of intermediate X in order to maintain the correct atom balance.

$$\Delta G_Z = G_Z + G_X - G_{REF} \qquad Eq.\ 25$$

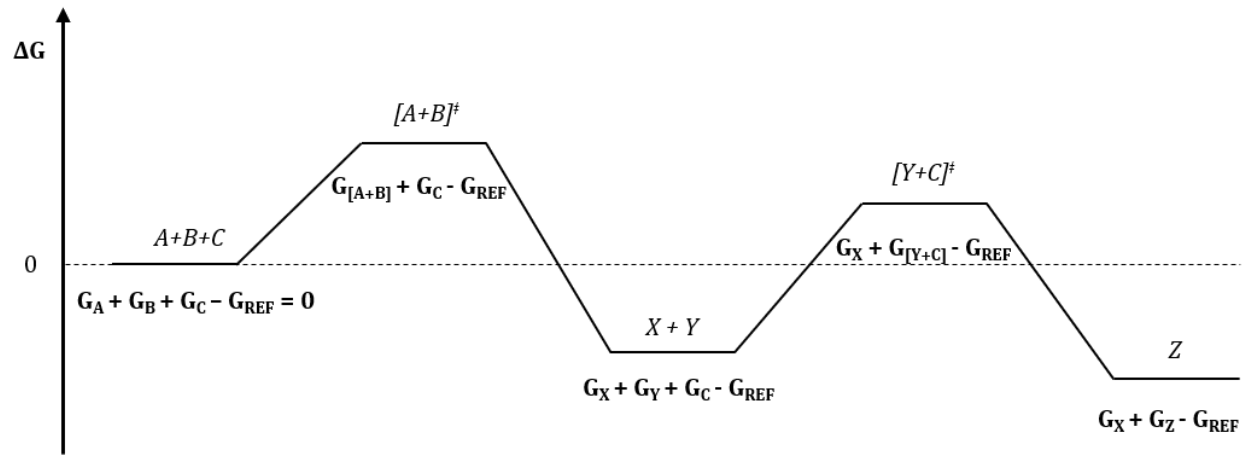


**Figure 8**: Gibbs free energy profile for the consecutive reactions A+B → X+Y and C+Y → Z with respect to the seperate reactants A, B and C.

### 3.2.2 Functionals and Basis Set

The hybrid functional B3LYP was used as the main method to report free energies. This functional combines Becke's exchange correlation functional (B3), which uses 3 parameters to mix in the exact Hartree-Fock exchange correlation, with the Lee Yang and Parr correlation functional (LYP) that recovers dynamic electron correlation. [58]–[61] Becke's original paper is one of the most cited papers of all time [54], which indicates how well established this method is among theoretical chemists. It's popularity is due to many reasons. It's fairly robust for a DFT method and consistently scores above average in studies benchmarking functionals for small and medium sized organic molecules. [62]–[64] Because it is not as heavily parameterized compared to other functionals, it performs generally faster than most other post Hartree-Fock methods, while yielding comparable results. A major drawback is the insufficient treatment of London dispersion interactions. [65], [66] Therefore the D3 version of Grimme's dispersion correction was included. [67]

Two extra functionals, ωB97XD and M06-2X, will be used for single-point energy calculations on the geometries obtained by B3LYP-D3 in order to validate the reported data. ωB97XD is a more recently developed functional which includes empirical dispersion. [68] M06-2X is part of the Minnesota group of functionals and performs well for main group thermochemistry, kinetics and non-covalent interactions. [69] All the functionals used are easily accessible in the Gaussian software package. The 6-311+G(d,p) basis set was chosen for all calculations. This is a split-valence triple-zeta basis with additional polarization and diffuse functions. [70], [71] Despite the relatively large size of the basis set, the duration of the computations were acceptable.

### 3.2.3 Thermochemistry

Throughout this computational study, Gibbs free energy differences ΔG associated with chemical reactions will be reported. The sign and magnitude of ΔG provide the chemist with information about the direction and speed in which a system will evolve. The general expression for G is given in equation 26.

$$G = H - TS \qquad Eq.\ 26$$

The entropy S is a measure for the disorder of a system and the enthalpy H is related to the internal energy U of a system via equation 27.

$$H = U + RT \qquad \textit{Eq. 27}$$

The internal energy of a system U is the result of four different contributions related to translation, electronic motion, rotational motion and vibrational motion. The principles of statistical physics can be applied to relate microscopic molecular quantities to the macroscopic quantities presented in equation 26 and 27. For each contribution i, the partition function $q_i$ can be derived which in turn can be used to calculate macroscopic quantities. The following equations are used in the Gaussian software to compute entropy $S_i$, internal thermal energy $E_i$ and heat capacity $C_{V,i}$ for each contribution i. [72]

$$S_i = R + R\ln\big(q_i(V,T)\big) + RT\left(\frac{\partial \ln q_i}{\partial T}\right)_V \qquad \textit{Eq. 28}$$

$$E_i = Nk_BT^2\left(\frac{\partial \ln q_i}{\partial T}\right)_V \qquad \textit{Eq. 29}$$

$$C_{V,i} = \left(\frac{\partial E_i}{\partial T}\right)_{N,V} \qquad \textit{Eq. 30}$$

Next the total entropy S and the internal energy U of the system can be derived. The term ZPVE in equation 32 refers to the zero-point vibrational energy which is the energy resulting from vibrational motion at 0 K.

$$S_{tot} = S_{trans} + S_{elec} + S_{rot} + S_{vibr} \qquad \textit{Eq. 31}$$

$$U = E_{trans} + E_{elec} + E_{rot} + E_{vibr} + ZPVE \qquad \textit{Eq. 32}$$

From this follows the Gibbs free energy and Gaussian predicts by default thermochemical values for 298,15 K and 1 atm.

### 3.2.4 Solvent Model

When dealing with the Staudinger β-lactam synthesis, a lot of polarized and ionized species appear on the reaction paths. Thus, it is of utmost importance to include possible stabilizing solvation effects in the calculations. Adding solvent molecules explicitly to the model would substantially increase the computational cost. Whether or not solvent molecules actively take part in the mechanisms under investigation might be subject for further investigation, but within the scope of this study it is assumed that this does not happen. Therefore, only stabilizing effects are accounted for by means of an implicit solvent model which is computationally less expensive than an explicit model. The Polarizable Continuum Model

using the Integral Equation Formalism (IEFPCM) was applied for all calculations. [73]–[75] This method places the solute in a cavity created by a set of overlapping spheres. This way a surrounding continuous medium is obtained, which is mainly characterized by the dielectric constant of the solvent.

## 3.3 Results

The subject of this theoretical study was the unexpected behavior concerning the reaction of 2,2-dichloroacetyl chloride with *(S)*-1-(2,2-dimethyl-1,3-dioxolan-4-yl)-*N*-(4-methoxyphenyl)methanimine in the presence of triethylamine. Usually, the applied method easily yields substituted β-lactams. However, upon applying the same conditions which are customary for the Staudinger β-lactam synthesis, the former reaction did not yield the desired β-lactam structure. **Scheme 15** presents a generalized overview of the reactions that will be investigated. The Staudinger Path pertains to the conventional mechanisms that govern the Staudinger β-lactam synthesis where β-lactams **4** are formed via reaction of acid chlorides **1** with imines **3** in the presence of a base. The Chloro-amide Path follows the direct acylation of imines **3** yielding *N*-(chloromethyl)amides **5**. An alternative ring-closure mechanism where β-lactams **4** are obtained from *N*-(chloromethyl)amides **5** by the action of a base will also be discussed briefly.

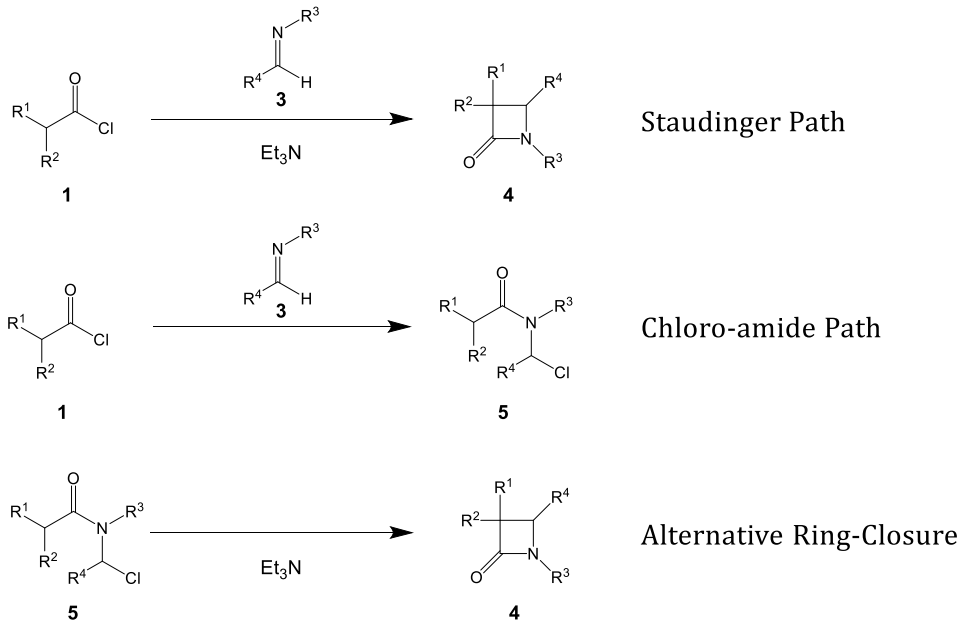


**Scheme 15**: Generalized overview of the reaction paths under investigation in this thesis.

## 3.3.1 Preliminary Study

In order to quickly identify the key intermediates and transition states, specific to the Staudinger β-lactam synthesis, and the proposed mechanisms responsible for the unexpectedly formed sideproducts, preliminary calculations were performed with *N*-methylethanimine **47** as the starting reactant. In this section the schemes and profiles will be presented individually for each path. Later, when the main results are discussed, these profiles will be combined, which will make it easier to compare the results obtained for different paths. Also, isomerization of the imine double bond (vide supra) will not be taken into account in this thesis. Therefore, all imine moieties of intermediates appearing on the following schemes are drawn in the (*E*)-configuration.

### 3.3.1.1 Staudinger Path

**Scheme 16** gives a mechanistic overview of the Staudinger Path for 2,2-dichloroacetyl chloride **8** and *N*-methylethanimine **47**.

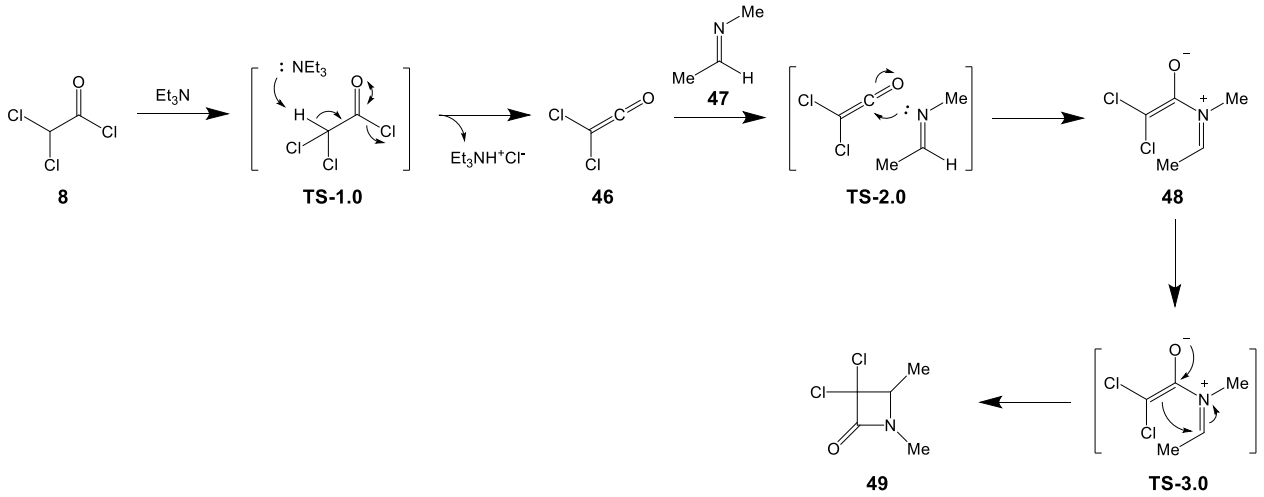


**Scheme 16:** Staudinger Path for the synthesis of 3,3-dichloro-1,4-dimethylazetidin-2-one **49** via [2+2]-cyclocondensation of 2,2-dichloroacetyl chloride **8** and *N*-methylethanimine **47**.

Three steps are required to obtain 3,3-dichloro-1,4-dimethylazetidin-2-one **49**. Firstly, 2,2-dichloroacetyl chloride **8** is converted to the corresponding ketene **46** by the action of triethylamine (**TS-1.0**). Addition of *N*-methylethanimine **47** onto the newly generated ketene produces zwitterionic intermediate **48** via **TS-2.0**. In the final step the zwitterionic intermediate **48** closes in a conrotatory fashion (**TS-3.0**), leading to 3,3-dichloro-1,4-dimethylazetidin-2-one **49**. The Gibbs free energies corresponding to **Scheme 16** are

visualized in **Profile 1**. The intrinsic barrier associated with **TS-1.0** amounts to 34.3 kJ/mol. This is followed by the expulsion of chloride from the post reactive complex (**post-TS-1.0**, **Figure 9**) and subsequently dichloroketene **46** is generated. The reported free energy of dichloroketene **46** takes into account the formation of triethylammonium hydrochloride, a salt that embodies the most stable form of hydrogen chloride, given the reaction conditions applied during synthesis, and is the product of the dehydrohalogenation of 2,2-dichloroacetyl chloride **8** by triethylamine. Based on calculations at the B3LYP-D3/6-311+G(d,p) level of theory, formation of triethylammonium hydrochloride from triethylamine and hydrogen chloride has a Gibbs free energy difference of -58.9 kJ/mol and -82.7 kJ/mol associated with it for toluene (ε = 2.3741) and dichloromethane (ε = 8.93), respectively.

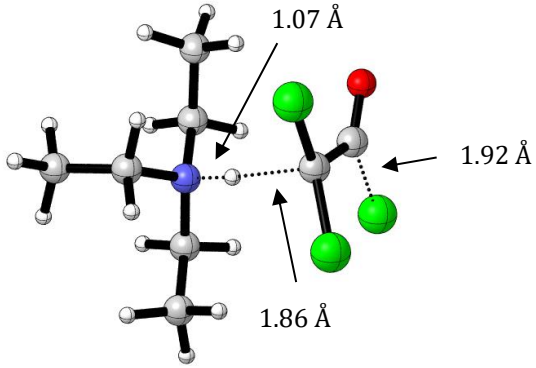


**Figure 9**: 3-D representation of **post-TS-1.0**, Level of theory: B3LYP-D3/6-311+g(d,p), IEFPCM: ε = 2,3741 (toluene).

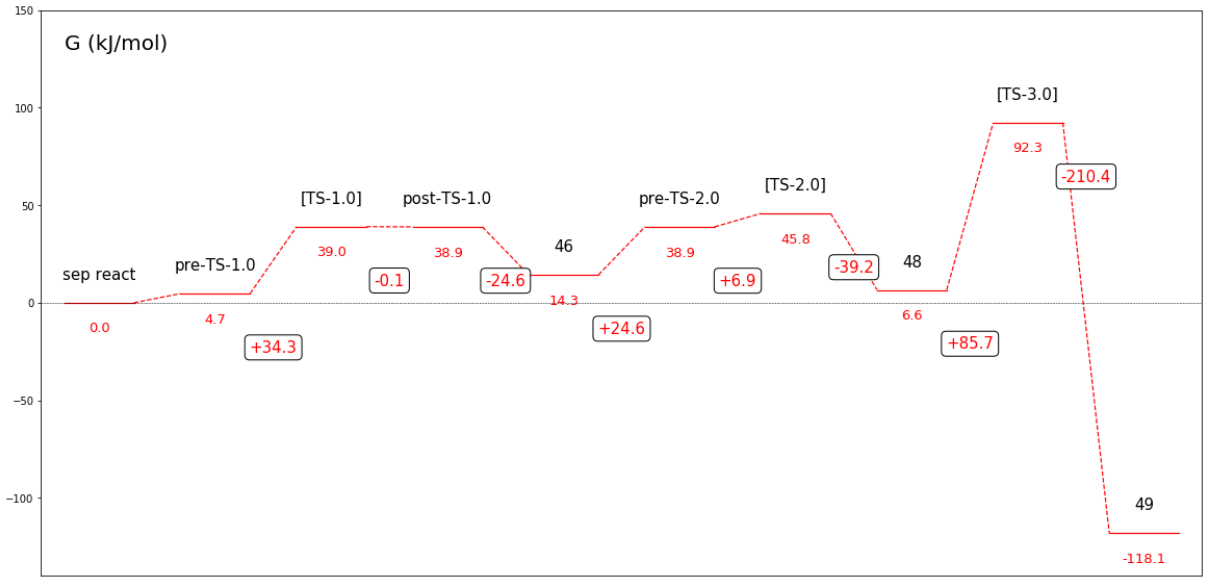


**Profile 1**: Gibbs free energies (kJ/mol) with respect to the separate reactants for the Staudinger Path of 2,2-dichloroacetyl chloride **8** and *N*-methylethanimine **47**. Dichloroketene **46** is generated via **TS-1.0**, ketene-imine addition occurs via **TS-2.0** and conrotatory cyclization of zwitterionic intermediate **48** occurs via **TS-3.0** yielding 3,3-dichloro-1,4-dimethylazetidin-2-one **49**. Level of theory: B3LYP-D3/6-311+G(d,p), IEFPCM: ε = 2,3741 (toluene).

We were unable to locate a transition state structure for **TS-2.0**, hence the given estimated value is derived from a structure which resembles what it should look like. This structure was obtained by performing a relaxed scan in zwitterionic intermediate **48** over the newly formed C-N bond. Next, the bond distance was fixed at a value of 2.52 Å and optimized to a transition state. The resulting structure had two imaginary frequencies (-148.2 and -75.0) and seemed like the best approximation since further calculations could not yield a structure with exactly one imaginary frequency. However, for the substituents of interest (vide infra) the ketene-imine addition transition states were correctly identified. The final barrier associated with the conrotatory ring-closure of **48** amounts to 85.7 kJ/mol and is therefore the rate-determining step in this path. The reverse barrier for **TS-3.0** is 210.4 kJ/mol and β-lactam **49** is thus 118.1 kJ/mol more stable than the separate reactants, which means that **49** is the thermodynamic product in this case.

### 3.3.1.2 Chloro-amide Path

A mechanistic overview of the Chloro-amide Path for 2,2-dichloroacetyl chloride **8** and *N*-methylethanimine **47** is given in **Scheme 17**. In the absence of a base, or when reactant addition happens prior to ketene generation, an iminium ion is formed through the direct acylation (**TS-4.0**) of imine **47** by acid chloride **8**. It would not be realistic to model the expelled chloride as a free anion since the Staudinger β-lactam synthesis is carried out in non-aqueous solvents such as toluene or dichloromethane. The newly generated iminium ion is the only positively charged specie present in the reaction mixture and is therefore modelled as a salt (**50**) with chloride as its counterion. Recombination of chloride at the C-terminus of the imine moiety in the iminium specie gives rise to stable adduct **51**. No transition state was found for the recombination, which could mean that the barrier associated with this reaction step is negligibly small or non-existing and hence occurs spontaneously.

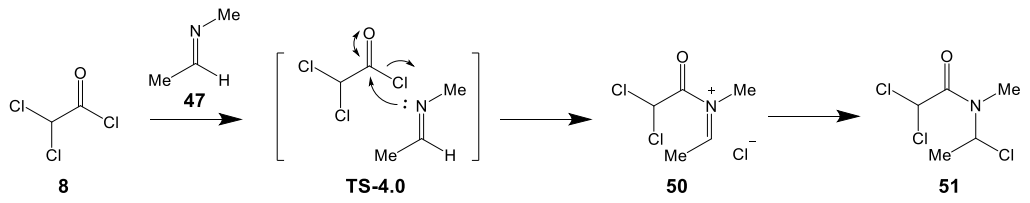


**Scheme 17**: Direct acylation via **TS-4.0** of *N*-methylethanimine **47** by 2,2-dichloroacetyl chloride **8** resulting in post-reactive complex **50** and subsequent recombination yielding *N*-(1-chloroethyl)amide **51**.

**Profile 2** presents the Gibbs free energies corresponding to the Chloro-amide Path for *N*-methylethanimine **47** and 2,2-dichloroacetyl chloride **8**. A forward barrier of 36.5 kJ/mol is obtained for the direct acylation step. Recombination of iminium salt **50** is favored, given the barrier of -84.3 kJ/mol, yielding the stable *N*-(1-chloroethyl)amide **51**.

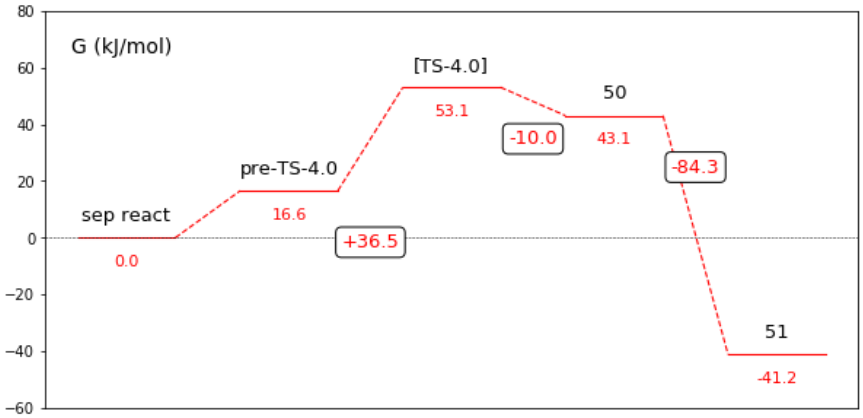


**Profile 2**: Gibbs free energies (kJ/mol) with respect to the separate reactants, for the direct acylation (Chloro-amide Path) of 2,2-dichloroacetyl chloride **8** and *N*-methylethanimine **47** yielding *N*-(1-chloroethyl)amide **51**. Level of theory: B3LYP-D3/6-311+G(d,p), IEFPCM: ε = 2,3741 (toluene).

### 3.3.1.3 Alternative Ring-Closure

An alternative ring-closure mechanism is often proposed in the literature to rationalize the preferential formation of *trans*-β-lactams when the addition of triethylamine to the reaction mixture is delayed. [22] The proposed mechanism, applied on *N*-(1-chloroethyl)amide **51**, is shown in **Scheme 18**. Deprotonation of *N*-(1-chloroethyl)amide **51** via **TS-5.0** yields anion **52** which forms 3,3-dichloro-1,4-dimethylazetidin-2-one **49** via a $S_N2$ displacement of chloride (**TS-6.0**).

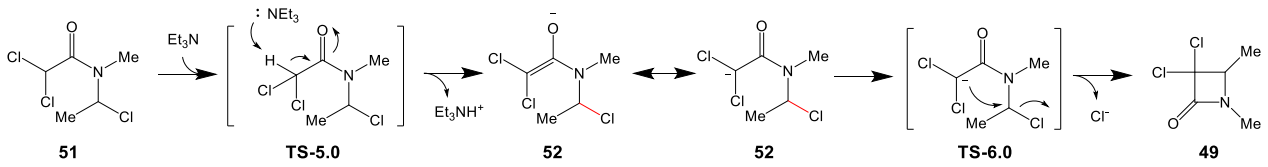


**Scheme 18**: Alternative ring-closure mechanism to obtain β-lactam **49** starting from *N*-(1-chloroethyl)amide **51**, depicted the way it was proposed in the literature. [22]

An attempt was made to model this path, but **TS-5.0** was not found for this imine substituent combination. In addition, anion **52** could not be identified as a stable intermediate due to the instability of the C-Cl bond (shown in red in **Scheme 18**). A transition state structure was found for **TS-6.0**, which is shown in **Figure 10** (middle). In order to obtain pre- and post-reactive complex, an IRC calculation was performed. The results are visualized in **Figure 10**. Anion **52** (**Scheme 18**) was not identified as the pre-reactive complex for **TS-6.0**. The C-Cl bond distance in **pre-TS-6.0** is 2.63 Å which is too high to be classified as a covalent bond (as a reference: this C-Cl bond distance in intermediate **51** is 1.87 Å). Also, the substituents at the C-terminus in **pre-TS-6.0** (indicated by * in **Figure 10**) are in a planar configuration, which indicates the presence of a double bond, thus confirming the absence of the C-Cl covalent bond (red bond in **Scheme 18**). A better representation of what is really happening in the simulation is shown in **Scheme 19**.

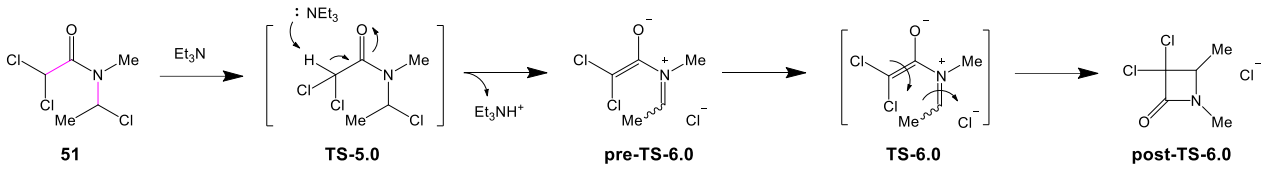


**Scheme 19**: Alternative ring-closure mechanism to obtain β-lactam **49** starting from *N*-(1-chloroethyl)amide **51**, depicted the way it was modelled at B3LYP-D3/6-311+G(d,p) level of theory. IEFPCM: ε = 2.3741 (toluene). Arrows in **TS-6.0** are used to indicate conrotatory torsion during cyclization.

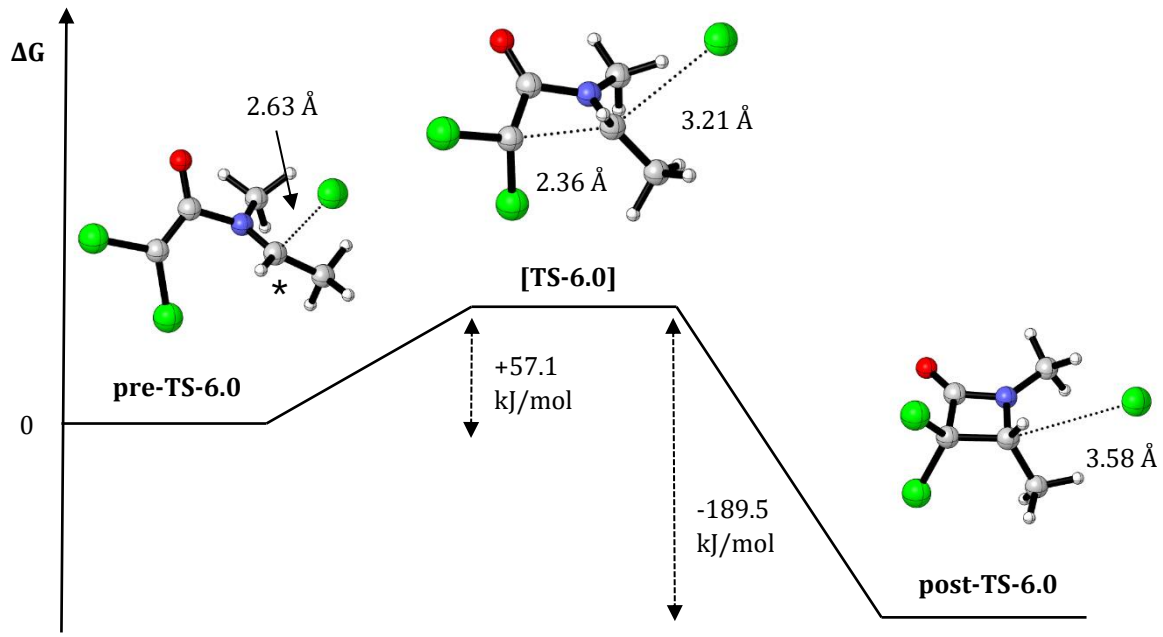


**Figure 10**: 3-D representation of **TS-6.0** and the pre- and post-reactive complex obtained by integrating the intrinsic reaction coordinate (IRC) and visualization of the Gibbs free energy barriers (not scaled). Level of theory: B3LYP-D3/6-311+G(d,p), IEFPCM: ε = 2.3741 (toluene).

When the enolate is formed via **TS-5.0** (**Scheme 18-19**), the formation of zwitterionic intermediate **pre-TS-6.0** (**Scheme 19**) via expulsion of chloride is favored over anionic intermediate **52** (**Scheme 18**). Furthermore, **TS-6.0** can be identified as a conrotatory cyclization yielding β-lactam as **post-TS-6.0** (**Scheme 19**). It should be stressed that **Scheme 19** is not a realistic depiction of what would happen in solution where the expelled chloride would form a salt with triethylammonium, but is used to clarify the simulated structures in **Figure 10**. Based on these results, one can assume that the alternative ring-closure mechanism, proposed in the literature to explain increased *trans*-selectivity, does not go via a $S_N2$ type reaction (**Scheme 18**), but via conrotatory cyclization of a zwitterionic intermediate which is formed spontaneously after delayed proton abstraction via **TS-5.0** (**Scheme 19**). The altered stereoselectivity can still be explained by the ability of *N*-(1-chloroethyl)amide **51** to rotate freely around the N1-C4 and C2-C3 bonds (pink bonds in **Scheme 19**) before they are converted to double bonds.

### 3.3.2 Main Results

The preliminary study was meant to identify the key intermediates and transition states which are of interest in this thesis. The goal of this section is to provide computational support for the unexpected behavior concerning the reaction of 2,2-dichloroacetyl chloride **8** with (*S*)-1-(2,2-dimethyl-1,3-dioxolan-4-yl)-*N*-(4-methoxyphenyl)methanimine **7a** (**Scheme 20**). The methyl groups of the imine discussed in the previous section are replaced by *para*-methoxyphenyl at the N-terminus and (*S*)-2,2-dimethyl-1,3-dioxolan-4-yl at the C-terminus, in correspondence to the experiment. [16], [17] The Gibbs free energy profiles are constructed for the Staudinger Path and the Chloro-amide Path. Toluene was the solvent of choice to include implicitly in the calculations but the effect of a more polar solvent, dichloromethane, is also discussed. Possible influences of different imine substituents will be investigated. The Staudinger and Chloro-amide Paths are also constructed for the reaction of (*S*)-1-(2,2-dimethyl-1,3-dioxolan-4-yl)-*N*-(4-methoxyphenyl)methanimine **7a** with the ketene derived from methoxyacetyl chloride. The choice of this ketene is based on in-house experiments where the Staudinger synthesis of this ketene with (*S*)-1-(2,2-dimethyl-1,3-dioxolan-4-yl)-*N*-(4-methoxyphenyl)methanimine did exhibit the expected formation of the corresponding β-lactam. [16]

### 3.3.2.1 Staudinger and Chloro-amide Paths

**Scheme 20** gives a mechanistic overview of the formation of *N*-(chloromethyl)amide **11a** via the Chloro-amide Path (**Scheme 20**, red) and β-lactam **9a** via the Staudinger Path (**Scheme 20**, blue). Experimentally, β-lactam **9a** could not be identified after work-up by NMR spectroscopy and it was assumed that this product was not produced at all during the reaction. Analysis of the NMR spectra lead to the observation of *N*-(chloromethyl)amide **11a** in 35% yield after purification and X-ray analysis showed that **11a** was only formed in the *(R)*-configuration. [16] Executing the same reaction in the absence of a base also yielded product **11a**, which confirms that triethylamine does not necessarily take part in the reaction path leading to amide **11a**. [17]

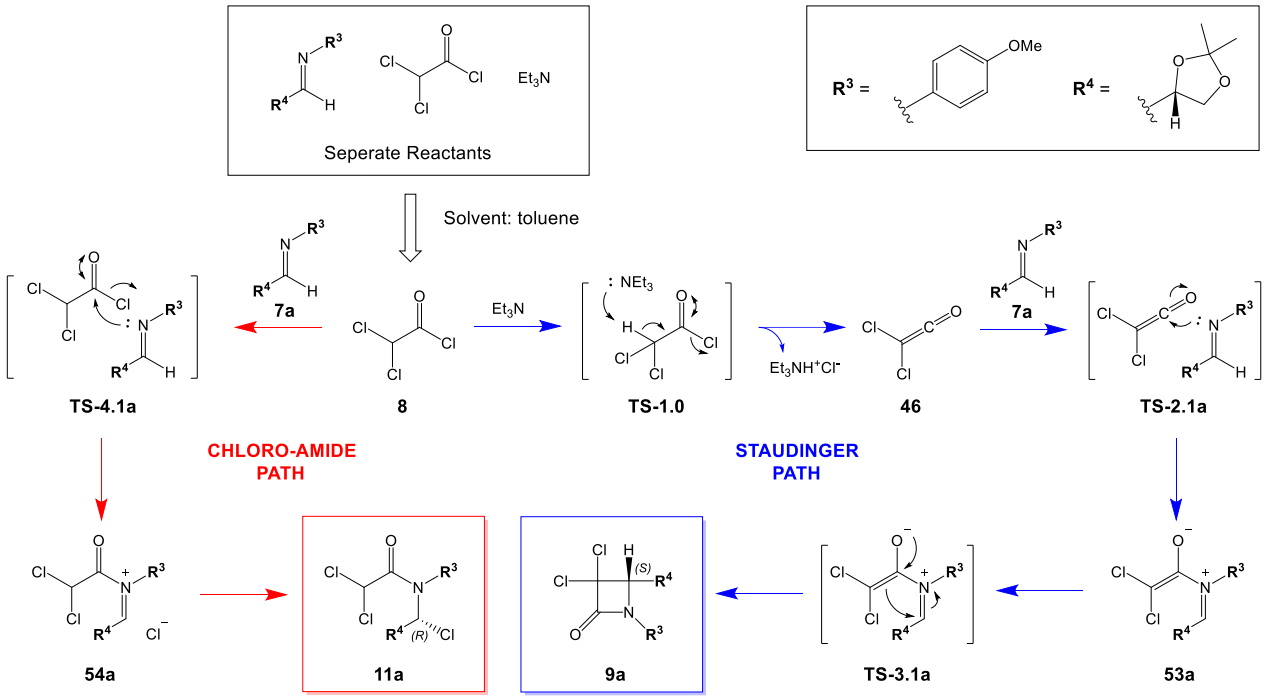


**Scheme 20**: The Chloro-amide Path ***(red)*** and the Staudinger Path ***(blue)*** for the formation of *N*-(chloromethyl)amide **11a** and β-lactam **9a**, respectively, starting from 2,2-dichloroacetyl chloride **8** and (*S*)-1-(2,2-dimethyl-1,3-dioxolan-4-yl)-*N*-(4-methoxyphenyl)methanimine **7a**. Conrotatory cyclization of **53a** via **TS-3.1a** is modelled in the conformation that yields (*S*)-β-lactam **9a**, due to the steric effect of chiral auxiliary $R^4$. This effect was investigated in a computational study by Cossío et al. (vide supra). [30]

An overview of the results for the Staudinger and Chloro-amide Paths is shown in **Profile 3**. The first step in the Chloro-amide Path (red) is the direct acylation of imine **7a** by 2,2-dichloroacetyl chloride **8** via **TS-4.1a** and has an intrinsic barrier of 52.7 kJ/mol associated with it. Two conformations are possible for this transition state (**TS-4.1a** and **TS-4.1a'**, **Figure 11**). The conformation **TS-4.1a** in which the chloride gets expelled at the side where

subsequent recombination of chloride onto iminium **54a** yields the (*R*)-configuration of the final product **11a**, is energetically favored (**Table 1**) over the conformation **TS-4.1a'** where subsequent recombination would yield the corresponding (*S*)-configuration of **11a**.

**Table 1**: Comparison of thermochemical data for **TS-4.1a** and **TS-4.1a'**. Values obtaines for **TS-4.1a'** are substracted from the values obtained for **TS-4.1a**. Level of theory: B3LYP-D3/6-311+G(d,p), IEFPCM: ε = 2.3741 (toluene).

| $\Delta H_{(TS\text{-}4.1a - TS\text{-}4.1a')}$ | $\Delta S_{(TS\text{-}4.1a - TS\text{-}4.1a')}$*298.15K | $\Delta G_{(TS\text{-}4.1a - TS\text{-}4.1a')}$ |
|---|---|---|
| -19.40 kJ/mol | +0.08 kJ/mol | -19.48 kJ/mol |

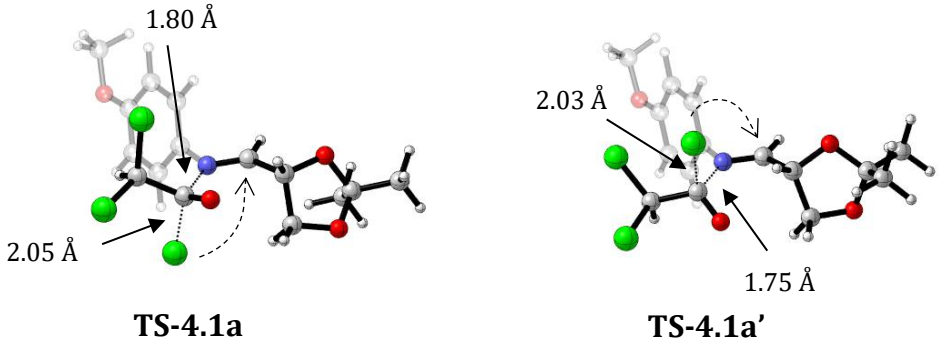


**Figure 11**: 3-D representation of two conformations for direct acylation of imine **7a** by 2,2-dichloroacetyl chloride **8**. The dashed arrows indicate the side where subsequent recombination of chloride onto the iminium carbon defines the stereochemistry of the final product **11a**, assuming recombination occurs immediately. Left structure, yielding *(R)*-**11a**, is favored over right structure, yielding *(S)*-**11a**. Level of theory: B3LYP-D3/6-311+G(d,p), IEFPCM: ε = 2.3741 (toluene).

Additional conformational analyses and comparison of Gibbs free energy barriers are required to obtain true confirmation for the exclusive observation of (*R*)-**11a** in experiments, [16] but this is not included in the scope of this study. Also, the reasoning described above assumes that recombination of chloride onto iminium **54a** occurs instantaneously. This can be justified by the large reverse barrier associated with the formation of *N*-(chloromethyl)amide **11a** which amounts to -102.4 kJ/mol (**Profile 3**). This is in contrast with authors claiming that the iminium chloride salt and it's covalent adduct can exist in equilibrium depending on experimental conditions. [76] Additional insights could be obtained from an explicit solvent environment.

Continuing on the results presented in **Profile 3**, the blue path corresponds to the formation of β-lactam **9a** via the mechanisms governing the Staudinger β-lactam synthesis (**Scheme 20**). Now triethylamine actively takes part and initiates the reaction by deprotonation of 2,2-dichloroacetyl chloride **8** via **TS-1.0** with an intrinsic barrier of +34.3 kJ/mol associated with it. The nucleophilic addition of imine **7a** onto ketene **46** via **TS-2.1a** is a low energy reversible reaction with an intrinsic barrier of +10.9 kJ/mol. The obtained intermediate **53a** is a stable

zwitterion which closes via **TS-3.1a** yielding β-lactam **9a**. This last step has a forward barrier of +58.7 kJ/mol and a reverse barrier of -192.6 kJ/mol, thus ring-closure of zwitterionic intermediate **53a** is, in accordance to the preliminary calculations, the rate-determining step and **9a** is the thermodynamic product for the Staudinger Path in this specific case.

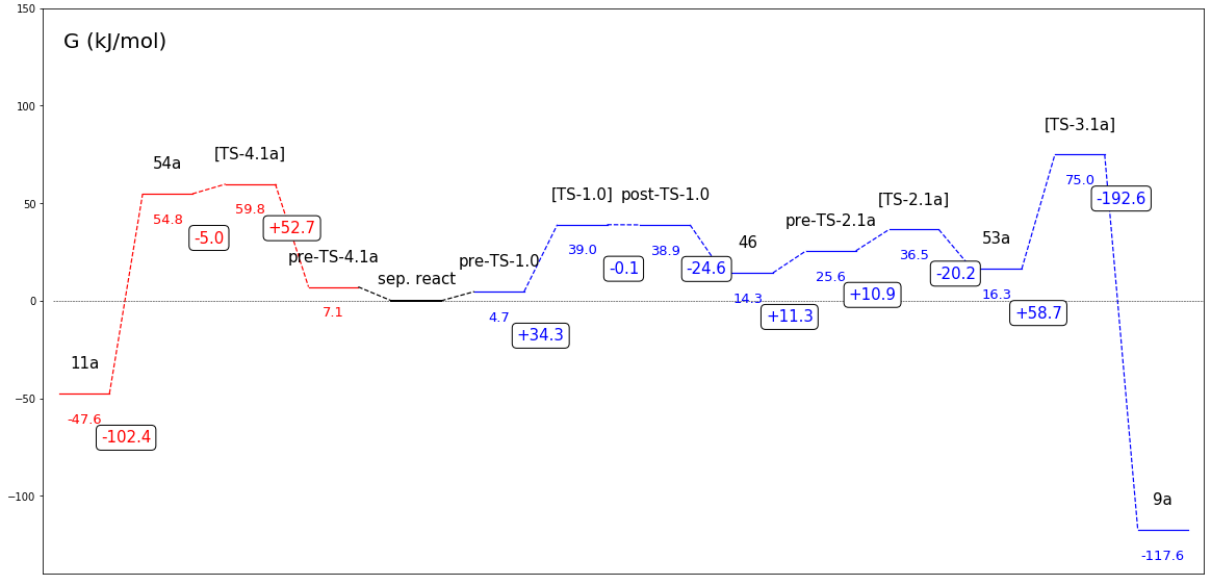


**Profile 3**: Gibbs free energy profile (kJ/mol), with respect to the separate reactants, for the Chloro-amide Path ***(red)*** and the Staudinger Path ***(blue)*** given in **Scheme 20**. Level of theory: B3LYP-D3/6-311+G(d,p), IEFPCM: ε = 2,3741 (toluene).

An additional path can be added to **Profile 3** but will be discussed briefly and seperately (**Scheme 21**) in order to maintain orderly profiles. In the preliminary study, an alternative ring-closure mechanism was discussed. However, the proposed $S_N2$ type reaction seemed unrealistic, given the unstability of the intermediate anion. On the other hand, this opened up a path (**Scheme 21**) to obtain zwitterionic intermediate **53a**, which appears on the Staudinger Path, from *N*-(chloromethyl)amide **11a**, which is formed via the Chloro-amide Path. The Gibbs free energy barrier for **TS-6.1a** (**Scheme 21**) with respect to the pre-reactive complex amounts to +78.2 kJ/mol and +98.4 kJ/mol with respect to the seperate reactants. Thus, one can assume that this reaction does not occur.

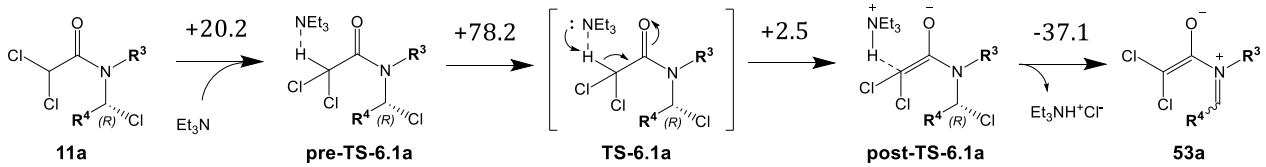


**Scheme 21**: Formation of zwitterionic intermediate **53a** from *N*-(chloromethyl)amide **11a** via **TS-6.1a**. ($R^3$ = *p*-methoxyphenyl, $R^4$ = (*S*)-2,2-dimethyl-1,3-dioxolan) The intrinsic Gibbs free energy barriers (kJ/mol) are shown above the reaction arrows. Level of theory: B3LYP-D3/6-311+G(d,p), IEFPCM: ε = 2,3741 (toluene).

Going back to the results in **Profile 3**, there is no reason to assume that β-lactam **9a** would not be formed at all, while *N*-(chloromethyl)amide **11a** would. The intrinsic Gibbs free energy barrier associated with the rate-determining step for β-lactam **9a** formation via **TS-3.1a** is only 6.0 kJ/mol higher than the intrinsic Gibbs free energy barrier for *N*-(chloromethyl)amide **11a** formation via **TS-4.1a**. With respect to the seperate reactants, **TS-3.1a** is 15.2 kJ/mol higher in Gibbs free energy than **TS-4.1a**. Therefore **Profile 3** indicates that both products are able to form with almost equal likelihood. In order to verify this trend, different levels of theory are used, namely: the M06-2X and ωB97-XD functionals. With these single-point calculations of the structures in **Profile 3** are performed. The forward intrinsic single-point energy barriers associated with the formation of *N*-(chloromethyl)amide **11a** and β-lactam **9a** via **TS-4.1a** and **TS-3.1a**, respectively are given in **Table 2**. The single-point energies with respect to the seperate reactants are also given between brackets.

**Table 2**: Single-point energy barriers (kJ/mol), with respect to pre-reactive complex (with respect to seperate reactants between brackets) associated with the rate-determining steps for the formation of *N*-(chloromethyl)amide **11a** and β-lactam **9a** via **TS-4.1a** and **TS-3.1a**, respectively. Note that these reported values are not based on Gibbs free energies but on single-point electronic energies. Basis set: 6-311+G(d,p), IEFPCM: ε = 2,3741 (toluene). A full comparison of the single-point energies computed with the validation functionals is given in **Table A1** (**Appendix**).

| | $\Delta E_{TS\text{-}4.1a}$ (kJ/mol) | $\Delta E_{TS\text{-}3.1a}$ (kJ/mol) |
|---|---|---|
| B3LYP-D3 | +36.8 (-8.6) | +50,4 (+4.3) |
| **M06-2X** | **+37,1 (-9.8)** | **+65,5 (+27.3)** |
| **ωB97-XD** | **+42,7 (-0.5)** | **+59,8 (+16.9)** |

The (intrinsic) single-point energy barrier for **TS-4.1a** does not change when computed with M06-2X while for ωB97-XD a slight increase is obtained (**Table 2**). On the other hand, B3LYP-D3 underestimates the (intrinsic) single-point energy barrier for **TS-3.1a** with respect to M06-2X and ωB97-XD. Therefore, all intermediates on **Profile 3** were optimized with the other functionals in order to assess Gibbs free energies and optimized geometries on different levels of theory. The results are visualized in **Profile 4**. M06-2X yields a higher intrinsic Gibbs free energy barrier for **TS-3.1a** (+62.9 kJ/mol) and a lower intrinsic Gibbs free energy barrier for **TS-4.1a** (+47.1 kJ/mol) with respect to B3LYP-D3 and ωB97-XD for which similar results are obtained (+52.7 kJ/mol and +54.9 kJ/mol for **TS-4.1a** and +58.7 kJ/mol and +58.9 kJ/mol for **TS-3.1a**, respectively). Also, with respect to the other functionals, B3LYP-D3 underestimates the intermediates appearing on the Staudinger Path and overestimates the stability of the final products **11a** and **9a**. But overall, no exceptional deviations from the trends are observed.

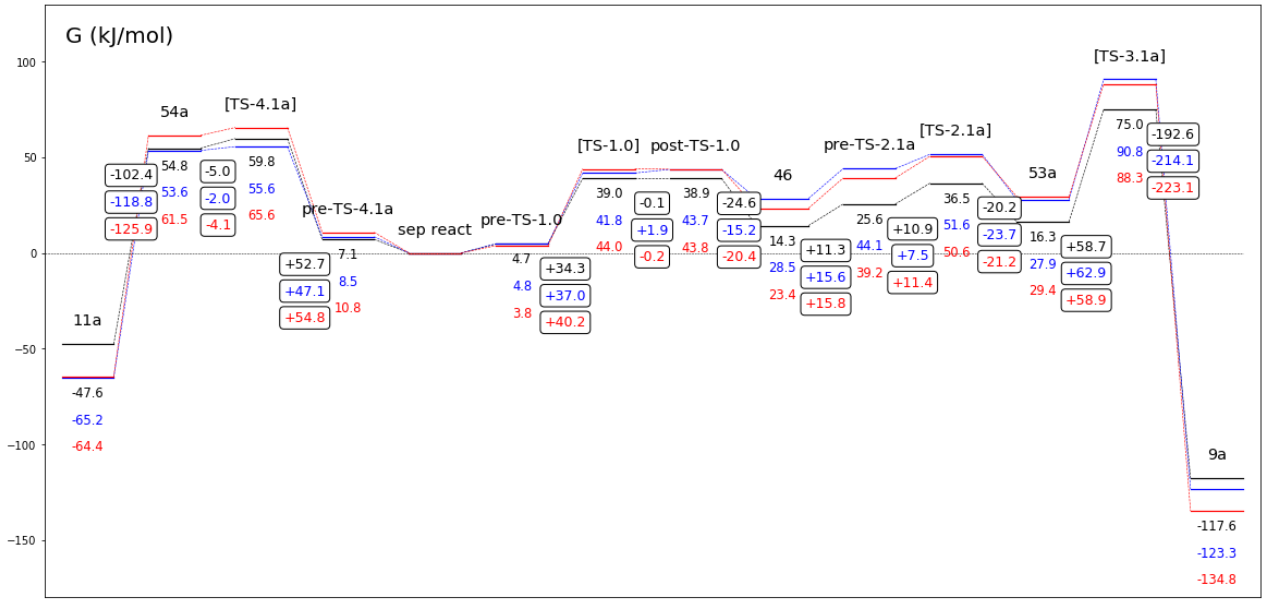


**Profile 4**: Gibbs free energy profiles of the Staudinger- and Chloro-amide Paths for formation of *N*-(chloromethyl)amide **11a** and β-lactam **9a**. Levels of theory: */6-311+G(d,p), IEFPCM: ε = 2,3741 (toluene).
(*): ***(black)*** : B3LYP-D3
***(blue)*** : M06-2X
***(red)*** : ωB97-XD

Next, possible stabilizing interactions involving zwitterionic intermediate **53a** will be investigated. It can be hypothesized that this precursor of β-lactam **9a** participates in the formation of a stable complex, hence complicating β-lactam formation via conrotatory cyclization. Possible participants are: the ammonium salt formed via dehydrohalogenation of acid chloride **8** by triethylamine, solvent molecules, the zwitterion itself or other compounds present in the mixture. One of the possibilities is hence a dimeric non-covalent interaction of zwitterion **53a** which is shown in **Figure 12**. Thermochemical values associated with the formation of this complex are given in **Table 3**. Energetic stabilization (ΔH = -79.19 kJ/mol) makes up for the reduced degree of freedom (T*ΔS = -69.24 kJ/mol) resulting in a ΔG-value of -9.95 kJ/mol in favor of the dimer. Two types of non-covalent interactions stabilizing the dimeric complex of zwitterion **53a** can be identified. First, there is a π-stacking interaction of the aromatic *p*-methoxyphenyl side chains. In addition, there is an electrostatic interaction between the negatively charged enolate oxygen and the positively charged imine carbon at the core of the complex. These cooperating forces hold the zwitterions in a conformation so that the chlorine groups and (*S*)-2,2-dimethyl-1,3-dioxolan side chains are pointing outwards, respectively in opposite directions.

**Table 3**: Thermochemical values associated with the formation of zwitterion **53a** dimer. Level of theory: B3LYP-D3/6-311+G(d,p), IEFPCM: ε = 2,3741 (toluene).

| **ΔH** (kJ/mol) | **ΔS*298.15 K** (kJ/mol) | **ΔG** (kJ/mol) |
|---|---|---|
| -79.19 | -69.24 | -9.95 |

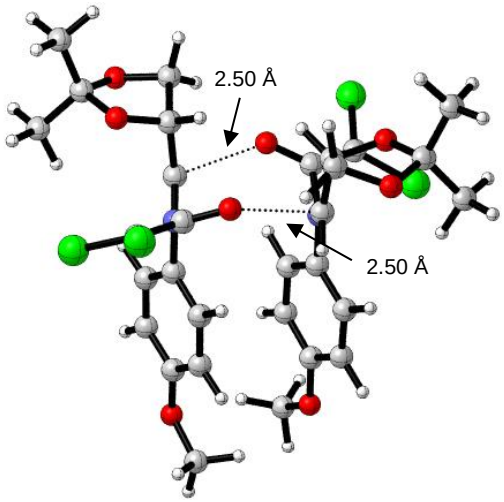


**Figure 12**: 3-D representation of zwitterion **53a** dimer. Optimized at the B3LYP-D3/6-311+G(d,p) level of theory. IEFPCM: ε = 2,3741 (toluene).

Of course, a Gibbs free energy difference of -9.95 kJ/mol is not extraordinarily high and there is no reference given to compare this value with. It's definitely not unlikely that zwitterions carrying other substituent combinations also interact in such a manner, without loss of β-lactam formation. However, many other types of complexes including the zwitterionic intermediate could exist, and in their turn complicate β-lactam synthesis. However, due to the time limitation of this thesis, we did not investigate this in more depth.

So far, the calculations in this study did not provide strong evidence to prove that β-lactam is not formed at all during synthesis. Based on this obervation, the analytic data obtained in the experimental phase were examined a second time. LC-MS analysis was not conclusive due to the complexity of the crude reaction mixtures and identical m/z values for *N*-(chloromethyl)amide **11a** and β-lactam **9**. In this respect, NMR analysis is more suitable for structure clarification. The presence of β-lactam in the crude reaction mixture could not be confirmed based on the available NMR spectra. However, in one of the attempts to purify the crude reaction mixture via column chromatography a fraction was found containing three products: 2,2-dichloroacetamide **60** (vide infra), *N*-(chloromethyl)amide **11a** and an unknown compound. [16] Based on the chemical shifts and integration of these signals in the $^{1}$H-NMR spectra ($CDCl_3$), the unknown compound could presumably be the envisioned β-lactam **9a**. Even if these signals are originating from β-lactam **9a**, only traces are present as these signals were not visible on the spectra of the crude reaction mixture and are blended in with the noise. However, additional NMR experiments are required to elucidate β-lactam **9a** formation.

### 3.3.2.2 Influence of different Imine Substituents on Staudinger and Chloroamide Paths

In this section the influence of different imine substituents on the Staudinger and Chloroamide Paths will be discussed. Two commonly used aromatic groups are chosen to replace *p*-methoxyphenyl ($R^3$) and (*S*)-2,2-dimethyl-1,3-dioxolan ($R^4$) in imine **7a**. The combinations under investigation are shown in **Table 4**.

**Table 4**: Combinations of varying imine substituents $R^3$ and $R^4$.

| | $R^3$ | $R^4$ |
|---|---|---|
| **a** | *p*-methoxyphenyl | (*S*)-DMDO* |
| **b** | phenyl | (*S*)-DMDO* |
| **c** | *p*-nitrophenyl | (*S*)-DMDO* |
| **d** | *p*-methoxyphenyl | phenyl |
| **e** | *p*-methoxyphenyl | *p*-nitrophenyl |

(*): (*S*)-DMDO = 

No aliphatic side chains were chosen to include in this comparison because the reaction of 2,2-dichloroacetyl chloride **8** with imines carrying aliphatic side chains at $R^3$ and (*S*)-DMDO at $R^4$ under Staudinger conditions yields complex reaction mixtures which are difficult to analyse. [16], [17] An electron-withdrawing group *p*-nitrophenyl (PNP) was chosen for comparison with the electron-donating nature of *p*-methoxyphenyl (PMP). Phenyl (Ph) was included as a reference for PNP and PMP, since it cannot be classified as an electron-donating, nor electron-withdrawing group, while having a similar steric effect.

First, PMP ($R^3$) was replaced by Ph and PNP (case **b** and **c**, respectively) and the corresponding structures included in the reaction paths in **Profile 3** were reoptimized. The results are visualized in **Profile 5** with case **b**, blue ($R^3$ = Ph, $R^4$ = (*S*)-DMDO), case **c**, red ($R^3$ = PNP, $R^4$ = (*S*)-DMDO) and case **a**, black ($R^3$ = PMP, $R^4$ = (*S*)-DMDO). The middle part of the profile remains unchanged as it refers to the generation of ketene **46** and thus not depends on imine substituents. The electron-withdrawing effect of PNP has an observable effect on the Gibbs free energy profile. With respect to the seperate reactants, intermediates from the red profile ($R^3$ = PNP) are the least stable. There is a clear correlation between the electronic character of $R^3$ and the Gibbs free energies with respect to the corresponding separate reactants. This effect is very pronounced for the zwitterionic intermediates **53a-c**. The PMP side chain in **53a** donates electron density to the positive moiety of the zwitterion and thereby stabilizes the precursor of β-lactam **9a**. On the other hand, the PNP side chain in **53c** withdraws electron density from the positive moiety of the zwitterion (**Figure 13**), hence disfavoring it's

formation. This destabilizing effect of PNP also applies to **TS-3.1c**. Therefore, there is no remarkable change observed for the intrinsic barriers associated with **TS-3.1a,c**.

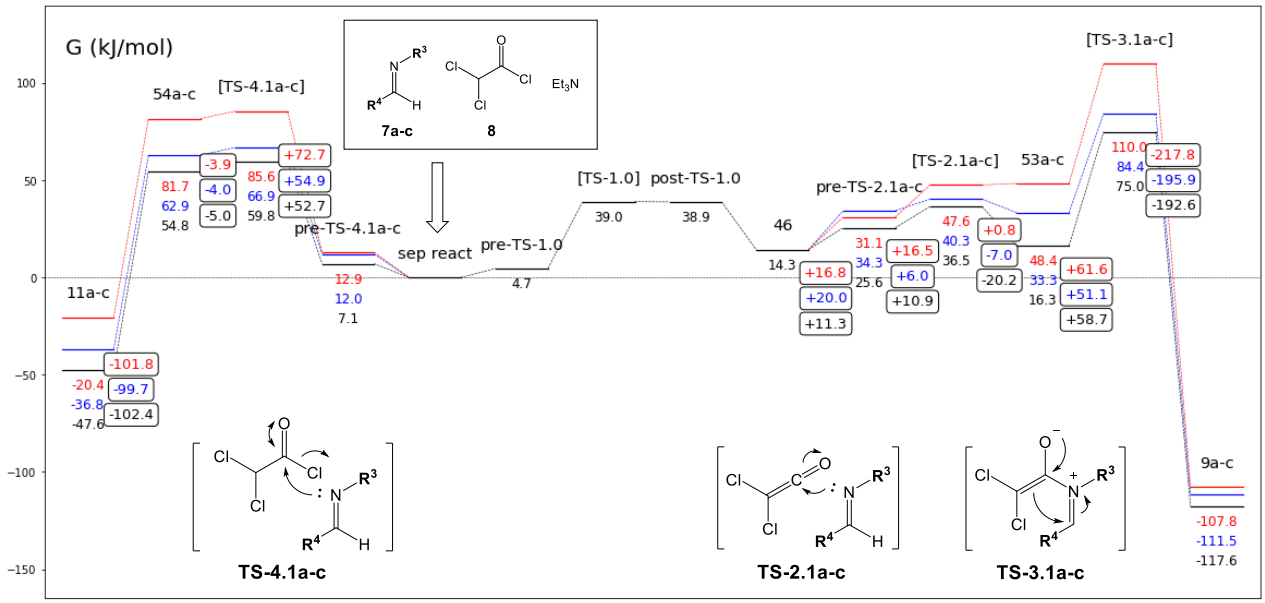


**Profile 5**: Gibbs free energy profile (kJ/mol) associated with the Chloro-amide Path (formation of **11a-c**) and the Staudinger Path (formation of **9a-c**) for imine substituent combinations **a-c**.
***(black)*** **a**: $R^3$ = PMP, $R^4$ = (*S*)-DMDO
***(blue)*** **b**: $R^3$ = Ph, $R^4$ = (*S*)-DMDO
***(red)*** **c**: $R^3$ = PNP, $R^4$ = (*S*)-DMDO
Level of theory: B3LYP-D3/6-311+G(d,p), IEFPCM: ε = 2,3741 (toluene).

Furthermore, the Gibbs free energy with respect to the seperate reactants for **TS-4.1c** is 25.8 kJ/mol higher than for **TS-4.1a** (left side **Profile 5**). This $R^3$ side chain dependence can be attributed to the increased/decreased electron density at the nitrogen atom in **TS-4.1a,c** which facilitates/complicates addition of imine **7a,c** onto the carbonyl of 2,2-dichloroacetyl chloride **8**. However, the Gibbs free energies with respect to the corresponding seperate reactants for **pre-TS-4.1a,c** remain similar (which was not the case for the zwitterionic pre-reactive complexes of **TS-3.1a,c**). Consequently, the intrinsic barrier associated with direct acylation and subsequent formation of **11a** is 20.0 kJ/mol lower than the intrinsic barrier for formation of **11c**.

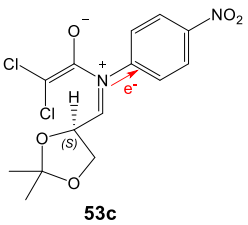


**53c**

**Figure 13**: Destabilizing effect of *p*-nitrophenyl (PNP) side chain at $R^3$ position in zwitterionic intermediate **53c**, due to the withdrawal of electron density from the positively charged moiety of the molecule.

Next, the effect of the $R^4$ substituent is examined by leaving *p*-methoxyphenyl at the $R^3$ position and replacing the (*S*)-DMDO-group at $R^4$ by phenyl (Ph) and *p*-nitrophenyl (PNP) (**d** and **e**, respectively). In an analogous way **Profile 6** was constructed by plotting the results of case **d**, blue ($R^3$ = PMP, $R^4$ = Ph) and **e**, red ($R^3$ = PMP, $R^4$ = PNP) with respect to the profile for case **a**, black ($R_3$ = PMP, $R_4$ = (*S*)-DMDO). Interestingly, replacing the (*S*)-DMDO group by an aromatic side chain results in a considerable increase of the Gibbs free energy barriers associated with **TS-4.1d-e** (with respect to separate reactants and to pre-reactive complexes). In addition, the electron-withdrawing nature of PNP at the $R^4$ position facilitates the formation of β-lactam **9e** via **TS-3.1e** by means of a lowered intrinsic barrier height (+39.1 kJ/mol and +58.7 kJ/mol for **TS-3.1e** and **TS-3.1a**, respectively).

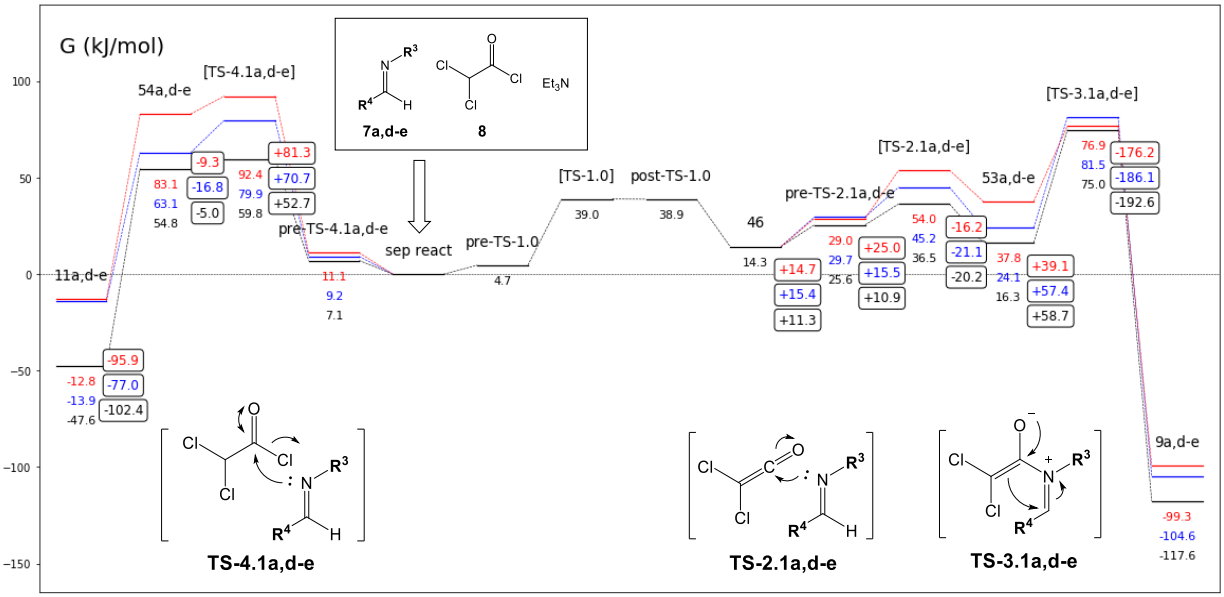


**Profile 6**: Gibbs free energy profile (kJ/mol) associated with the Chloro-amide Path (formation of **11a,d-e**) and the Staudinger Path (formation of **9a,d-e**) for imine-substituent combinations **a, d** and **e**.
***(black)*** **a**: $R^3$ = PMP, $R^4$ = (*S*)-DMDO
***(blue)*** **d**: $R^3$ = PMP, $R^4$ = Ph
***(red)*** **e**: $R^3$ = PMP, $R^4$ = PNP
Level of theory: B3LYP-D3/6-311+G(d,p), IEFPCM: ε = 2,3741 (toluene).

To conclude, based on intrinsic Gibbs free energy barriers, the specific combination of $R^3$ = PMP and $R^4$ = (*S*)-DMDO (case **a**) shows the most preference for the formation of *N*-(chloromethyl)amide **11a** compared to other imine substituent combinations **b-e**. In terms of relative Gibbs free energies with respect to the separate reactants, imine combination **a** yields the most stable intermediates for the entire profile. This is definitely the case for *N*-(chloromethyl)amide **11a**, where the (*S*)-DMDO side chain exhibits the most pronounced stabilizing effect on this final product (left side **Profile 6**, **11a** is -47.6 kJ/mol more stable than the separate reactants, while **11d,e** are respectively -13.9 kJ/mol and -12.8 kJ/mol more stable with respect to the separate reactants). Also, case **a** yields the most stable zwitterionic precursor of β-lactam for all combinations **a-e**.

### 3.3.2.3 Influence of different Acid Chloride Substituents on Staudinger and Chloro-amide Paths

In order to gain more insight into the effect of the acid chloride substituents on the preference for different reaction paths, 2-methoxyacetyl chloride **12** was applied to model the Staudinger Path (**Scheme 22**, right) and the Chloro-amide Path (**Scheme 22**, left). This choice was based on earlier in-house experiments where 2-methoxyacetyl chloride **12** was used for a Staudinger β-lactam synthesis in dichloromethane. In this case, imine **7a** was successfully incorporated in the β-lactam structure, yielding product **13**. Even though *N*-(chloromethyl)amide **58** was not formed in this reaction, since it was not identified with the spectra obtained for the crude reaction mixture, the path leading to this product was included in the model for comparison.

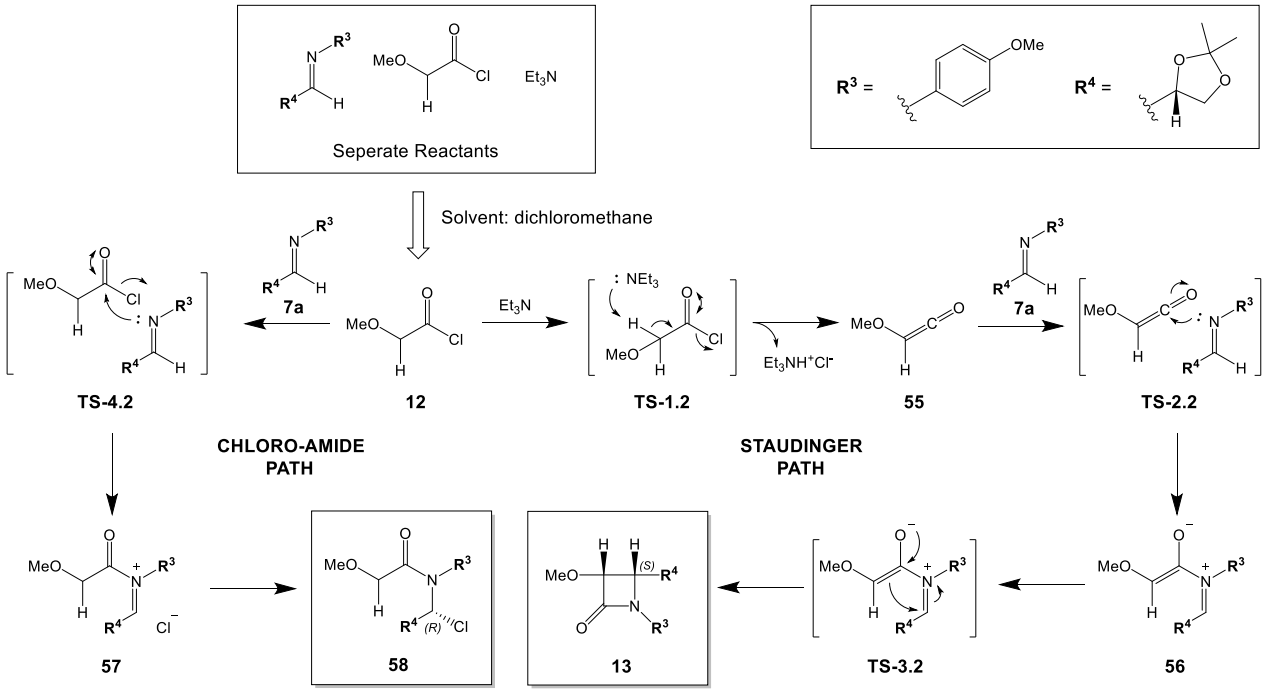


**Scheme 22**: The Chloro-amide Path (left) and Staudinger Path (right) for the formation of *N*-(chloromethyl)amide **58** and β-lactam **13**, respectively, starting from 2-methoxyacetyl chloride **12** and (*S*)-1-(2,2-dimethyl-1,3-dioxolan-4-yl)-*N*-(4-methoxyphenyl)methanimine **7a**. Only formation of (*S*)-β-lactam **13** was modelled, due to steric effect of chiral auxiliary $R^4$ (vide supra). [30]

The Gibbs free energies associated with these paths are visualized in **Profile 7**. This figure also includes the profile for the reaction of 2,2-dichloroacetyl chloride **8** with imine **7a** in toluene (**Profile 7**, red) discussed in section 3.3.2.1 (**Scheme 20**). This way the comparison can be made between a successful and an unsuccessful attempt to incorporate imine **7a** in a β-lactam structure. The experimental details corresponding to the blue and red profile are summarized in **Table 5**.

**Table 5**: Experimental details [16], [17] corresponding to the computational data plotted in **Profile 7**.

| Profile | Imine | Acid chloride | Solvent | Base | *N*-(chloromethyl)amide observed? | β-lactam observed? |
|---|---|---|---|---|---|---|
| ***(blue)*** | **7a** | 2-methoxyacetyl chloride **12** | $CH_2Cl_2$ | $Et_3N$ | No | Yes |
| ***(red)*** | **7a** | 2,2-dichloroacetyl chloride **8** | toluene | $Et_3N$ | Yes | No* |

(*): Presumably, trace amounts of β-lactam **9a** were detected. (vide supra)

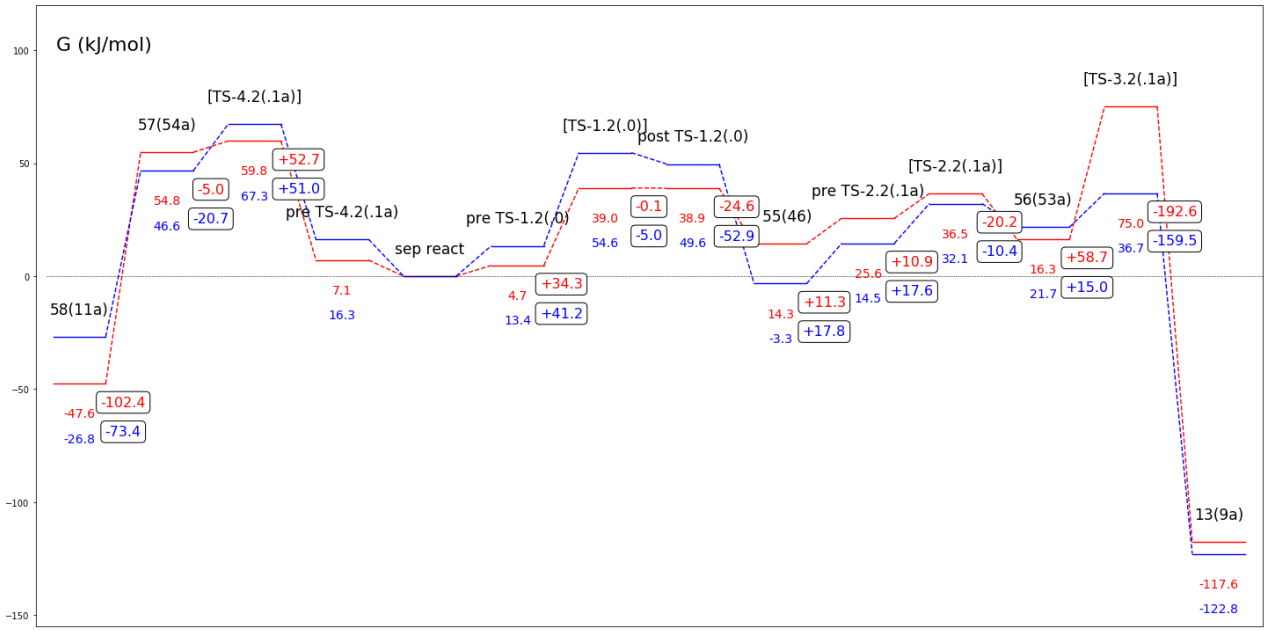


**Profile 7**: Gibbs free energy profile (kJ/mol) associated with the Chloro-amide Path (left) and the Staudinger Path (right) for the reaction of imine **7a** with:
***(blue)*** 2-methoxyacetyl chloride **12** in dichloromethane
***(red)*** 2,2-dichloroacetyl chloride **8** in toluene
The label-indices between round brackets are referring to the red profile. Level of theory: B3LYP-D3/6-311+G(d,p), IEFPCM: ε = 8,93 (dichloromethane) for blue profile and ε = 2,3741 (toluene) for red profile.

Apart from the relative stability of *N*-(chloromethyl)amides **58** and **11a** with respect to the separate reactants (-26.8 kJ/mol and -47.6 kJ/mol, respectively), there is no remarkable difference observed for the Chloro-amide Path (left side **Profile 7**). The Staudinger Path (right side **Profile 7**) on the other hand is affected by the different acid chloride substituents. The rate-determining step for the formation of β-lactam **13** is no longer associated with the ring-closure mechanism **TS-3.2** ($\Delta G_{\text{TS-3.2,forward}}$ = +15.0 kJ/mol), but now generation of ketene **55** via **TS-1.2** ($\Delta G_{\text{TS-1.2,forward}}$ = +41.2 kJ/mol) is the rate-limiting step of the Staudinger synthesis of β-lactam **13**. The acid chloride substituents have a major impact on the Gibbs free energy barrier for ring-closure (+15.0 kJ/mol and +58.7 kJ/mol for **TS-3.2** and **TS-3.1a**, respectively). The thermochemical values associated with this barrier are given in **Table 6**.

**Table 6**: Thermochemical values corresponding to the barrier for **TS-3.2** (blue profile) and **TS-3.1a** (red profile), with respect to the pre-reactive complexes.

| | **ΔH** (kJ/mol) | **ΔS*298.15K** (kJ/mol) | **ΔG** (kJ/mol) |
|---|---|---|---|
| **TS-3.2** ***(blue)*** | +8.5 | -6.5 | +15.0 |
| **TS-3.1a** ***(red)*** | +50.5 | -8.2 | +58.7 |

Based on **Table 6**, the difference between **TS-3.2** and **TS-3.1a** is mainly attributed to energetic effects while steric effects are similar. The electron-donating nature of the methoxy side chain significantly facilitates the ring-closure via **TS-3.2** due to the increased electron density of the ketene moiety in zwitterionic intermediate **56** (**Scheme 22**) and thereby assists the attack of the enolate on the electron-deficient moiety in **TS-3.2**. Also, the methoxy side chain is directed outwards in **TS-3.2** (**Figure 14**, left) while for **TS-3.1a** (**Figure 14**, right) one of the chlorine side chains is directed inwards, causing a repulsive interaction between the outer shell electron clouds of chlorine and the σ-bond being formed between C2 and C3.

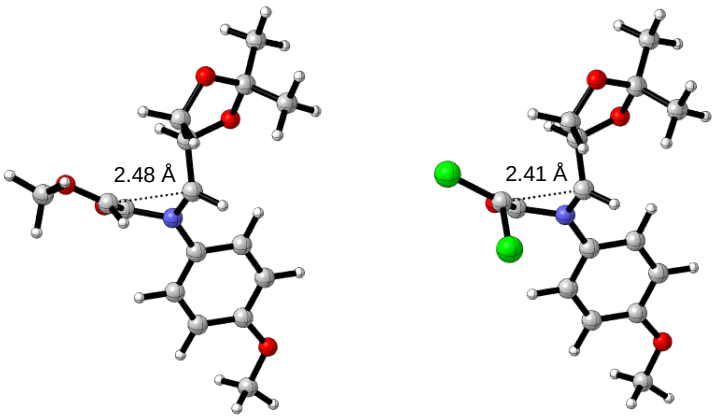


**TS-3.2** **TS-3.1a**

**Figure 14**: 3-D representation of **TS-3.2** (left) and **TS-3.1a** (right). Optimized at the B3LYP-D3/6-311+G(d,p) level of theory. IEFPCM: ε = 8,93 (dichloromethane) for **TS-3.2** and ε = 2,3741 (toluene) for **TS-3.1a**.

To conclude, Staudinger synthesis of imine **7a** with 2-methoxyacetyl chloride **12** favors the formation of β-lactam **13**, in accordance with experiment. This can be generalized for acid chlorides carrying -OR substituents. [16]

### 3.3.2.4 Influence of Solvent on Staudinger and Chloro-amide Paths

In the previous section a comparison was made for different acid chlorides as starting components. One should be attentive however that different solvents were applied in the model. This was done in order to be in accordance with experiments. Whether or not a more polar solvent like dichloromethane would affect the reaction of 2,2-dichloroacetyl chloride **8** with imine **7a** is looked into in this section. The results are visualized in **Profile 8**. The reaction of 2-methoxyacetyl chloride **12** with imine **7a** was also modelled for toluene, but will not be discussed here. (**Table A2**, **Appendix**)

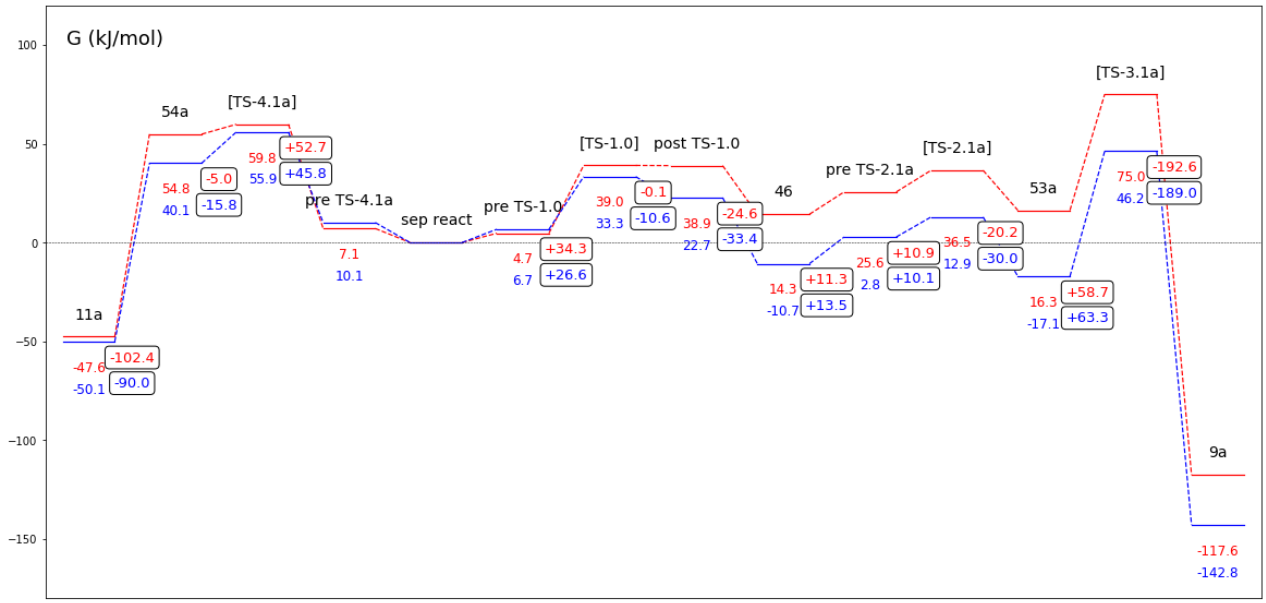


**Profile 8**: Gibbs free energy profile (kJ/mol) associated with the Chloro-amide Path (left) and the Staudinger Path (right) for the reaction of 2,2-dichloroacetyl chloride **8** with imine **7a** in toluene ***(red)*** and in dichloromethane ***(blue)***. Level of theory: B3LYP-D3/6-311+G(d,p), IEFPCM: ε = 2,3741 (toluene) for red profile and ε = 8,93 (dichloromethane) for blue profile.

One can observe a significant stabilizing effect of dichloromethane on the intermediates appearing in the Staudinger Path (right side **Profile 8**). This is obviously not a surprise given the polar and ionic nature of some of the intermediates, such as ketene **46** and zwitterion **53a**. On the other hand, this effect is less pronounced for the Chloro-amide Path leading to product **11a**. In terms of intrinsic barrier heights there is no considerable change observed. Therefore, these results imply that application of dichloromethane as a solvent for the reaction of 2,2-dichloroacetyl chloride **8** with imine **7a** would not drastically alter the outcome of the reaction, which is in accordance with experiments. [17]

### 3.3.2.5 Hydrolysis of *N*-(chloromethyl)amide

*N*-(chloromethyl)acetamide **11a** proved to be rather unstable, since structure clarification of the reaction mixtures revealed 1/1-ratios of **11a** and 2,2-dichloroacetamide **60** (**Scheme 23**). [17] The latter side product was always observed both in toluene and dichloromethane, with or without addition of base. 2,2-Dichloroacetamide **60** can be formed due to the attack of free primary amine **59** onto 2,2-dichloroacetyl chloride **8**. These free amines are applied in previous steps to produce imine **7a** via condensation with (*R*)-2,2-dimethyl-1,3-dioxolane-4-carboxaldehyde **58**. However, it was shown that free amines were no longer present and hence could not be the cause for formation of 2,2-dichloroacetamides **60**. It was hypothesized that hydrolysis of **11a** due to the presence of trace amounts of water during work-up is causing this side reaction. This was modelled via the mechanisms shown in **Scheme 24**.

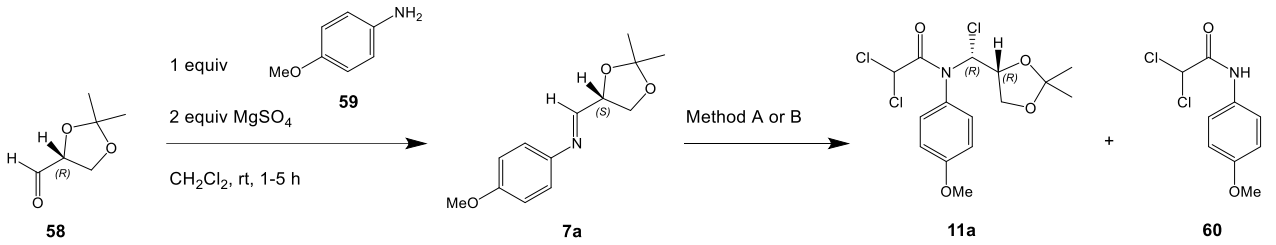


**Scheme 23**: Condensation of aldehyde **58** with amine **59** to form imine **7a** and consequent formation of *N*-(chloromethyl)amide **11a** and 2,2-dichloroacetamide **60**.
Method A: 2 equiv 2,2-dichloroacetyl chloride **8**, 3 equiv $Et_3N$, toluene, rt, 4 h
Method B: 1 equiv 2,2-dichloroacetyl chloride **8**, dichloromethane, rt, 16 h

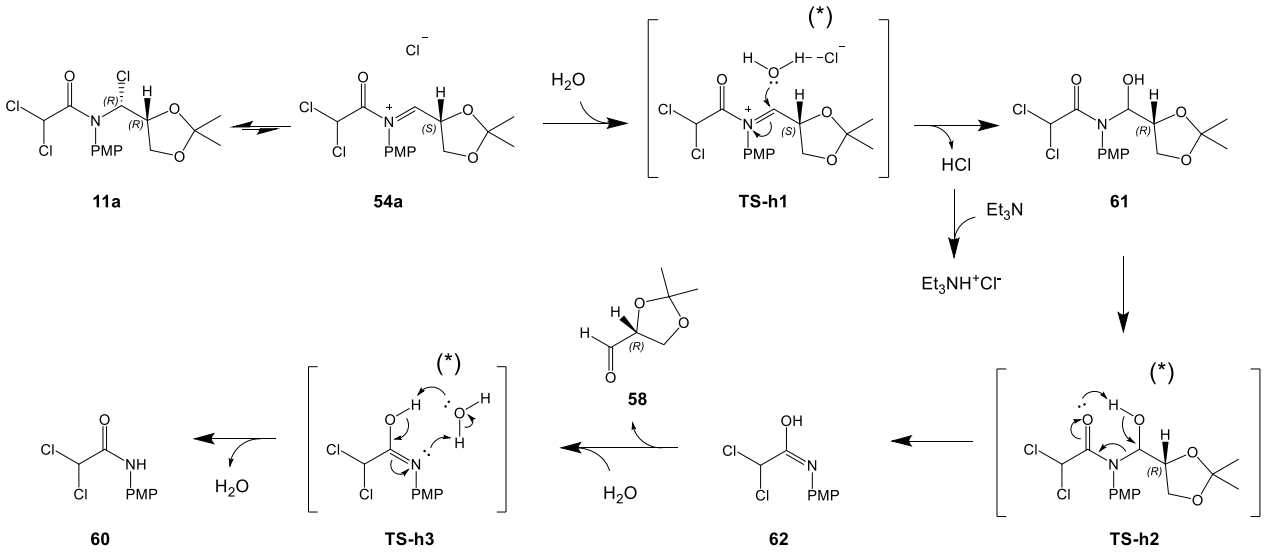


**Scheme 24**: Hydrolysis pathway, presented the way it was modelled, starting from *N*-(chloromethyl)amide **11a** yielding (*R*)-2,2-dimethyl-1,3-dioxolane-4-carboxaldehyde **58** and 2,2-dichloroacetamide **60**. (*): more realistic mechanisms exist, (vide infra) but were not modelled due to the time limitation of this thesis.

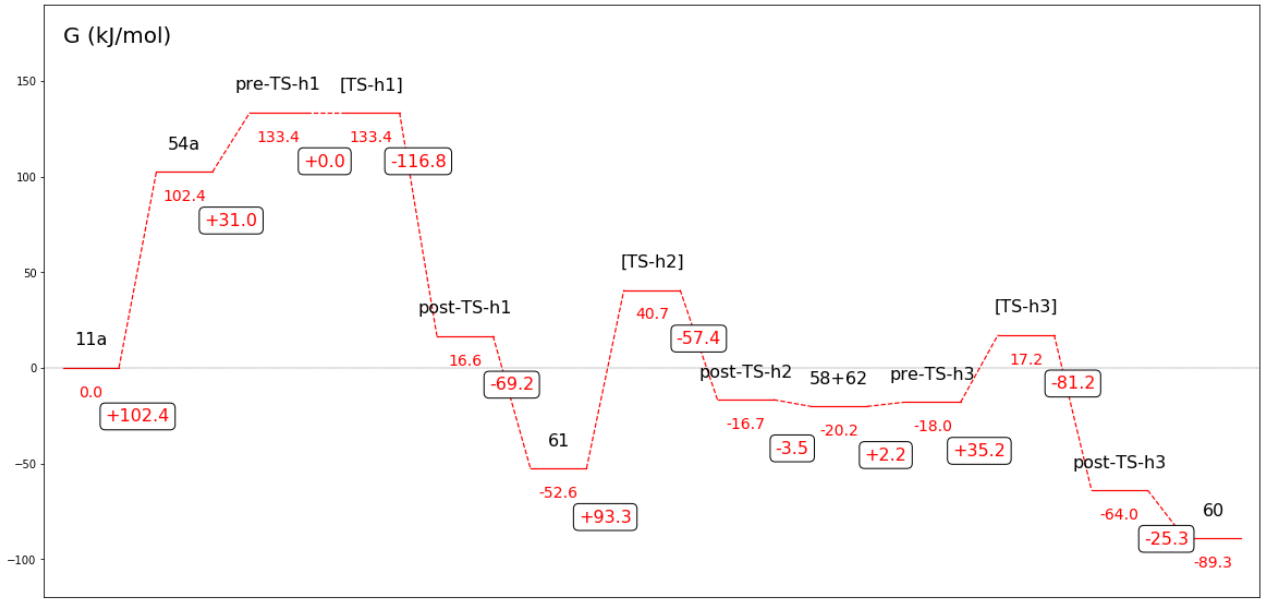


**Profile 9**: Gibbs free energy profile (kJ/mol) for to the hydrolysis of *N*-(chloromethyl)amide **11a** via the mechanisms shown in **Scheme 24**. Level of theory: B3LYP-D3/6-311+G(d,p), IEFPCM: ε = 2,3741 (toluene).

The initial addition of water onto the substrate was modelled via **TS-h1** (**Figure 15**, left) where chloride stabilizes the oxonium cation under formation and has an intrisic barrier of +31.0 kJ/mol. Due to the presence of chloride in the modelled system, an oxonium cation was not obtained as the post-reactive complex after IRC calculation. Instead, alcohol **61** (**Scheme 24**) and hydrogen chloride were obtained. The newly generated hydrogen chloride is removed from the post-reactive complex (**post-TS-h1**, **Profile 9**) with the formation of triethylammonium hydrochloride. In a more realistic way to model **TS-h1**, chloride is replaced by triethylamine, which abstracts a proton from the oxonium cation. Subsequently, triethylammonium hydrochloride is formed after combination of chloride with triethylammonium.

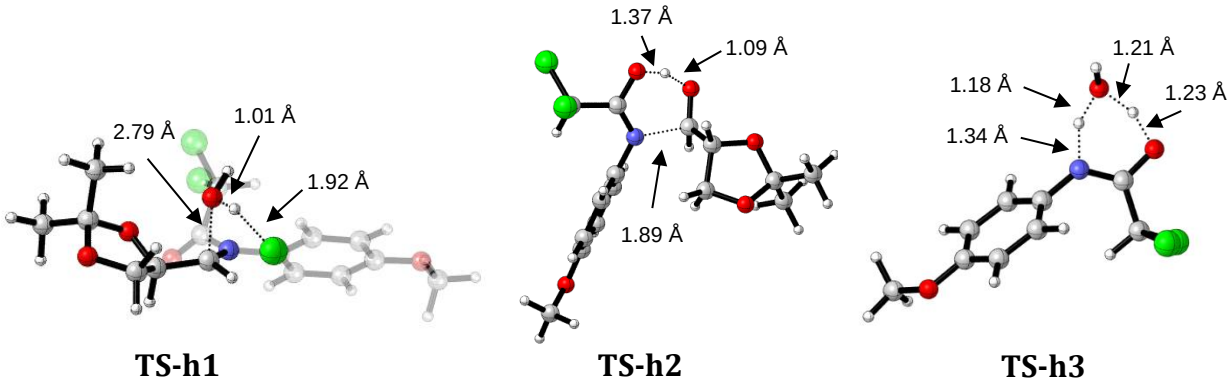


**Figure 15**: 3-D representation of **TS-h1,2,3**. Level of theory: B3LYP-D3/6-311+G(d,p), IEFPCM: ε = 2,3741 (toluene).

Cleavage of alcohol **61** yielding iminol **62** and aldehyde **58** was modelled as a six-membered ring transition state via **TS-h2** (**Figure 15**, middle) with an intrinsic barrier of +93.3 kJ/mol. This large barrier is due to the unrealistic way the cleavage was modelled. In solution, intervention of additional water molecules can catalyze this step. [77] The same applies for tautomerization of iminol **62** via **TS-h3** (**Figure 15**, right) which was modelled with the intervention of one additional watermolecule, facilitating the protontransfer. An iminol **62** dimeric transition state could also be a more efficient way for tautomerization of iminol **62**.

Apart from the large barrier associated with the transition from **11a** to **54a**, there is nothing unusual to be noticed about this hydrolysis pathway. Barriers obtained for **TS-h1,2**,**3** can be decreased even further by means of more realistic transition state structures, which are lower in Gibbs free energy, for example by intervention of additional water molecules. [77] However, the requirement for the formation of iminium salt **54a** in this model raises a red flag. Even though some authors state that there exists an equilibrium between **11a** and **54a** [76], this might not be the case for the specific substrate under investigation given the high stability obtained for *N*-(chloromethyl)amide **11a**. Again it should be mentioned that additional calculations may shed new light on the latter, both statically by including solvent molecules explicitly, or via dynamic simulations (vide infra). Furthermore, we were unable to identify a transition state for the addition of water onto **11a** directly and based on the steric hindrance caused by the (*S*)-DMDO group at the site of water addition, one can assume that the corresponding barrier would also amount to a relatively large value. These findings indicate that hydrolysis of **11a** might not be the main pathway responsible for the formation of **60**. Alternatively, 2,2-dichloroacetamide **60** could be the result of hydrolysis of zwitterion **53a**. Nonetheless, acetamide **60** is also formed in the absence of base [17], and thus in the absence of zwitterion **53a**. In this case free amines might still be responsible for acetamide **60** formation. Additional research is required to further elaborate on these findings.

# Chapter 4

# Summary, Conclusion and Outlook

This thesis was a computational continuation on the experimental findings of D. Deturck and L. Cools. [16], [17] An attempt to produce β-lactam **9a** from imine **7a** and 2,2-dichloroacetyl chloride **8** applying Staudinger conditions did not yield the envisioned β-lactam structure but instead a mixture of *N*-(chloromethyl)amide **11a** and 2,2-dichloroacetamide **60** was obtained. (**Scheme 25**) This was rather unexpected, given that imine **7a** has been applied before to succesfully yield β-lactams **13** and 2,2-dichloroacetyl chloride also proved to yield β-lactams in combination with a variety of imines. This reactivity was investigated by means of a DFT study on the B3LYP-D3/6-311+G(d,p) level of theory using an implicit solvent model.

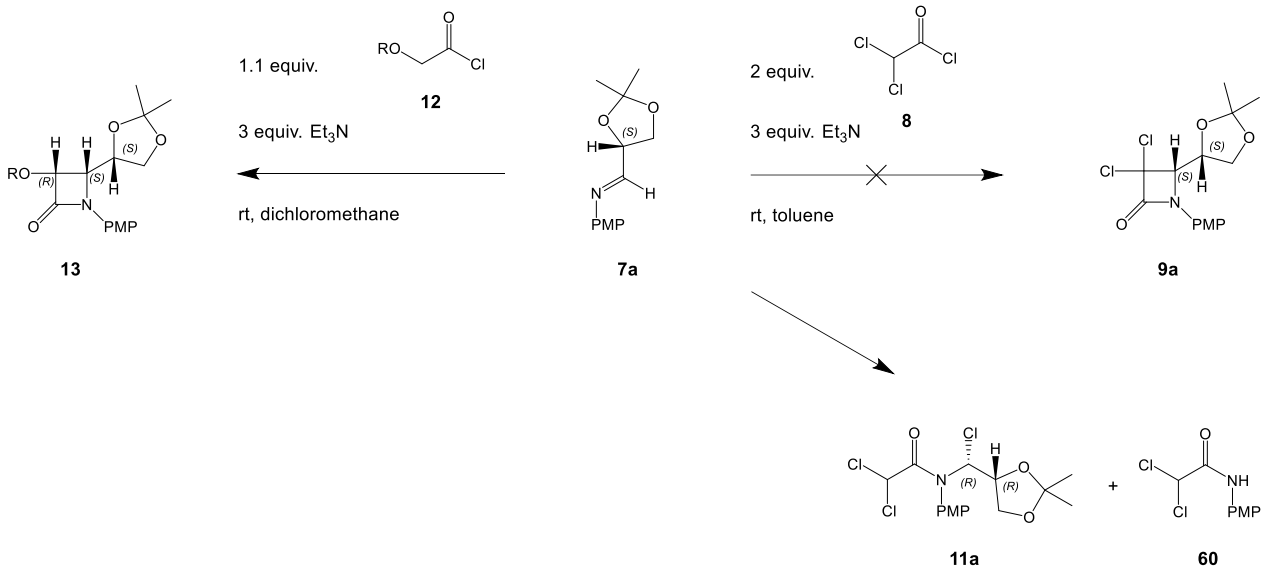


**Scheme 25**: Experimental findings of D. Deturck and L. Cools. [16], [17]

## 4.1 Summary

Throughout this thesis a systematic approach was followed to investigate the issue presented in **Scheme 25**. In the preliminary study a simplified imine system was used to examine two pathways for the formation of the corresponding β-lactam and *N*-(chloromethyl)amide. Next, the Gibbs free energy profile for the formation of β-lactam **9a** and *N*-(chloromethyl)amide **11a** was discussed. It was expected that the obtained profile would reveal a clear preference for formation of *N*-(chloromethyl)amide **11a**. However, this was not the case and based on the results one can assume that there should be competition between formation of β-lactam **9a** and *N*-(chloromethyl)amide **11a** given the similar intrinsic Gibbs free energy barriers for the rate-determining steps corresponding to the formation of these products (+58.7 kJ/mol and +52.7 kJ/mol, respectively). This trend obtained at the B3LYP-D3/6-311+G(d,p) level of theory was validated by means of single-point energy calculation with the M06-2X and ωB97-XD functionals. In addition, the Gibbs free energy profile was also constructed with the other levels of theory, but no noticeable difference was observed which confirmes the trend obtained with B3LYP-D3/6-311+G(d,p). Additional calculations were performed in order to examine this discrepancy between the computational model and experiments. A possible stabilizing interaction of the zwitterionic precursor of β-lactam **9a** was examined by means of a dimeric complex of this zwitterionic intermediate. This was not investigated in further detail due to the time limitation of this thesis.

In a next stage the influence of the imine substituents was assessed. The *p*-methoxyphenyl (PMP) and (*S*)-2,2-dimethyl-1,3-dioxolan ((*S*)-DMDO) side chains were in turn replaced by *p*-nitrophenyl and phenyl and the corresponding Gibbs free energy profiles were constructed. From this comparison the infuence of the electron-donating nature of PMP on the Gibbs free energy profile was deduced. This influence was mainly expressed by stabilization of the zwitterionic intermediate and by facilitating direct acylation of the imine. However, the effect of (*S*)-DMDO was more pronounced. Upon replacing this side chain by an aromatic group, a considerable increase of the intrinsic barrier for *N*-(chloromethyl)amide **11a** formation was obtained (from +52.7 kJ/mol for $R^4$ = (*S*)-DMDO to +70.7 kJ/mol and +81.3 kJ/mol for $R^4$ = phenyl and *p*-nitrophenyl, respectively). Next, the effect of a different acid chloride, that is known to succesfully yield β-lactams in combination with imine **7a**, was examined. The profile corresponding to the reaction between imine **7a** and 2-methoxyacetyl chloride **12** (**Scheme 25**, R = Me) was compared with the profile for reaction between imine **7a** and 2,2-dichloroacetyl chloride **8**. The results showed that for the former reaction, ring-closure of the zwitterionic intermediate was no longer the rate-determining step (ΔG = +15.0 kJ/mol) but instead, generation of the corresponding ketene determined the rate of β-lactam formation (ΔG = +41.2 kJ/mol). From the comparison of the barriers for ring-closure of the zwitterionic

intermediates, it was deduced that the chlorine substituents complicate ring-closure by means of energetic destabilization of the corresponding transition state.

Since the latter comparison was done for different solvents in order to be in accordance with experiments (**Scheme 25**), the reaction of imine **7a** with 2,2-dichloroacetyl chloride **8** was also modelled for dichloromethane. It was found that the path leading to *N*-(chloromethyl)amide **11a** was not affected by the more polar solvent, while the intermediates appearing on the path leading to β-lactam **9a** were stabilized by dichloromethane. However, there was no considerable difference in the intrinsic barriers for both solvents.

In the final stage of this thesis, a pathway for the hydrolysis of *N*-(chloromethyl)amide **11a** yielding 2,2-dichloroacetamide **60** was modelled. This pathway starts with the elimination of chloride from *N*-(chloromethyl)amide **11a**, resulting in the corresponding iminium chloride salt on which initial addition of water occurs. After two additional steps, 2,2-dichloroacetamide **60** is obtained and the separate products formed via this pathway have a combined Gibbs free energy of -89.3 kJ/mol with respect to *N*-(chloromethyl)amide **11a**.

## 4.2 Conclusion

Examination of the Gibbs free energy profiles for starting reactants with different substituents revealed that the specific combination of 2,2-dichloroacetyl chloride **8** with imine **7a** (**Scheme 25**) exhibits a slight preference for the formation of *N*-(chloromethyl)amide **11a**, with respect to the other substituent combinations that were investigated. The imine side chains ($R^3$ = *p*-methoxyphenyl and $R^4$ = (*S*)-DMDO) had a stabilizing effect on the zwitterionic precursor of β-lactam **9a**, while facilitating direct acylation of the imine **7a** by 2,2-dichloroacetyl chloride **8**. The most determining factor was the nature of the acid chloride substituents. The two chlorine groups complicate β-lactam formation via conrotatory cyclization, while similar barriers were obtained for direct acylation of the imine by the two acid chlorides that were applied in this study. However, purely based on the profile obtained for the reaction of 2,2-dichloroacetyl chloride **8** with imine **7a** one can assume that there should be competition between the formation of β-lactam **9a** and *N*-(chloromethyl)amide **11a**. The analytic spectra were reanalyzed, which lead to the observation of an unknown compound in one of the fractions obtained after purification via columnchromatography. These signals could presumable originate from the envisioned β-lactam **9a**, but only trace amounts of this compound were detected. Based on the calculations discussed in this study, it remains rather peculiar that only trace amounts can be detected, following the assumption that β-lactam **9a** is formed after all. However, based on the available analytic data, the latter assumption can't be confirmed, nor denied.

## 4.3 Outlook

During this computational study, a pathway was modelled for the hydrolysis of *N*-(chloromethyl)amide **11a** yielding the observed 2,2-dichloroacetamide **60**. The model assumes that elimination of chloride from the substrate, resulting in the corresponding iminium chloride salt, occurs prior to addition of water. However, the calculations indicate that the covalent adduct is considerably more stable than the salt (ΔG = -102.4 kJ/mol). This is in contradiction with authors claiming that the latter species can exist in equilibrium, depending on reaction conditions. These findings could be refined via simulation techniques, both static and dynamic, that take into account a more realistic solvent environment. One or more solvent molecules could be included explicitly in static calculations. Molecular dynamic simulations are computationally more expensive but are a better representation of a realistic solution. In order to analyze the presence of the iminium chloride salt versus the presence of the corresponding covalent adduct, one can analyze the distance Δr between the carbon atom, on which chloride adds, and the plane formed by the adjacent atoms (**Figure 16**). Since the iminium ion has a planar configuration (Δr ≈ 0 Å) and it's corresponding covalent adduct, shown in **Figure 16**, a tetraedic configuration (Δr ≈ 0.3 Å), analysis of this coordinate during molecular dynamic simulations could reveal additional insights into this matter. In order to obtain equilibrium constants, more advanced methods such as metadynamica can be applied.

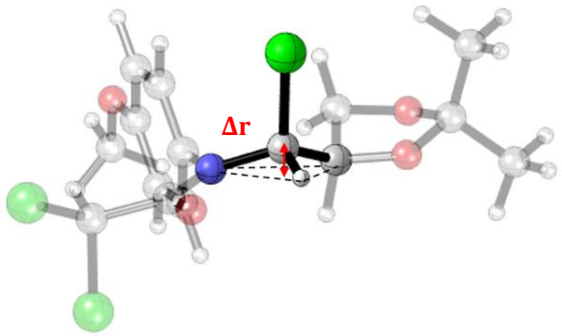


**Figure 16**: 3-D representation of *N*-(chloromethyl)amide **11a**, optimized at B3LYP-D3/6-311+G(d,p) level of theory, IEFPCM: ε = 2,3741 (toluene). Red arrow indicates distance between carbon atom, bound to the chlorine group, and the plane formed by the adjacent atoms.

On the other hand, it can be hypothesized that 2,2-dichloroacetamide **60** is formed via hydrolysis of the zwitterionic intermediate. Proving this statement would also explain the failed attempts to obtain β-lactam **9a**, due to the loss of it's precursor. In addition, further investigation could also focus on the formation of stable complexes of the zwitterionic intermediate, hence complicating β-lactam **9a** formation. Finally, if additional NMR experiments would prove that formation of β-lactam **9a** during synthesis definitely occurs, then further investigation could focus on pathways resulting in ring-opening of the obtained β-lactam **9a**. This was observed for a similar β-lactam ($R^3$ = OAc) in alkaline aqueous conditions. [78]

# Chapter 5

# Samenvatting, Besluit en Vooruitzichten

Deze thesis was een computationele verderzetting op de experimentele resultaten van D. Deturck en L. Cools. Een poging om β-lactam **9a** te produceren door reactie van imine **7a** met 2,2-dichloroacetyl chloride **8** in Staudinger condities leverde niet de verwachte β-lactam structuur op. In de plaats werd een mix van *N*-(chloromethyl)amide **11a** en 2,2-dichloroacetamide **60** bekomen. (**Schema 26**) Dit was eerder onverwacht, aangezien imine **7a** reeds succesvol werd gebruikt om β-lactamen **13** te produceren. Ook werd er al aangetoond dat 2,2-dichloroacetyl chloride **8** kan worden gebruikt om β-lactamen te vormen door reactie met verschillende imines. Deze reactiviteit werd onderzocht aan de hand van een DFT studie met het B3LYP-D3/6-311+G(d,p) theoretisch niveau, gebruik makend van een impliciet solvent model.

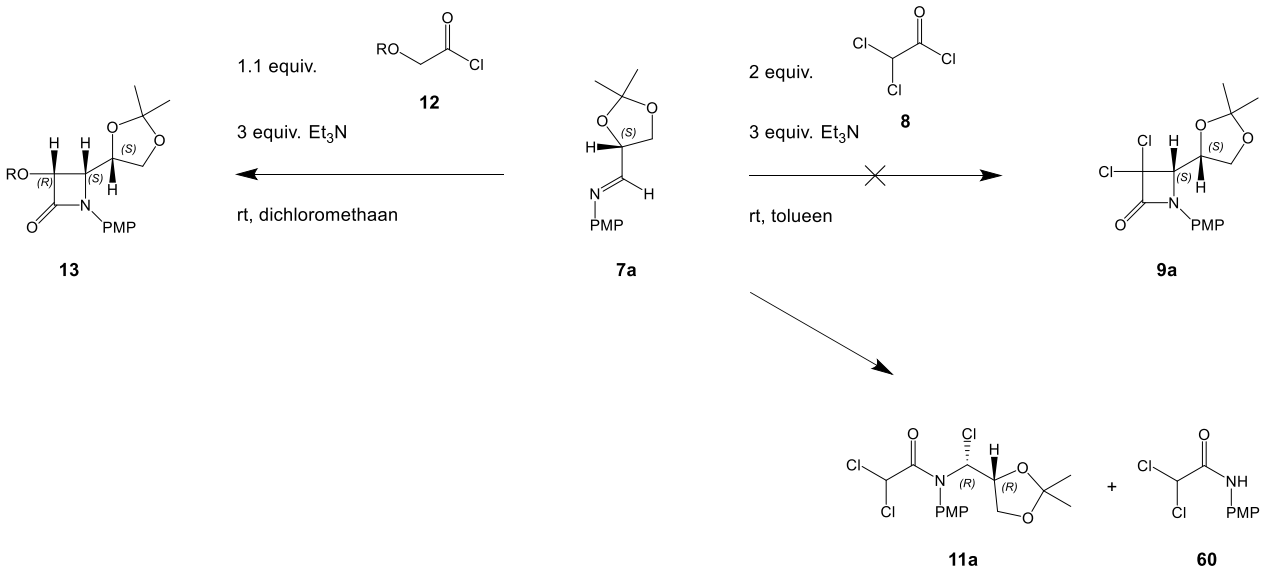


**Schema 26**: Experimentele bevindingen van D. Deturck en L. Cools. [16], [17]

## 5.1 Samenvatting

Tijdens deze thesis werd een systematische aanpak gevolgd om de kwestie, voorgesteld in **Schema 26**, te onderzoeken. In de voorafgaande studie werd een vereenvoudigd imine systeem toegepast om twee reactiepaden te bestuderen, die leiden tot de vorming van het overeenkomstig β-lactam en *N*-(chloromethyl)amide. Daarna werd het Gibbs vrije energie profiel voor de vorming van β-lactam **9a** en *N*-(chloromethyl)amide **11a** besproken. Er werd verwacht dat dit profiel een duidelijke voorkeur voor de vorming van *N*-(chloromethyl)amide **11a** zou aantonen. Dit was echter niet het geval en gebaseerd op het profiel kan worden verondersteld dat vorming van beide producten in competitie is, aangezien de barrières voor de snelheidsbepalende stappen voor de vorming van β-lactam **9a** en *N*-(chloromethyl)amide **11a** gelijkaardig zijn (+58,7 kJ/mol en +52,7 kJ/mol, respectievelijk). Deze trend, bekomen op het B3LYP-D3/6-311+G(d,p) theoretisch niveau, werd gevalideerd aan de hand van single-point energieberekeningen met de M06-2X en ωB87-XD functionalen. Daarnaast werd het Gibbs vrije energie profiel ook geconstrueerd op deze twee andere theoretische niveaus, maar er werd geen opmerkelijk verschil waargenomen, wat de trend verkregen met B3LYP/6-311+G(d,p) bevestigt. Aanvullende berekeningen werden uitgevoerd om deze discrepantie tussen de experimenten en het theoretisch model te onderzoeken. Een mogelijke stabiliserende interactie van de zwitterionische precursor van β-lactam **9a** werd onderzocht door middel van een dimerisch complex van dit zwitterionisch intermediair. Dit was vanwege de tijdslimiet van deze thesis niet nader onderzocht.

In een volgende fase werd de invloed van de imine substituenten beoordeeld. De *p*-methoxyfenyl (PMP) en (*S*)-2,2-dimethyl-1,3-dioxolaan ((*S*)-DMDO) zijketens werden op hun beurt vervangen door *p*-nitrofenyl en fenyl en vervolgens werden de overeenkomstige Gibbs-vrije energie profielen opgesteld. Door deze vergelijking te maken werd de invloed van het elektrongevend karakter van PMP op het Gibbs vrije energie profiel afgeleid. Deze invloed kwam voornamelijk tot uiting door stabilisatie van het zwitterionisch intermediair en door facilitatie van de directe acylering van het imine. Het effect van (*S*)-DMDO was echter meer uitgesproken. Vervanging van deze zijketen door een aromatische groep leverde een aanzienlijke toename op van de intrinsieke barrière voor de vorming van *N*-(chloromethyl) amide **11a** (van +52,7 kJ/mol voor $R^4$ = (*S*)-DMDO tot +70,7 kJ/mol en + 81,3 kJ/mol voor $R^4$ = fenyl en p-nitrofenyl, respectievelijk). Vervolgens werd het effect onderzocht van een ander zuurchloride, namelijk 2-methoxyacetyl chloride **12**, waarvoor is aangetoond dat het succesvol β-lactam **13** oplevert in combinatie met imine **7a**. Het profiel voor deze reactie (**Schema 25**, R = Me) werd vergeleken met het profiel voor de reactie tussen imine **7a** en 2,2-dichlooracetyl chloride **8**. De resultaten toonden aan dat voor de reactie tussen 2-methoxyacetyl chloride **8** en imine **7a** ringsluiting van het zwitterionische intermediair niet langer de snelheidsbepalende stap was (ΔG = +15,0 kJ/mol). In plaats daarvan bepaalde de vorming van het overeenkomstig keteen de snelheid in dit reactiepad (ΔG = +41,2 kJ/mol). Uit

de vergelijking van de barrières voor ringsluiting van de zwitterionische intermediairen werd afgeleid dat de chloorsubstituenten de ringsluiting bemoeilijken door middel van energetische destabilisatie van de overeenkomstige transitietoestand.

Aangezien de vorige vergelijking van profielen werd uitgevoerd voor verschillende solventen, om in overeenstemming te zijn met experimentele condities (**Schema 26**), werd de reactie tussen imine **7a** met 2,2-dichloroacetyl chloride **8** ook gemodelleerd voor dichloromethaan. Hieruit konden we opmaken dat het pad, dat naar *N*-(chloromethyl)amide **11a** leidt, niet werd beïnvloed door het meer polaire solvent, terwijl de intermediairen, die voorkomen op het pad dat leidt naar β-lactam **9a**, wel werden gestabiliseerd door dichloromethaan. Er was echter geen noemenswaardige verandering voor de intrinsieke Gibbs vrije energie barrières in vergelijking met tolueen.

In de laatste fase van deze thesis werd een reactiepad gemodelleerd voor de hydrolyse van *N*-(chloromethyl)amide **11a** met de vorming van 2,2-dichlooracetamide **60**. Dit pad begint met de eliminatie van chloride uit *N*-(chloromethyl)amide **11a**, wat resulteert in het overeenkomstige iminiumchloride zout, waar vervolgens de initiele aanval van water op plaatsvindt. Na twee extra stappen wordt 2,2-dichloroacetamide **60** verkregen en de afzonderlijke producten die via hydrolyse worden verkregen, hebben een gecombineerde Gibbs vrije energie van -89,3 kJ/mol ten opzichte van *N*-(chloromethyl)amide **11a**.

## 5.2 Besluit

Onderzoek van de Gibbs vrije energie profielen voor beginproducten met verschillende substituenten toonde aan dat de specifieke combinatie van 2,2-dichloroacetyl chloride **8** en imine **7a** het meest voorkeur vertoonde voor de vorming van *N*-(chloromethyl)amide **11a**, ten opzichte van de andere onderzochte substituentcombinaties. De imine zijketens ($R^3$ = *p*-methoxyfenyl en $R^4$ = (*S*)-DMDO) hebben een stabiliserend effect op de precursor van β-lactam **9a**, terwijl ze de directe acylering van imine **7a** door 2,2-dichloroacetyl chloride **8** faciliteren. De meest bepalende factor was de aard van de zuurchloride substituenten. De twee chloorgroepen vermoeilijken de vorming van β-lactam via conrotationele cyclisatie, terwijl min of meer gelijke barrières werden verkregen voor directe acylering van imine **7a** door de twee zuurchloriden die in dit onderzoek werden toegepast. Puur op basis van het verkregen profiel voor de reactie tussen 2,2-dichloroacetyl chloride **8** en imine **7a** kan men echter veronderstellen dat er competitie moet zijn tussen de vorming van β-lactam **9a** en *N*-(chloromethyl)amide **11a**. De analytische spectra werden opnieuw geanalyseerd, wat leidde tot de waarneming van een onbekende verbinding in een van de fracties die werd verkregen na opzuivering via kolomchromatografie. Deze signalen kunnen vermoedelijk afkomstig zijn van het beoogde β-lactam **9a**, maar slechts sporen van deze verbinding werden gedetecteerd.

Op basis van de berekeningen die in deze studie zijn besproken, blijft het echter eigenaardig dat alleen sporen kunnen worden gedetecteerd, uitgaande van de veronderstelling dat β-lactam **9a** wel degelijk wordt gevormd. Op basis van de beschikbare analytische data kan deze laatste veronderstelling echter niet worden bevestigd noch ontkend.

## 5.3 Vooruitzichten

Tijdens deze computationele studie werd een route gemodelleerd voor de hydrolyse van *N*-(chloromethyl)amide **11a**, resulterend in 2,2-dichloroacetamide **60**. In het model werd ervan uit gegaan dat eliminatie van chloride uit het substraat, met de vorming van het overeenkomstige iminium chloride zout, plaatsvindt voor de initiele aanval van water. De berekeningen geven echter aan dat het covalente adduct aanzienlijk stabieler is dan het zout (ΔG = -102,4 kJ/mol). Dit is in tegenspraak met auteurs die beweren dat deze twee componenten in evenwicht kunnen voorkomen, afhankelijk van de reactieomstandigheden. Deze bevindingen kunnen worden verfijnd met simulatietechnieken, zowel statische als dynamische, die een meer realistische solventomgeving in rekening kunnen brengen. Een of meerdere solventmoleculen kunnen expliciet worden toegevoegd aan statische berekeningen. Moleculaire dynamische simulaties zijn computationeel veeleisender, maar zijn een betere weergave van een reële oplossing. Om de aanwezigheid van het iminium chloride zout versus de aanwezigheid van het overeenkomstig covalent adduct te onderzoeken, kan men de afstand Δr analyseren tussen het koolstofatoom, waarop chloride addeert, en het vlak gevormd door de aangrenzende atomen (**Figuur 17**). Aangezien het iminiumion een vlakke structuur heeft (Δr ≈ 0 Å) en het overeenkomstig covalent adduct, weergegeven in **Figuur 17**, een tetraedische configuratie (Δr ≈ 0,3 Å), zou analyse van deze coördinaat tijdens moleculaire dynamische simulaties aanvullende inzichten in deze materie kunnen onthullen. Om evenwichtsconstanten te verkrijgen kunnen meer geavanceerde methoden zoals metadynamica worden toegepast.

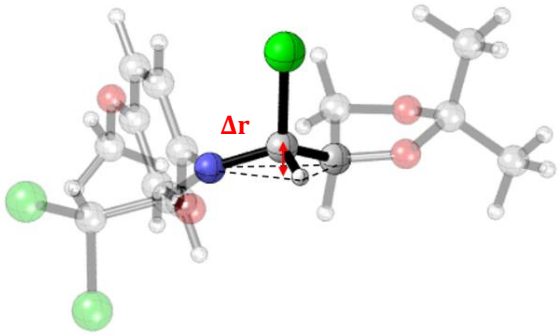


**Figuur 17**: 3-D weergave van *N*-(chloromethyl)amide **11a**, geoptimaliseerd op B3LYP-D3/6-311+G(d,p) theoretisch niveau, IEFPCM: ε = 2,3741 (tolueen). De rode pijl duidt de afstand aan tussen het koolstofatoom, waarop chloor is gebonden, en het vlak gevormd door de aangrenzende atomen.

Aan de andere kant kan worden verondersteld dat 2,2-dichloroacetamide **60** wordt gevormd via hydrolyse van het zwitterionische intermediair. Deze stelling bewijzen zou ook de mislukte pogingen om β-lactam **9a** te produceren verklaren, aangezien de precursor via hydrolyse verloren gaat. Bovendien zou verder onderzoek zich ook kunnen richten op de vorming van stabiele complexen van het zwitterionische intermediair, wat de vorming van β-lactam **9a** gecompliceert. Tot slot, als aanvullende NMR experimenten zouden bewijzen dat de vorming van β-lactam **9a** tijdens synthese zonder twijfel plaatsvindt, dan zou verder onderzoek zich kunnen concentreren op reacties die resulteren in ringopening van het verkregen β-lactam **9a**. Dit werd ook al waargenomen voor een vergelijkbaar β-lactam ($R^3$ = OAc) in alkalische waterige omstandigheden. [78]

**Table A1**: Single-point energies (kJ/mol) with respect to the seperate reactants for the Chloro-amide and Staudinger Path, obtained via single-point energy calculations on the structures obtained with B3LYP-D3/6-311+G(d,p) level of theory. IEFPCM: ε = 2,3741 (toluene)

| | **11a** | **54a** | **TS-4.1a** | **pre-TS-4.1a** | **sep. react.** | **pre-TS-1.0** | **TS-1.0** | **post-TS-1.0** | **46** | **pre-TS-2.1a** | **TS-2.1a** | **53a** | **TS-3.1a** | **9a** |
|---|---|---|---|---|---|---|---|---|---|---|---|---|---|---|
| **B3LYP-D3** | -123.5 | -15.4 | -8.6 | -45.5 | 0 | -47.1 | -14.0 | -23.9 | 11.9 | -19.7 | -16.1 | -46.1 | 4.3 | -195.7 |
| **M06-2X** | -140.7 | -13.1 | -9.8 | -46.9 | 0 | -41.7 | -8.3 | -14.5 | 27.3 | -1.7 | 3.3 | -38.2 | 27.3 | -199.0 |
| **ωB97-XD** | -141.0 | -7.0 | -0.5 | -43.2 | 0 | -46.7 | -9.0 | -17.3 | 19.1 | -8.6 | -3.2 | -42.9 | 16.9 | -214.6 |

**Table A2**: Gibbs free energies (kJ/mol) with respect to the seperate reactants of the Chloro-amide and Staudinger Path for the reaction of imine **7a** with 2,2-dichloroacetyl chloride **8** (first row) and with 2-methoxyacetyl chloride **12** (second row). Level of theory: B3LYP-D3/6-311+G(d,p), IEFPCM: ε = 2,3741 (toluene)

| | **11a/58** | **54a/57** | **TS-4.(1a/2)** | **pre-TS-4.(1a/2)** | **sep. react.** | **pre-TS-1.(0/2)** | **TS-1.(0/2)** | **post-TS-1.(0/2)** | **46/55** | **pre-TS-2.(1a/2)** | **TS-2.(1a/2)** | **53a/56** | **TS-3.(1a/2)** | **9a/13** |
|---|---|---|---|---|---|---|---|---|---|---|---|---|---|---|
| **$R^1 = R^2 = Cl$** | -47.6 | 54.8 | 59.8 | 7.1 | 0 | 4.7 | 39.0 | 38.9 | 14.3 | 25.6 | 36.5 | 16.3 | 75.0 | -117.6 |
| **$R^1 = H, R^2 = OMe$** | -25.2 | 60.0 | 68.8 | 12.3 | 0 | 10.2 | 61.3 | 63.0 | 20.3 | 34.4 | 58.4 | 54.8 | 68.6 | -99.5 |

# References


[1] E. D. Brown and G. D. Wright, "Antibacterial drug discovery in the resistance era," *Nature*, vol. 529, no. 7586, pp. 336–343, 2016, doi: 10.1038/nature17042.

[2] H. Cho, T. Uehara, and T. G. Bernhardt, "Beta-Lactam Antibiotics Induce a Lethal Malfunctioning of the Bacterial Cell Wall Synthesis Machinery," *Cell*, vol. 159, no. 6, pp. 1300–1311, 2014, doi: 10.1016/j.cell.2014.11.017.

[3] S. Shaikh, J. Fatima, and S. Shakil, "Antibiotic resistance and extended spectrum beta-lactamases: Types, epidemiology and treatment," *Saudi J. Biol. Sci.*, vol. 22, no. 1, pp. 90–101, 2015, doi: 10.1016/j.sjbs.2014.08.002.

[4] M. D'hooghe *et al.*, "Synthesis of novel 2-alkoxy-3-amino-3-arylpropan-1-ols and 5-alkoxy-4-aryl-1,3-oxazinanes with antimalarial activity," *J. Med. Chem.*, vol. 52, no. 13, pp. 4058–4062, 2009, doi: 10.1021/jm9002632.

[5] B. Alcaide, P. Almendros, and C. Aragoncillo, "β-lactams: Versatile building blocks for the stereoselective synthesis of non-β-lactam products," *Chemical Reviews*, vol. 107, no. 11. pp. 4437–4492, 2007, doi: 10.1021/cr0307300.

[6] I. F. Discovery, J. Burdon-sanderson, J. Lister, and T. H. Huxley, "History of β-Lactam Antibiotics," pp. 1–14, 1983.

[7] A. Bruggink, "Synthesis of β-lactam antibiotics: chemistry, biocatalysis & process integration.," *Springer Sci. Bus. Media*, vol. 1, 2011.

[8] L. S. Hegedus, J. Montgomery, Y. Narukawa, and D. C. Snustad, "A contribution to the confusion surrounding the reaction of ketenes with imines to produce .beta.-lactams. A comparison of stereoselectivity dependence on the method of ketene generation: acid chloride/triethylamine vs photolysis of chromium carbene compl," *J. Am. Chem. Soc.*, vol. 113, no. 15, pp. 5784–5791, Jul. 1991, doi: 10.1021/ja00015a036.

[9] Y. Liang, L. Jiao, S. Zhang, and J. Xu, "Microwave- and Photoirradiation-Induced Staudinger Reactions of Cyclic Imines and Ketenes Generated from α-Diazoketones . A Further Investigation into the Stereochemical Process," *J. Org. Chem.*, vol. 70, no. 1, pp. 334–337, 2005.

[10] F. Duran and L. Ghosez, "Cycloaddition of haloketenes to imines: A convenient synthesis of functionally substituted β-lactams and 2-pyridones.," *Tetrahedron Lett.*, vol. 11, no. 3, pp. 245–248, 1970, doi: 10.1016/0040-4039(70)80037-5.

[11] A. K. Bose, G. Spiegelman, and M. S. Manhas, "Studies on lactams. Part XVI. Stereochemistry of β-lactam formation," *Tetrahedron Lett.*, vol. 12, no. 34, pp. 3167–3170, 1971, doi: 10.1016/S0040-4039(01)97121-7.

[12] A. Bolognese, M. V. Diurno, O. Mazzoni, and F. Giordano, "on the azetidin-2-one ring formation. A 1H NMR investigation.," *Tetrahedron*, vol. 47, no. 35, pp. 7417–7428, 1991, doi: 10.1016/S0040-4020(01)89743-X.

[13] D. A. Nelson, "Synthesis of cis- and trans-3-chloroazetidinones. II. Direct acylation of imines," *J. Org. Chem.*, vol. 37, no. 9, pp. 1447–1449, May 1972, doi: 10.1021/jo00974a038.

[14] K. Mollet, M. D'hooghe, and N. De Kimpe, "Stereoselective synthesis of bicyclic tetrahydrofuran-fused β-lactams and their conversion into methyl cis-3-aminotetrahydrofuran-2-carboxylates," *Tetrahedron*, vol. 68, no. 52, pp. 10787–10793,

2012, doi: 10.1016/j.tet.2012.01.001.
[15] M. D'hooghe, Y. Dejaegher, and N. Kimpe, "Synthesis of trans-4-aryl-3-(3-chloropropyl)azetidin-2-ones and their transformation into trans- and cis-2-arylpiperidine-3-carboxylates," *Tetrahedron*, vol. 64, pp. 4575–4584, May 2008, doi: 10.1016/j.tet.2008.03.006.
[16] D. Deturck, "Synthese en reactiviteitsstudie van 4-imidoyl-β-lactamen.," UGent, 2018.
[17] L. Cools, "Onderzoek naar de synthese van 3,3-dichloor- en 3-imino-β-lactamen," UGent, 2019.
[18] L. Decuyper *et al.*, "A nitrilase-mediated entry to 4-carboxymethyl-β-lactams from chemically prepared 4-(cyanomethyl)azetidin-2-ones," *RSC Adv.*, vol. 6, no. 59, pp. 54573–54579, 2016, doi: 10.1039/c6ra08213k.
[19] F. Tato, V. Reboul, and P. Metzner, "A novel synthesis of 1-nosyl 3,3-dichloro-β-lactams and derivatives," *J. Org. Chem.*, vol. 73, no. 19, pp. 7837–7840, 2008, doi: 10.1021/jo8014193.
[20] Y. Dejaegher, S. Mangelinckx, and N. De Kimpe, "Rearrangement of 2-aryl-3,3-dichloroazetidines: Intermediacy of 2-azetines," *J. Org. Chem.*, vol. 67, no. 7, pp. 2075–2081, 2002, doi: 10.1021/jo010914j.
[21] F. P. Cossio, J. M. Ugalde, X. Lopez, B. Lecea, and C. Palomo, "A semiempirical theoretical study on the formation of β-lactams from ketenes and imines," *J. Am. Chem. Soc.*, vol. 115, no. 3, pp. 995–1004, Feb. 1993, doi: 10.1021/ja00056a026.
[22] A. Arrieta, B. Lecea, and F. P. Cossío, "Origins of the Stereodivergent Outcome in the Staudinger Reaction between Acyl Chlorides and Imines," *J. Org. Chem.*, vol. 63, no. 17, pp. 5869–5876, 1998, doi: 10.1021/jo9804745.
[23] B. K. Banik, "Cycloaddition Reaction of Imines with Acid Chlorides in the Presence of a Tertiary Base: Variation of the Methods for the Synthesis of Beta Lactams," *Mod. Chem. Appl.*, vol. 05, no. 04, pp. 4–6, 2017, doi: 10.4172/2329-6798.1000240.
[24] J. E. Lynch *et al.*, "Mechanism of An Acid Chloride-imine Reaction By Low-temperature Ft-ir: β-lactam Formation Occurs Exclusively Through A Ketene Intermediate," *J. Org. Chem.*, vol. 54, no. 16, pp. 3792–3796, 1989, doi: 10.1021/jo00277a011.
[25] Y. Liang, L. Jiao, S. Zhang, Z. X. Yu, and J. Xu, "New insights into the torquoselectivity of the staudinger reaction," *J. Am. Chem. Soc.*, vol. 131, no. 4, pp. 1542–1549, 2009, doi: 10.1021/ja808046e.
[26] B. K. Banik, B. Lecea, A. Arrieta, A. De Cózar, and F. P. Cossío, "On the stereodivergent behavior observed in the staudinger reaction between methoxyketene and (E)-N-benzylidenearyl amines," *Angew. Chemie - Int. Ed.*, vol. 46, no. 17, pp. 3028–3032, 2007, doi: 10.1002/anie.200605231.
[27] L. Jiao, Y. Liang, and J. Xu, "Origin of the Relative Stereoselectivity of the β-Lactam Formation in the Staudinger Reaction," *J. Am. Chem. Soc.*, vol. 128, no. 18, pp. 6060–6069, May 2006, doi: 10.1021/ja056711k.
[28] Y. Wang, Y. Liang, L. Jiao, D. M. Du, and J. Xu, "Do reaction conditions affect the stereoselectivity in the staudinger reaction?," *J. Org. Chem.*, vol. 71, no. 18, pp. 6983–6990, 2006, doi: 10.1021/jo0611521.
[29] B. Li, Y. Wang, D.-M. Du, and J. Xu, "Notable and Obvious Ketene Substituent-Dependent Effect of Temperature on the Stereoselectivity in the Staudinger Reaction," *J. Org. Chem.*, vol. 72, no. 3, pp. 990–997, Feb. 2007, doi: 10.1021/jo0622734.

[30] F. P. Cossío, A. Arrieta, J. M. Ugalde, and B. Lecea, "Chiral Control in the Staudinger Reaction between Ketenes and Imines. A Theoretical SCF-MO Study on Asymmetric Torquoselectivity," *J. Am. Chem. Soc.*, vol. 116, no. 5, pp. 2085–2093, 1994, doi: 10.1021/ja00084a054.
[31] J. Xu, "Stereoselectivity in the synthesis of 2-azetidinones from ketenes and imines via the staudinger reaction," in *Arkivoc*, 2009, vol. 2009, no. 9, pp. 21–44, doi: 10.3998/ark.5550190.0010.903.
[32] B. Komjáti, B. Szokol, B. Kováts, P. Kegye, and J. Nagy, "DFT study of stereoselective Ketene-imine cycloadditions, evaluation of possible solvent effects with IEF-PCM," *Period. Polytech. Chem. Eng.*, vol. 62, no. 4, pp. 503–509, 2018, doi: 10.3311/PPch.12527.
[33] M. S. Khajavi, F. Sefidkon, and S. S. Sadat Hosseini, "Reaction of Imines with Trichloroacetic Esters or Anhydride Promoted by Iron Carbonyl or Microwave Irradiation. Preparation of 3,3-Dichloro-β-Lactams," *J. Chem. Res. - Part S*, no. 11, pp. 724–725, 1998, doi: 10.1039/a804314k.
[34] A. Dandia, R. Singh, and P. Sharma, "Solvent-Free Cycloaddition Reaction of 3-Indolylimines with Chloroacetyl Chloride Under Microwave Irradiation," *Heteroat. Chem.*, vol. 14, no. 5, pp. 468–473, 2003, doi: 10.1002/hc.10180.
[35] D. Bandyopadhyay, J. Cruz, and B. K. Banik, "Novel synthesis of 3-pyrrole substituted β-lactams via microwave-induced bismuth nitrate-catalyzed reaction," *Tetrahedron*, vol. 68, no. 52, pp. 10686–10695, 2012, doi: 10.1016/j.tet.2012.06.009.
[36] M. R. Linder, W. U. Frey, and J. Podlech, "Diazoketones as precursors in β-lactam synthesis. New insights into the mechanism of the photochemically induced Staudinger reaction," *J. Chem. Soc., Perkin Trans 1*, pp. 2566–2577, 2001, doi: 10.1039/b105748k.
[37] M. K. Beyer and H. Clausen-schaumann, "Mechanochemistry: The Mechanical Activation of Covalent Bonds," *Chem. Rev.*, vol. 105, no. 8, pp. 2921–2948, 2005.
[38] T. Stauch and A. Dreuw, "Advances in Quantum Mechanochemistry: Electronic Structure Methods and Force Analysis," *Chem. Rev.*, vol. 116, no. 22, pp. 14137–14180, 2016, doi: 10.1021/acs.chemrev.6b00458.
[39] P. Ramachandra Reddy, A. Padmaja, and V. Padmavathi, "Synthesis of Heteroaryl Thiazolidinones and Azetidinones under Conventional and Ultrasonication Methods," *J. Heterocycl. Chem.*, vol. 52, no. 5, pp. 1474–1482, 2015, doi: 10.1002/jhet.2254.
[40] J. Ribas-arino, M. Shiga, and D. Marx, "Understanding Covalent Mechanochemistry," *Angew. Chemie - Int. Ed.*, vol. 48, no. 23, pp. 4190–4193, 2009, doi: 10.1002/anie.200900673.
[41] M. J. Robb and J. S. Moore, "A Retro-Staudinger Cycloaddition: Mechanochemical Cycloelimination of a β-Lactam Mechanophore," *J. Am. Chem. Soc.*, vol. 137, no. 34, pp. 10946–10949, 2015, doi: 10.1021/jacs.5b07345.
[42] D. Marx and M. I. Menéndez, "Torquoselective Mechanochemical Activation of the Staudinger Reaction To Form β-Lactams," *J. Am. Chem. Soc*, vol. 83, no. 4, pp. 2438–2441, 2018, doi: 10.1021/acs.joc.7b03036.
[43] F. P. Cossío, A. Arrieta, and M. A. Sierra, "The mechanism of the ketene-imine (Staudinger) reaction in its centennial: Still an unsolved problem?," *Acc. Chem. Res.*, vol. 41, no. 8, pp. 925–936, 2008, doi: 10.1021/ar800033j.

[44] R. Lopez, T. L. Sordo, J. A. Sordo, and J. Gonzalez, "Torquoelectronic effect in the control of the stereoselectivity of ketene-imine cycloaddition reactions," *J. Org. Chem.*, vol. 58, no. 25, pp. 7036–7037, Dec. 1993, doi: 10.1021/jo00077a022.
[45] E. Rutherford, "The scattering of alpha and beta particles by matter and the structure of the atom," *Phil. Mag. Ser. 6*, vol. 21, pp. 669–688, 1911, doi: 10.1080/14786440508637080.
[46] N. Bohr, "I. On the constitution of atoms and molecules," *London, Edinburgh, Dublin Philos. Mag. J. Sci.*, vol. 26, no. 151, pp. 1–25, Jul. 1913, doi: 10.1080/14786441308634955.
[47] E. Schrödinger, "An Undulatory Theory of the Mechanics of Atoms and Molecules," *Phys. Rev.*, vol. 28, no. 6, pp. 1049–1070, Dec. 1926, doi: 10.1103/PhysRev.28.1049.
[48] M. Born and R. Oppenheimer, "Zur Quantentheorie der Molekeln," *Ann. Phys.*, vol. 389, no. 20, pp. 457–484, Jan. 1927, doi: 10.1002/andp.19273892002.
[49] D. R. Hartree, "The Wave Mechanics of an Atom with a Non-Coulomb Central Field. Part I. Theory and Methods," *Math. Proc. Cambridge Philos. Soc.*, vol. 24, no. 1, pp. 89–110, 1928, doi: 10.1017/S0305004100011919.
[50] D. R. Hartree, "The Wave Mechanics of an Atom with a Non-Coulomb Central Field. Part II. Some Results and Discussion," *Math. Proc. Cambridge Philos. Soc.*, vol. 24, no. 1, pp. 111–132, 1928, doi: 10.1017/S0305004100011920.
[51] J. C. Slater, "The Theory of Complex Spectra," *Phys. Rev.*, vol. 34, no. 10, pp. 1293–1322, Nov. 1929, doi: 10.1103/PhysRev.34.1293.
[52] W. Pauli, "Über den Zusammenhang des Abschlusses der Elektronengruppen im Atom mit der Komplexstruktur der Spektren," *Zeitschrift für Phys.*, vol. 31, no. 1, pp. 765–783, 1925, doi: 10.1007/BF02980631.
[53] C. Møller and M. S. Plesset, "Note on an Approximation Treatment for Many-Electron Systems," *Phys. Rev.*, vol. 46, no. 7, pp. 618–622, Oct. 1934, doi: 10.1103/PhysRev.46.618.
[54] R. Haunschild, A. Barth, and B. French, "A comprehensive analysis of the history of DFT based on the bibliometric method RPYS," *J. Cheminform.*, vol. 11, no. 1, pp. 1–15, 2019, doi: 10.1186/s13321-019-0395-y.
[55] P. Hohenberg and W. Kohn, "Inhomogeneous Electron Gas," *Phys. Rev.*, vol. 136, no. 3B, pp. B864--B871, Nov. 1964, doi: 10.1103/PhysRev.136.B864.
[56] W. Kohn and L. J. Sham, "Self-Consistent Equations Including Exchange and Correlation Effects," *Phys. Rev.*, vol. 140, no. 4A, pp. A1133--A1138, Nov. 1965, doi: 10.1103/PhysRev.140.A1133.
[57] K. Fukui, "The path of chemical reactions - the IRC approach," *Acc. Chem. Res.*, vol. 14, no. 12, pp. 363–368, Dec. 1981, doi: 10.1021/ar00072a001.
[58] A. D. Becke, "Density-functional exchange-energy approximation with correct asymptotic behavior," *Phys. Rev. A*, vol. 38, no. 6, pp. 3098–3100, Sep. 1988, doi: 10.1103/PhysRevA.38.3098.
[59] A. D. Becke, "Density-functional thermochemistry. III. The role of exact exchange," *J. Chem. Phys.*, vol. 98, no. 7, pp. 5648–5652, Apr. 1993, doi: 10.1063/1.464913.
[60] A. D. Becke, "A new mixing of Hartree-Fock and local density-functional theories," *J. Chem. Phys.*, vol. 98, no. 2, pp. 1372–1377, 1993, doi: 10.1063/1.464304.
[61] C. Lee, W. Yang, and R. G. Parr, "Development of the Colle-Salvetti correlation-energy

formula into a functional of the electron density," *Phys. Rev. B*, vol. 37, no. 2, pp. 785–789, Jan. 1988, doi: 10.1103/PhysRevB.37.785.
[62] É. Brémond *et al.*, "Benchmarking Density Functionals on Structural Parameters of Small-/Medium-Sized Organic Molecules," *J. Chem. Theory Comput.*, vol. 12, no. 2, pp. 459–465, 2016, doi: 10.1021/acs.jctc.5b01144.
[63] L. Goerigk, A. Hansen, C. Bauer, S. Ehrlich, A. Najibi, and S. Grimme, "A look at the density functional theory zoo with the advanced GMTKN55 database for general main group thermochemistry, kinetics and noncovalent interactions," *Phys. Chem. Chem. Phys.*, vol. 19, no. 48, pp. 32184–32215, 2017, doi: 10.1039/c7cp04913g.
[64] M. Gruden *et al.*, "Benchmarking density functional tight binding models for barrier heights and reaction energetics of organic molecules," *J. Comput. Chem.*, vol. 38, no. 25, pp. 2171–2185, 2017, doi: 10.1002/jcc.24866.
[65] H. Kruse, L. Goerigk, and S. Grimme, "Why the standard B3LYP/6-31G* model chemistry should not be used in DFT calculations of molecular thermochemistry: Understanding and correcting the problem," *J. Org. Chem.*, vol. 77, no. 23, pp. 10824–10834, 2012, doi: 10.1021/jo302156p.
[66] B. J. Lynch and D. G. Truhlar, "How well can hybrid density functional methods predict transition state geometries and barrier heights?," *J. Phys. Chem. A*, vol. 105, no. 13, pp. 2936–2941, 2001, doi: 10.1021/jp004262z.
[67] S. Grimme, J. Antony, S. Ehrlich, and H. Krieg, "A consistent and accurate ab initio parametrization of density functional dispersion correction (DFT-D) for the 94 elements H-Pu," *J. Chem. Phys.*, vol. 132, no. 15, p. 154104, Apr. 2010, doi: 10.1063/1.3382344.
[68] J.-D. Chai and M. Head-Gordon, "Long-range corrected hybrid density functionals with damped atom–atom dispersion corrections," *Phys. Chem. Chem. Phys.*, vol. 10, no. 44, pp. 6615–6620, 2008, doi: 10.1039/B810189B.
[69] Y. Zhao and D. G. Truhlar, "The M06 suite of density functionals for main group thermochemistry, thermochemical kinetics, noncovalent interactions, excited states, and transition elements: two new functionals and systematic testing of four M06-class functionals and 12 other function," *Theor. Chem. Acc.*, vol. 120, no. 1, pp. 215–241, 2008, doi: 10.1007/s00214-007-0310-x.
[70] M. J. Frisch, J. A. Pople, and J. S. Binkley, "Self-consistent molecular orbital methods 25. Supplementary functions for Gaussian basis sets," *J. Chem. Phys.*, vol. 80, no. 7, pp. 3265–3269, Apr. 1984, doi: 10.1063/1.447079.
[71] T. Clark, J. Chandrasekhar, G. W. Spitznagel, and P. V. R. Schleyer, "Efficient diffuse function-augmented basis sets for anion calculations. III. The 3-21+G basis set for first-row elements, Li–F," *J. Comput. Chem.*, vol. 4, no. 3, pp. 294–301, 1983, doi: 10.1002/jcc.540040303.
[72] J. Ochterski, "Thermochemistry in Gaussian," 2000. http://gaussian.com/thermo/.
[73] S. Miertuš, E. Scrocco, and J. Tomasi, "Electrostatic interaction of a solute with a continuum. A direct utilizaion of AB initio molecular potentials for the prevision of solvent effects," *Chem. Phys.*, vol. 55, no. 1, pp. 117–129, 1981, doi: 10.1016/0301-0104(81)85090-2.
[74] S. Miertuš and J. Tomasi, "Approximate evaluations of the electrostatic free energy and internal energy changes in solution processes," *Chem. Phys.*, vol. 65, no. 2, pp. 239–245,

1982, doi: 10.1016/0301-0104(82)85072-6.
[75] J. L. Pascual-ahuir, E. Silla, and I. Tuñon, “GEPOL: An improved description of molecular surfaces. III. A new algorithm for the computation of a solvent-excluding surface,” *J. Comput. Chem.*, vol. 15, no. 10, pp. 1127–1138, 1994, doi: 10.1002/jcc.540151009.
[76] B. E. Maryanoff, H.-C. Zhang, J. H. Cohen, I. J. Turchi, and C. A. Maryanoff, “Cyclizations of N-Acyliminium Ions,” *Chem. Rev.*, vol. 104, no. 3, pp. 1431–1628, Mar. 2004, doi: 10.1021/cr0306182.
[77] Y. Zeng and Y. Ren, “Density functional theory study of tautomerization of 2-aminothiazole in the gas phase and in solution,” *Int. J. Quantum Chem.*, vol. 107, no. 1, pp. 247–258, 2007, doi: 10.1002/qua.21059.
[78] S. Deketelaere, “Unpub,” 2020.